Response to Reviewer #1:

We appreciate the reviewer who reviewed the manuscript and revision carefully and provided insightful follow-up comments. We have tried our best to address all concerns and revised the manuscript accordingly. The comments are in normal font. A point-by-point response is listed as below in bold italics.

This the third around review. The authors did not take good use of the chances to address the concerns I raised. Besides they still missed some points (examples below), they even did not try to make effort to organize the paper and present the most important points. The paper gets so lengthy and appears lack of organization (see the comment #1 below for an example below). They now got 20 formal figures and 15 supplemental figures. It appears they added lengthy text and figures to address comments but did not think of how to better organize and only present the most important points. Another evidence showing the lack of effort in presenting the study is that the figures are out of orders, for example, it is jumped from Figure S2 to Figure S6 in referencing figures. The first appearance of Figure S3 and S4 is after Figure S7. The first appearance of Figure S5 is after Figure S7 but before the first appearance of Figures S3 and S4. The first reference to Figure 1 is also after Figure 2.

Response: Per your suggestions, the main text has been restructured and the order of the figures in both the main text and supplement has been corrected accordingly.

I did not have time to read the whole paper but only read their response and changes and the following corrections and clarifications are needed:

1. To address my first comment of the second round review, the authors conveniently only added a few figures to the end of the supplemental materials and discussed it in the Summary and Discussion section, which does not address the point. I emphasized before that the point is to explain the opposite precipitation response at the different sectors of the system. So, to address this point well, it is equally important to describe both the increase of the precipitation at the convergence zone and warm sector and the decrease of the precipitation in the cold sector.

Then explain the reasons causing the increase and the decrease, respectively. Therefore, the changes should be started from the first paragraph in P8 where Figure 3 is discussed.

Response: Thanks for your suggestions. In the latest version, we mention the cold front system firstly. The responses of rainfall amount to increased aerosols are described at the beginning of the result part, with increase in the warm sector and decrease in the cold sector. Given the details discussed with enough text length, it would be tedious if we equally explain the mechanism of both precipitation increase and decrease. It may be more appropriate to focus on the aggravated side with precipitation enhancement where also covers most developed cities over southern China. However, the discussion about the mechanism of the precipitation decrease in the cold sector is revised per your suggestions in comment #4.

2. Also, the authors argued “There are lots of ice crystals with cloud ice extending up to 16 km, indicating strong deep convection”. At the cold sector of a frontal system, generally there is no mechanism to form deep convective clouds. It should be deep stratiform clouds, not strong convective clouds. If this case is different from the general understanding, then needs to present evidence such as large CAPE or large low-level upward motion to support the argument of deep convective clouds.

Response: Figure R 1 shows the spatial distribution of CAPE on December 15 in 2013. There is a salient gradient between the northwest and southeast of the domain 2 which is consistent with the surface temperature gradient (Figure S3). We agree that the relatively low CAPE over the northwest of the domain 2 suggests the stable situation there. It is more likely to form stratiform clouds. The corresponding description has been revised in the main text.

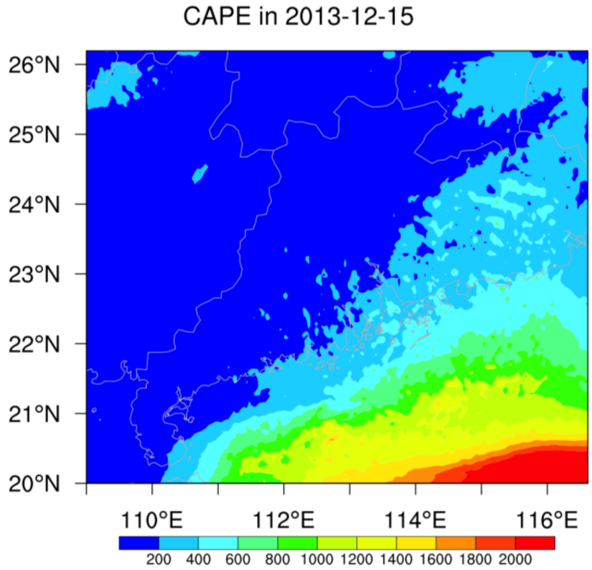

Figure R 1. Spatial distribution of CAPE (unit: J kg^{-1}) on December 15 in 2013 in the CTL run.

3. "The reduction of rain water and ice crystals (particularly in graupel) suggest that both the warm rain and cold rain are suppressed" - wrong statement. As I emphasized previously, ice crystals are non-precipitating particles which does not suggest precipitation information, but graupel is precipitating particle but it is not ice crystal, it is just one type of ice particles. They made such mistakes in terminology in many places throughout the paper. When talking about specific hydrometeors types, you may use ice crystal (or cloud ice), snow, graupel. When you want to take about ice particle in general covering different types, use "ice particle" not "ice crystal". This need to be changed throughout the paper.

Response: Thanks for your explanation and clarification. In this sentence, the ice crystals referred to snow and graupel. The misuse of hydrometeor terminology has also been corrected in the main text.

4. The suppressed precipitation for cold-based clouds should be mainly because the reduced warm rain formation at the early times and reduced graupel formation at the later time period based on Figure S12. This is a typical response of deep stratiform clouds to CCN since the most dominant changes by aerosols for this type of clouds are collision processes including autoconversion and riming, which are less efficient due to smaller droplet size. This should be

the major argument for the suppressed precipitation. The three reasons listed by authors are mainly for deep convective clouds.

Response: Per your suggestions. There is a strong surface temperature gradient between the southeast and northwest of the domain 2, indicating a front system. In the cold sector, the clouds tends to be stratiform clouds, which is most winter precipitation falls from. We remove the mechanism for convective clouds and revised it for stratiform clouds as you suggested.

5. The sentence in the abstract that I pointed out previously still did not make sense. As I asked previously, how can the changes of precipitation between a polluted and clean condition resemble that from control run since the changes mean the differences?

Response: Per you Suggestions. This sentence has been revised as "In response to 10× aerosol emissions, the pattern of precipitation and cloud property changes resembled the differences between CTL and CLEAN, but with a much greater magnitude."

6. In response of #7 comments in the last round, I read their changes and still have the following problems,

(1) "The warm rain is still suppressed before 15Z on December 15 (Figure 6c) even though with strong latent heat release through cloud water formation": Warm rain will be always suppressed with the two-moment bulk scheme with the parameterization of autoconversion. This is very different from the treatment of in bin microphysics used in Fan et al. 2018. This needs to be clarified. Also, warm rain means the rain formed from autoconversion. Rain mass below 0 C level can be contributed by the melted particles. You only can discuss the warm rain at the times when there are no ice particles at all above 0 C level in Figure 6c.

Response: Thanks for pointing this out. We agree that the warm rain is always suppressed as the number of converted droplets into rain drops is inversely proportional to cloud droplet numbers (Khairoutdinov and Kogan, 2000). This is also clarified in the main text. Per your suggestions, the description of warm rain has been removed.

(2) "To further analyze the source of this latent heat release, following Fan et al. (2018), the

latent heat released from condensation, deposition, and freezing during cold and warm cloud processes are diagnosed", I do not think you can say "following Fan et al. (2018)". The author's response did not give a clear description about how the latent heat is calculated. They should not have sent a bunch of codes, instead, it should be easily described with words about how the latent heat is calculated for each process. I think the latent heat calculation should be the part of Morrison scheme since this is the feedback to temperature that a full coupled model should consider. The authors should not need to add additional code for such calculation (probably only need to find the right variable name to output it). Because the authors had wrong statements about latent heat and also said they diagnosed it in the code before, I asked these details to check if this important part was done and interpreted correctly. I did not get the answer from their response.

Response: Yes, the latent heat is calculated in the Morrison scheme. However, in the calculation, the latent heat is only derived for warm cloud and cold cloud rather than attributed to different microphysical processes. The latent heat of each process is not calculated based on the mass. To avoid the confusion, we revise the description as follows:

The latent heat for each process is calculated as the product of mass conversion between different phases and its associate latent heat release rate in the model.

The Appendix A part is removed per your suggestion.

(3) P10 Line 5-28, the lengthy statements they added need to revised due to misunderstandings. First, it is the basic cloud microphysics that latent heat from freezing is not a major component deep clouds as I explained last round. Condensation and deposition are always the very important condensate forming process in deep convective clouds. Second, in those past studies that the author mentioned, when they discussed the effect from freezing changed by aerosols, it is not just about the latent heat from freezing only, instead about the latent heat changes from all the processes due to the change of freezing induced by aerosols. For example, when there are more freezing, more ice crystals form, then riming and deposition will change as well.

Response: Thanks for pointing this out. Yes, latent heat release is dominated by condensation and deposition. Sorry for the misunderstanding, we revise the description of the marginal role of freezing by attribution to amount of latent heat. In the mentioned

literature, the effect of freezing is indeed not only due to its latent heat release. The statement has been shortened and modified as follows:

"The latent heat released for each process, which is calculated as the product of mass conversion between different phases and its associate latent heat release rate in the model, is further analyzed for both cold and warm clouds (Figure 7). The salient latent heat changes mentioned above in Figure 5g is caused by deposition in cold cloud (Figure 7e). Figure S9 shows the time-height distribution of mass and number concentrations for different hydrometers in control run. Note the magnitude of snow and graupel mass is ten times of that of rain water. There are affluent snow and graupel before 15Z on 15 December located where the distinct changes in depositional heat appears. With aerosols, the snow and graupel grows at the expenses of ice crystals and rain water via aggregation and riming, respectively (Figure 6c–e). The former refers to the collision and coalescence of ice crystals to form snow while the latter represents the accretion of cloud drops and rain drops by snow and graupel to form larger graupels. These are the main processes of converting liquid mass to solid phase, contributing to additional precipitating particles. However, the latent heat due to riming is relatively small (Figure 7f) because the latent heat release per unit for freezing (334 kJ kg–1) is only 1/8 of that for deposition (2256 kJ kg–1). The latent heat release due to deposition in cold cloud is stronger than that due to condensation in warm cloud even though the latter is also important (Figure 7a and 7e). In deep convection, the strong updraft usually makes the atmospheric condition saturated for water which is supersaturated with respect to ice. With the presence of snow and graupel (Figure S9), the formation of ice particles is enhanced accompanied by additional latent heat release due to deposition (Figure 6 and Figure 7). After 15Z on December 15, most of the snow and graupel sedimentate. Compared with depositional heating, the condensational heating plays a dominant role in intensifying convective strength. The rain water increases through accretion of added cloud droplets, leading to precipitation increases. These findings highlight two different processes and mechanisms in the precipitation increase before and after 15Z on December 15. The dominant source for latent heat release is depositional heating in the former case (cold rain enhancement) while condensational heating in the latter (warm rain enhancement). Due to latent heat release with aerosols, the vertical motion is boosted (Figure 5g) which further enhance the supersaturation and associated with latent heat release. Via microphysics–dynamics feedback, the convection is intensified, and precipitation increased. This feedback has been widely discussed in ACI effects on deep convection (Fan et al., 2018; Koren et al., 2015; Tao et al., 2012)."

With through rounds of review, I have tried hard to correct many basic knowledges and results about cloud microphysics and aerosol-cloud interaction processes to improve the quality of this paper. I urge the authors to take the opportunity to do a careful job in writing and organizing the results so that the paper can reach a certain level of qualify for publication.

Response: We appreciate your great effort in improving this study significantly. We have tried our best to write precisely and organise the structure smoothly.

Reference:

Khairoutdinov, M. and Kogan, Y.: A New Cloud Physics Parameterization in a Large-Eddy Simulation Model of Marine Stratocumulus, Mon. Weather Rev., doi:10.1175/1520-0493(2000)128<0229:ancppi>2.0.co;2, 2000.

Contribution of local and remote anthropogenic aerosols to ~~intensification of~~ a record-breaking torrential rainfall event in Guangdong P~~p~~rovince, China

Z. Liu[1,2,3], Y. Ming[5~~4~~], C. Zhao[6~~5~~], N.C. Lau[1,2,4~~3~~], J~~.ian~~P~~.ping~~ Guo[7~~6~~], M. Bollasina[3], Steve H.L. Yim[~~1,~~4,1~~3~~,2]

Formatted: Superscript

[1]Institute of Space and Earth Information Science, The Chinese University of Hong Kong, Hong Kong, China
[2]Institute of Environment, Energy and Sustainability, The Chinese University of Hong Kong, Sha Tin, N.T., Hong Kong
[3]School of Geosciences, University of Edinburgh, UK

Formatted: Font: 10 pt, (Asian) Chinese (Hong Kong SAR)

[4~~3~~]Department of Geography and Resource Management, The Chinese University of Hong Kong, Sha Tin, N.T., Hong Kong
[5~~4~~]Geophysical Fluid Dynamics Laboratory/NOAA, Princeton, New Jersey, USA
[6~~5~~]School of Earth and Space Sciences, University of Science and Technology of China, Hefei, Anhui, China
[7~~6~~]State Key Laboratory of Severe Weather, Chinese Academy of Meteorological Sciences, Beijing 100081, China

Correspondence to: Steve H.L. Yim (steveyim@cuhk.edu.hk)

Abstract. A torrential rainfall case, which happened in Guangdong Province during December 14–16, 2013, broke the historical rainfall record in the province in terms of duration, affected area, and accumulative precipitation. The influence of anthropogenic aerosols on this extreme rainfall event ~~was~~ is examined using a coupled meteorology-~~-~~chemistry-aerosol model. Enhancement of precipitation in the estuary and near the coast up to 33.7 mm ~~was~~ is mainly attributed to aerosol-~~-~~cloud interactions (ACI), whereas aerosol-radiation interaction~~s~~ partially ~~compensated~~ offsets 14% of the precipitation increase. F~~Our F~~further analysis ~~of different~~on~~by varying~~ changes in hydrometeors and latent heat sources suggests that the ACI effects on the intensification of~~ying the~~ precipitation can be divided into two stages: cold rain enhancement in the former stage followed by~~ while~~ warm rain enhancement in the latter~~ stage~~. Responses of precipitation to the changes in anthropogenic aerosols concentration ~~s~~ from local (i.e., Guangdong P~~p~~rovince) and remote (i.e., outside Guangdong P~~p~~rovince) sources ~~were~~ are also investigated through simulations with reduced aerosol emissions from either local or remote sources. Accumulated aerosol concentration from local sources ~~aggregated~~ aggregates mainly near the ground surface and ~~diluted~~ dilutes quickly after the precipitation initiated. By contrast, the aerosols ~~concentration~~ from remote emissions ~~extended~~ extend up to 8 km and ~~lasted~~ lasts much longer before decreasing until peak rainfall beg~~a~~ins, because aerosol~~s~~ ~~were~~are continuously transported by the strong northerly winds. ~~Although~~ T~~t~~he patterns of precipitation response to remote and local aerosol~~s~~ concentrations~~s~~ resemble~~d~~ each other.~~,~~ However, compared with local aerosol~~s~~ through warm rain enhancement, remote aerosol~~s~~ ~~contributed~~ contribute more than twice the precipitation increase via intensifying both cold and warm rain~~ compared with local aerosols~~, occupying a predominant role. A ~~T~~ten-times~~s of the~~ emission sensitivity test ~~resulted~~ shows~~in~~ about ten times of PM$_{2.5}$ concentration compared with the control run. Cold (w~~W~~arm) rain is drastically enhanced (suppressed) in 10× run. In response to 10× aerosol emissions, the pattern of ~~Compared with CLEAN experiment, t~~~~The patterns of~~ precipitation and cloud property changes~~ in 10× run also~~ resemble~~sd~~ ~~that in~~ the differences between CTL~~control run~~ and CLEAN, but with a much greater

magnitude. sT~~T~~he ~~average~~ precipitation average over~~in~~ Guangdong ~~Pprovince~~ decrease~~d~~s by 1.0 mm in 10× run but ~~increased~~ increases by 1.4 mm in the control run by comparing with the CLEAN run. We note~~d~~ that the ~~reinforced~~ precipitation increase ~~was~~ is concentrated within a more narrowed downstream region of aerosol source, whereas the precipitation decrease ~~was~~ is more dispersed across the upstream region. This indicates that the excessive aerosols~~s~~ not only suppress rainfall but also change the spatial distribution of precipitation, increasing the rainfall range, thereby potentially exacerbating flood and drought elsewhere. This study highlights the importance of considering aerosols~~s~~ in meteorology to improve extreme weather forecasting. Furthermore, aerosols~~s~~ from remote emissions may outweigh those from local emissions in the convective~~loud~~ invigoration effect.

1 Introduction

Synoptic weather is a key factor driving air pollution events through photochemical, turbulence, wet deposition, and transport processes (Ding et al., 2009; Guo et al., 2017; Liu et al., 2001; Liu et al., 2019b; Madronich, 1987). Numerous studies have predicted air quality either numerically or statistically based on weather conditions (Dutot et al., 2007; Otte et al., 2005). In recent years, ~~more and more~~~~Few~~ efforts have been increasingly made to identify the influence of air pollution (e.g., aerosols~~s~~)~~aerosols~~ on synoptic weather (Ding et al., 2013; Grell et al., 2011), particularly~~especially~~ on different types of~~in~~ extreme weather, such as tropical cyclone (Wang et al., 2014; Zhao et al., 2018), hail storm (Ilotoviz et al., 2016), and extreme rainfall~~ cases~~ (Fan et al., 2015; Zhong et al., 2015)~~. However, the climate effects of aerosols have long been analyzed (Hansen et al., 1997; Myhre et al., 2013; Twomey, 1977)~~.

For decades, China has been affected by severe pollution induced by rapid urbanization and economic development (He et al., 2002). The Pearl River Delta (PRD) region, situated on the south coast of China, is one of the most developed and also the most polluted regions. The aerosol optical depth retrieved from the Moderate Resolution Imaging Spectroradiometer is typically higher than 0.6 in Guangzhou, a megacity in the PRD region (Wu et al., 2005).

In addition to reducing visibility and inducing respiratory diseases (Cohen et al., 2015; Gu and Yim, 2016; Chen et al., 2017), high aerosol concentration~~s~~ can also affect weather and climate through interactions with radiation and clouds (Bollasina et al., 2011; Lau and Kim, 2006; Liu et al., 2019c; Wang et al., 2011). Aerosols~~s~~ absorb and scatter solar radiation and serve as cloud condensation nuclei and ice nuclei, which are referred to as aerosol-~~–~~radiation interactions (ARI) and aerosol-~~–~~cloud interactions (ACI), respectively (IPCC, 2013). Both ARI and ACI influence deep convection and hence precipitation (Fan et al., 2008, 2013; Koren et al., 2004; Liu et al., 2018; Rosenfeld et al., 2008; Fan et al., 2018). Liu et al. (2018) found that ARI suppressed deep convection by reducing the relative humidity in the middle-~~–~~upper troposphere and weakening the upward motion. Fan et al. (2015) revealed that ARI ~~weakened convergence, enhanced atmospheric stability, and~~ suppressed convection in the basin during the daytime but~~. Excess moist static energy was transported to mountains, thus~~ enhanced~~generating heavy~~ rainfall at night on ~~the~~ mountains. ~~This suppression effect is dramatically modulated by the intensity of synoptic forcing (Zhong et al., 2017).~~ Compared with the effects of ARI, those of ACI on deep convection and precipitation have received more attention and are more controversial in both observational and modeling studies. Increased aerosols~~s~~ can suppress or enhance precipitation depending on environmental conditions such as humidity, cloud type, cloud phase, and vertical wind shear (Khain, 2009; Lee et al., 2008; Tao et al., 2012; Liu et al., 2019a). Khain (2009) and Fan et al. (2007) have reported that increases in humidity generate more condensate than lose~~t~~, resulting in more precipitation from deep convective clouds~~, especially in a polluted environment~~. Studies have reported that aerosols~~s~~ inhibit precipitation from shallow clouds (Andreae et al., 2004; Chen et al., 2016; Rosenfeld, 2000), whereas they invigorate deep convection with warm (>15°C) cloud bases (Bell et al., 2008; Koren et al., 2010, 2014). By contrast, smaller cloud droplets induced by aerosols~~s~~ could remain liquid ~~the slowing autoconversion rate induced by aerosols forms airborne cloud droplets in clouds with bases~~ below ~~near or above~~ 0°C when lacking ice nuclei, inhibiting precipitation (Cui et al., 2006; Rosenfeld and Woodley, 2000). Fan et al. (2009, 2012) have suggested that increased aerosols~~s~~ enhanced convection under weak wind shear ~~and~~ whereas suppressed convection under strong wind shear by increasing evaporative cooling for an isolated storm. ~~However, the evaporative cooling induced by aerosols has also been found to enhance precipitation under strong wind shear for cloud systems (Lee et al., 2008; Tao et al., 2007).~~ Recently, Fan et al. (2018) found that the latent heat release could be mainly attributed to condensational heating rather than ice-related processes at upper levels, differing from cold convective~~-cloud~~ invigoration (Rosenfeld et al., 2008).

~~Few studies have discussed~~ T~~t~~he competition between~~relative importance of~~ the effects of ~~-~~ARI and ACI~~-~~ has been discussed on both cloud-resolving scale (Lin et al., 2017; Wang et al., 2018) ~~as well as~~and regional scale (Wang et al., 2016)~~on deep convection and precipitation~~. Fan et al. (2008) suggested that the suppressive effects of ARI can outweigh the invigorative effects of ACI on deep convection and precipitation as the absorption of ~~aerosols~~aerosols enhances. Koren et al. (2008) showed ~~that~~ the net effect of two opposite influences~~, those of ARI and ACI,~~ on clouds over the Amazon which depends on the initial cloud fraction. Large cloud cover fractions were mostly invigorated by ACI, whereas small cloud cover fractions were suppressed by ARI. Different aerosol types can also be a critical factor to ~~their~~the radiative or microphysical properties of clouds, thus determining the invigoration or suppression effect of ~~aerosols~~aerosols on deep convection (Jiang et al., 2018). ~~However, much less attention is payed to aerosol impact on stratiform clouds and associated precipitation. Fan et al. showed that increased aerosols contribute to more condensation but less precipitation because of much smaller droplet size. The precipitation enhancement in the downwind area of a polluted environment could be induced mainly by either ARI or ACI (Fan et al., 2015; Zhong et al., 2015).~~ Most of the~~Both~~ studies have focused on summer season ~~extreme rainfall cases~~ when~~because~~ most extreme rainfall events occur ~~in summer~~ over China (Fu et al., 2013).

We select~~ed~~ a torrential rainfall case in winter, which ~~broke~~ breaks the record of Guangdong Province since 1951 in terms of duration, affected area, and cumulative rainfall (Deng et al., 2015) ~~over the PRD region~~, to further understand the combined effects and relative importance of ARI and ACI on precipitation. Before this heavy rainfall, the PRD region ~~was~~ is affected by a strong haze with $PM_{2.5}$ concentration~~s~~ ~~approaching~~ reaching to 174 μg m^{-3}. The significant transboundary nature of air pollution in China has been well recognized (e.g., Gu and Yim, 2016). Effects of local and remote aerosol emissions on monsoons and associated precipitation~~, particularly the Indian summer monsoon,~~ have been examined in recent years (Bollasina et al., 2014; Cowan and Cai, 2011; Guo et al., 2016b; Jin et al., 2016), which ~~was~~ were comprehensively reviewed by Li et al. (2016). The effects of local and remote aerosol emissions on extreme rainfall events remain mostly unexplored. Given the strong monsoonal flow and severe air pollution over the northeast of China (Figure 1b), the aerosol concentration~~s~~ could be either from local emissions or transport by prevailing northeasterly winds~~s~~. A critical question, therefore, is whether the aerosol~~s concentrations~~~~s~~ that affect~~ed~~ this extreme rainfall case ~~was~~is originated from local or remote aerosol emission sources. The remainder of this study proceeds as follows: Section 2 describes the regional model associated with the experimental design as well as the observation datasets of this study. Main findings on the effects of ~~aerosols~~aerosols on the extreme rainfall event are discussed in section 3. The main conclusions are summarized and discussed in section 4.

~~ACI strongly depend on cloud regimes~~

Formatted: Font: 10 pt

2 Model configurations and observational datasets

The principal tool for this work is~~was~~ the Weather Research and Forecasting (WRF) model coupled with Chemistry (WRF-Chem) v3.5.1 (Grell et al., 2005), with some recent improvement by the University of Science and Technology of China (Zhao et al., 2013~~a~~, 2014, 2016; Hu et al., 2016). The details of the WRF-Chem configuration are ~~documented in section 2.1~~provided in Supporting Information (SI).~~, followed by~~ The model experiment design is described in section 2.1~~2~~. The observational datasets used for validating the simulated precipitation performance, along with hourly in situ $PM_{2.5}$ observations are described in section 2.2~~3~~.

~~2.1 WRF-Chem~~

~~WRF-Chem is a fully online model coupled with gas-phase chemistry mechanisms and aerosol physiochemical modules. In this model, chemical and meteorological components use the same grid coordinates, time steps, transport schemes, and subgrid physics. The meteorological component (WRF) of this coupled model uses an Eulerian dynamical core with a nonhydrostatic solver (Skamarock et al., 2008). Gas-phase chemical reactions are estimated using the carbon bond chemical mechanism (Zaveri and Peters, 1999). Aerosol physics and chemistry are treated using the Model for Simulating Aerosol Interactions and Chemistry (MOSAIC) scheme (Zaveri et al., 2008) with aqueous chemistry. The aerosol size distribution is represented by four discrete size bins within the MOSAIC scheme: 0.039–0.156 μm, 0.156–0.625 μm, 0.625–2.5 μm, and 2.5–10 μm (Fast et al., 2006). The approach to aerosol dry deposition is based on Binkowski and Shankar (1995). In-cloud (rainout) and below-cloud (washout) removal of aerosols by resolved clouds and precipitation are simulated following Easter et al. (2004) and Chapman et al. (2009), respectively. The transport and wet removal of aerosols by convective clouds are also considered using the Kain–Fritsch (KF) scheme (Kain and Fritsch, 1990) following Zhao et al. (2009, 2013b). The major physical schemes of meteorological components comprise the KF cumulus scheme; the Yonsei University (YSU) planetary boundary layer (PBL) scheme (Hong et al., 2006); the National Center for Environmental Prediction, Oregon State University, Air Force, and Hydrologic Research Lab's (NOAH) land surface model (Chen and Dudhia, 2001); the Morrison two-moment scheme for cloud microphysics (Morrison et al., 2009); and the rapid radiative transfer for global (RRTMG) for both longwave and~~

~~shortwave radiation schemes (Iacono et al., 2008). Aerosol interactions with shortwave and longwave radiation are incorporated into the model by linking aerosol optical properties, including optical depth, single-scattering albedo, and asymmetry factor, to RRTMG shortwave and longwave schemes, respectively (Zhao et al., 2010, 2011). The effects of ACI are estimated by considering the activation of aerosols to form cloud droplets based on the maximum supersaturation in the Morrison microphysical scheme (Chapman et al., 2009; Yang et al., 2011).~~

2.1~~2~~ Experiment design

WRF-Chem simulations a~~we~~re conducted to investigate the effect of ~~aerosols~~aerosols on the extreme rainfall event of December 14–16, 2013~~, at~~. Unless ~~otherwise~~ specified, all time points in this study refer to local standard time (LST), which is equal to UTC+8. Two nested grids (run simultaneously with one-way nesting) cover~~ed~~ most of China (87.47°–131.67° E, 11.42°–41.22° N) and Guangdong P~~p~~rovince (109.59°–117.32° E, 20.07°–25.62° N) with a horizontal resolution of 20 km and 4 km, respectively (Figure S1a). The cumulus scheme i~~wa~~s turned off in the inner domain. Both nested grids use~~d~~ 41 vertical levels extending from the surface to 100 hPa. The meteorological initial and boundary conditions (ICs and BCs) a~~we~~re derived from 6-hourly National Center for Environmental Prediction global final analysis data with a horizontal resolution of 1° × 1°. The 6-hourly chemical ICs and BCs a~~we~~re generated from the Model for Ozone and Related Chemical Tracer version 4 (MOZART-4), which is an offline global chemical transport model suited for tropospheric studies, at a horizontal resolution of 1.9° × 2.5° with 56 vertical levels (Emmons et al., 2010). Anthropogenic emissions a~~we~~re obtained from the Emissions Database for Global Atmospheric Research Hemispheric Transport of Air Pollution v2 inventory (Janssens-Maenhout et al., 2015) for the year 2010 with a resolution of 0.1° × 0.1° (http://edgar.jrc.ec.europa.eu/htap_v2/). Biomass burning emission data a~~we~~re extracted from FINN 1.5 (Wiedinmyer et al., 2010). Dust and sea salt emission schemes a~~we~~re updated following Zhao et al. (2010) and Zhao et al. (2013a), respectively. The results show~~ed~~ marginal differences between simulations with and without dust and sea salt emissions (figure not shown) in our study case; possible reasons for this are discussed in section 4.

Six sets of experiments a~~we~~re performed in total (Table 1~~Table 1Table 1~~). To isolate robust signals from the model's natural variations, five ensemble members with perturbed ICs at 3-h intervals a~~we~~re conducted for each experiment. The simulations start~~ed~~ from 08Z to 20Z on December 13 with 3-h intervals, and all end~~ed~~ at 02Z on December 17. The simulation before December 14 i~~wa~~s for model spin up, and the following analysis focuses on the results of ~~from~~ December 14–16. In the first experiment (CTL), current emissions a~~we~~re used in the simulation with both ARI and ACI effects included (Table 1~~Table 1Table 1~~). Following Fan et al. (2015), we scale~~d~~ the anthropogenic and fire emissions by a factor of 0.1 and perform~~ed~~ the CLEAN simulation. We adjust the factor to 0.1 from 0.3 in Fan et al. (2015) to represent the background aerosol concentration as the emissions in 2010 is much higher than that in 2006 (Chang et al., 2018). It is used to mimic the situation in which the background of aerosol concentration~~s~~ serves as cloud condensation nuclei before the economic development in China. The differences between CTL and CLEAN denote the total effects of aerosols including both ARI and ACI effects ~~on this extreme rainfall case~~. To examine the role and relative importance of ARI and ACI, the ARIoff run i~~wa~~s conducted based on CTL run

Formatted: Font: 10 pt, (Asian) Chinese (PRC)

Formatted: Font: 10 pt, (Asian) Chinese (PRC)

Formatted: Font: 10 pt, (Asian) Chinese (PRC)

Formatted: Font: 10 pt, (Asian) Chinese (PRC)

Formatted: Font: 10 pt, (Asian) Chinese (PRC)

Formatted: Font: 10 pt, (Asian) Chinese (PRC)

by excluding the ARI effect. Thus, the differences between CTL and ARIoff~~(CTL minus ARIoff and ARIoff minus CLEAN)~~ represent ARI effects ~~and ACI effects, respectively~~ (Zhong et al., 2015). The ACI effects are approximated by looking at differences between CTL – CLEAN and CTL – ARIoff. To distinguish and isolate the effects induced by local (i.e., domain 2, Guangdong P~~p~~rovince) emissions and remote (i.e., domain 1, outside Guangdong P~~p~~rovince) emissions, two other experiments a~~we~~re designed. In D1 (Table 1) experiment, the ICs, BCs, and emissions are kept as same with control run for domain 1. Meanwhile, the ICs and emissions are scaled by a factor of 0.1 for domain 2. Similarly, in D2 experiment, the ICs, BCs, and emissions are scaled by a factor of 0.1 for domain 1. The ICs and emissions are kept as same with control run for domain 2. ~~that~~ a~~were identical to the CTL run, except for scaling the emissions and chemical ICs and BCs by a factor of 0.1 in domain~~ 2~~1 (hereafter D1 run, Table 1) and domain~~ 1~~2 (hereafter D2 run).~~ Note that the offline chemical BCs extracted from MOZART a~~we~~re only applicable to domain 1. Along with CTL run, these experiments allow~~ed~~ us to interpret and ascertain aerosol-related changes that would have occurred with either local or remote aerosol emissions by observing differences between CTL – ~~minus~~ CLEAN and either D2 – ~~minus~~ CLEAN or D1 – ~~minus~~ CLEAN. To test the sensitivity of precipitation to aerosol concentration~~s~~, one more experiment for extreme polluted case i~~wa~~s conducted. In parallel to that in CLEAN run, w~~We~~e scale the emissions and chemical ICs and BCs in control run by a factor of 10 (10×)~~ in parallel to that in CLEAN run~~.

2.~~3~~2 Observational datasets

The model-simulated precipitation performance i~~wa~~s evaluated with satellite-based precipitation products and in situ rainfall observations.

Climate Prediction Center morphing technique (CMORPH) data is produced by the National Oceanic and Atmospheric Administration covering the period from December 2002 to present~~ awere used~~. In this technique, infrared geostationary satellites observe the motion vectors of precipitation patterns to generate half-hourly precipitation estimates by using passive microwave (PMW) sensors. Time-weighted linear interpolation is exploited to morph the shape and intensity of precipitation features when and where PMW data are unavailable. This provides data for global (60° S–60° N) precipitation analysis with a horizontal resolution of 0.07277° (approximately 8 km at the equator) and temporal resolution of 30 minutes. More details of CMORPH products are documented by Joyce et al. (2004).

The in situ hourly precipitation dataset i~~wa~~s developed at the National Meteorological Information Center of the China Meteorological Administration (source: http://data.cma.cn). A total of 115 stations a~~we~~re within domain 2. Their locations are represented as colored circles in Figure 2~~Figure 2Figure 2~~a.

The ERA-Interim version 2 is used to evaluate the model performance in simulating large-scale circulation. This data is a global atmospheric reanalysis ~~containing~~making data publicly accessible since 1979, provided by the European Centre for Medium-Range Weather Forecasts (ECMWF) (Dee et al., 2011). The data is available at a horizontal resolution of approximately 0.25˚ which is comparable to the resolution of domain 1.

Formatted: Font: 10 pt

Formatted: Font: 10 pt, (Asian) Chinese (PRC)

Formatted: Font: 10 pt, (Asian) Chinese (PRC)

Formatted: Font: 10 pt, (Asian) Chinese (PRC), (Other) English (United States)

Formatted: Font: 10 pt, (Asian) Chinese (PRC), (Other) English (United States)

Formatted: Font: 10 pt, (Asian) Chinese (PRC), (Other) English (United States)

Formatted: Font: 10 pt, (Asian) Chinese (PRC), (Other) English (United States)

Formatted: Font: 10 pt, (Asian) Chinese (PRC), (Other) English (United States)

Formatted: Font: 10 pt, (Asian) Chinese (PRC), (Other) English (United States)

Formatted: Font: 10 pt, (Asian) Chinese (PRC), (Other) English (United States)

The hourly $PM_{2.5}$ concentration in situ dataset i~~wa~~s obtained from the website of the Ministry of Environmental Protection (source: http://106.37.208.233:20035) (Zhang and Cao, 2015). In total, 58 stations a~~we~~re within domain 2. Their locations are denoted as colored circles in Figure 1~~Figure 1Figure 1~~c.

3 Results

During December 14–16, 2013, there i~~wa~~s a rare continuous rainstorm over most~~all~~ of Guangdong Province. The 3-day accumulated rainfall at most stations exceeds~~ed~~ 100 mm (Figure 2~~Figure 2Figure 2~~a), which may benefit winter and spring water usage, promote air cleaning, and reduce forest fire risk. ~~This iwas the most extreme precipitation event in the province in terms of duration, affected area, and cumulative rainfall in December since the meteorological record of Guangdong province set in 1951 (Deng et al., 2015).~~ The mid-tropospheric flow pattern, with a ridge to the northeast of the Tibet Plateau and a trough over the west of the Indo-China Peninsula, facilitates~~is favorable for~~ cold and dry air to move~~ing~~ southward, whereas moist and warm air to ~~from the Bay of Bengal and the South China Sea~~ move northward (~~see~~ Figure S2~~a of Deng et al., 2015~~). At the surface, prevailing northeasterlies blow over East China (Figure 1b), indicating a strong monsoonal flow (Chang et al., 2006). The passage of a cold front results in sharp temperature gradient with northwest-southeast tilt (Figure S3). Deep stratiform and convective clouds form at the cold and warm side, respectively, as shown ~~The persistent meeting of these two flows results in intense convergence (Figure S1b) at lower levels over domain 2 (Figure 1b),and resulting in strong deep convection indicated by bright white color~~ in the natural-color satellite image captured by NASA's Terra (Figure 1a)~~thus produces torrential rainfall~~. The simulated cloud top temperature ~~average~~ over Guangdong Province ~~the land in domain 2~~ is lower than –15 °C ~~almost everywhere~~ with the minimum reaching to about –35 °C (Figure S1b). Before the study case occurs~~red~~, Guangdong province i~~wa~~s affected by severe pollution on December 13. The hourly-averaged $PM_{2.5}$ concentration~~s~~ exceeds~~ed~~ 100 μg m^{-3} over~~in~~ the delta region~~, peaking at 173.58 μg m~~$^{\cancel{-3}}$ (Figure 1~~Figure 1Figure 1~~c). ~~The Canton Tower, the second tallest tower in the world and the landmark of Guangzhou City (denoted by a star in Figure 1c), was almost invisible under this extreme haze (as seen in the photo in Figure 1b). The area Tto t~~The north of Guangdong ~~province, the area,~~ including Zhejiang, Jiangsu, and Anhui P~~p~~rovinces, i~~wa~~s blanketed in grey haze ~~in the natural-color satellite image captured by NASA's Terra~~ (Figure 1~~Figure 1Figure 1~~a). ~~Note the grey haze area iwas smog, whereas whiter areas with more defined features awere clouds.~~ The column-integrated $PM_{2.5}$ concentration~~s~~ ~~in these areas~~ reaches~~ed~~ up to 2000 μg m^{-2} during December 14–16, 2013, in CTL ~~the simulated control~~ run (Figure 1~~Figure 1Figure 1~~b). ~~Strong prevailing northeasterly (Figure 1b) winds south of 30° N along the east coast of China indicatesed a strong monsoonal flow East Asian winter monsoon (Chang et al., 2006).~~ The pattern configurations~~s~~ of circulation and pollutant ~~patterns~~ a~~we~~re favorable for aerosol transport to the south of China. In the analysis~~Built on the observational and modeling works discussed above~~, we firstly examine~~d~~ ~~in section 3.2~~ the total effects and relative importance of ARI and ACI on this extreme rainfall event in section 3.2. The contribution of ~~We also distinguish and isolate the response to~~ local and remote aerosol emissions to their total impact is disentangled in section 3.3. In section 3.4, the sensitivity of precipitation to aerosol emissions is explored.

Formatted: Font: 10 pt, (Asian) Chinese (PRC)

Formatted: Font: 10 pt, (Asian) Chinese (PRC)

Formatted: Font: 10 pt, (Asian) Chinese (PRC)

Formatted: Font: 10 pt, (Asian) Chinese (PRC)

Formatted: Font: 10 pt

Formatted: Font: 10 pt, (Asian) Chinese (PRC)

Formatted: Font: 10 pt, (Asian) Chinese (PRC)

Formatted: Font: 10 pt, (Asian) Chinese (PRC)

Formatted: Font: 10 pt, (Asian) Chinese (PRC)

Formatted: Font: 10 pt, (Asian) Chinese (PRC)

Formatted: Font: 10 pt, (Asian) Chinese (PRC)

Formatted: Font: 10 pt, (Asian) Chinese (PRC)

Formatted: Font: 10 pt, (Asian) Chinese (PRC)

3.1 Model~~Rainfall~~ evaluation compared with observational datasets

~~The 500-hPa geopotential height and wind pattern simulated in the control run are evaluated with ERA-interim data (Figure S2).~~ The model well replicates the trough over the west of the Indo-China Peninsula and sub-tropical high over the South China Sea and the northwest Pacific (Figure S2). The pattern correlation~~s~~ of 500~~-~~h~~-~~Pa geopotential height reaches 0.99 at the 99% significance level. Modeled ~~simulated~~ $PM_{2.5}$ concentration is evaluated by comparing with the 58 in-situ station data in~~over~~ Guangdong Province. The spatial distribution of $PM_{2.5}$ concentration is generally reproduced with high ~~concentration~~ over mega cities and low over the surrounding areas (Figure S4~~6~~). The failure to capture the hot spot near the estuary may be related to the coarse grid resolution or uncertainty of emissions. In the time series, both the simulation and observation show a dramatically decreasing trend of $PM_{2.5}$ concentration~~s~~ after~~once~~ the rainfall initiated (Figure S5~~7~~). The model ~~could~~ generally replicates the spatial distribution and time evolution of $PM_{2.5}$ concentration~~s~~ with some underestimation during the first two days. This bias may underestimate the aerosol impact on rainfall.

~~The model-simulated precipitation performance~~ i~~was evaluated through comparison with in situ observation and satellite data, as shown in~~ ~~Figure 2Figure 2.~~ The precipitation from model output and satellite retrievals ~~aw~~is~~ere~~ interpolated to the locations of in situ observation through bilinear interpolation (Figure 2~~Figure 2Figures 2~~a–2c). ~~Approximately 100 mm of precipitation accumulatesd during December 14–16, 2013, covering the entirety of Guangdong Province.~~ The ~~However,~~ CMORPH satellite data, which is~~are~~ often used to evaluate model rainfall performance, underestimates~~d~~ the ~~-~~amount~~precipitation~~, particularly near the coast. Previous studies have reported that this ~~CMORPH~~ products substantially underestimates~~ed~~ heavy rainfall (Jiang et al., 2018; Qin et al., 2014) and cold season rainfall (Xie et al., 2017). By contrast, the control simulation yields a higher pattern correlation of 0.50–0.55 and a lower bias of 5%–20% (Figure 2~~Figure 2f~~). The time series of the average rain rate over Guangdong Province reveals~~ed~~ a remarkable ~~extreme rainfall event with a~~ lasting rain rate of 2.5 mm h^{-1} on the second and third days when~~;~~ satellite~~CMORPH~~ data distinctly underestimates~~d~~ ~~rainfall for these days~~ (Figure 2~~Figure 2Figure 2~~d). The model reproduces~~d~~ a comparable~~similar~~ magnitude to the observations with an earlier peak ~~in the early morning~~ near 08Z~~8:00 a.m.~~ on December 15. The initial time and physics schemes including microphysics, land surface, and PBL are tuned but only ~~tuned to check whether the peak time will be different. However,~~ the rainfall amplitude changes ~~are mostly happened in amplitude~~ rather than the peak time.~~,~~ Thus, ~~thus we conclude that~~ the bias may be induced by the meteorology boundary conditions from global model. ~~The Taylor diagram for 3-day accumulated rainfall in Figure 2Figure 2f suggests that the model simulation yieldsed a higher pattern correlation of 0.50–0.55 and a lower bias of 5%–20% than the CMORPH retrieval doesid (0.4 and >20% for pattern correlation and bias, respectively). Signs of bias are represented by inverted (negative) or upright (positive) triangles, indicating that the model overestimated the rainfall amount while the satellite products underestimatesd it.~~ ~~The TRMM data is also used to evaluate this extreme case in Figure S5d.~~ Precipitation in TRMM data is also underestimated along the coast as well as that in CMORPH data (Figure S6d). Overall, the model replicates~~d~~ the spatial distribution, time evolution, and the intensity of this extreme rainfall event. Note that all the analyses in the following sections are based on simulation results from domain 2.

Formatted: Font: 10 pt, (Asian) Chinese (PRC)
Formatted: Subscript
Formatted: Subscript
Formatted: Font: 10 pt, (Asian) Chinese (PRC)
Formatted: Font: 10 pt, (Asian) Chinese (PRC), Subscript
Formatted: Font: 10 pt, (Asian) Chinese (PRC)
Formatted: Font: 10 pt, (Asian) Chinese (PRC)
Formatted: Font: 10 pt, (Asian) Chinese (PRC)
Formatted: Font: 10 pt, (Asian) Chinese (PRC)
Formatted: Font: 10 pt, (Asian) Chinese (PRC)
Formatted: Font: 10 pt, (Asian) Chinese (PRC)
Formatted: Font: 10 pt, (Asian) Chinese (PRC)
Formatted: Font: 10 pt, (Asian) Chinese (PRC)
Formatted: Font: 10 pt, (Asian) Chinese (PRC)
Formatted: Font: 10 pt, (Asian) Chinese (PRC)
Formatted: Font: 10 pt, (Asian) Chinese (PRC)
Formatted: Font color: Text 1
Formatted: Font color: Text 1
Formatted: Font color: Text 1
Formatted: Font color: Text 1

3.2 Effects of ARI versus those of ACI

In this section, ~~Aerosols can change cloud properties and precipitation through two processes, radiative and microphysical (Graf, 2004; Kaufman and Koren, 2006), which contribute to the largest uncertainty in human-induced climate changes. We attempted to isolate~~ the total effects of ARI and ACI as well as ~~and thus investigate~~ their ~~roles and~~ relative importance in this extreme rainfall event are investigated. Figure 3~~Figure 3Figure 3~~ shows the spatial distribution of the daily accumulated rainfall~~precipitation~~ changes ~~differences~~ for December 14 and 15 between ~~the~~ different scenarios. Because the results on ~~the third day,~~ December 16~~,~~ illustrate a similar mechanism to those on December 15, our analysis focuses~~ed~~ on December 15. The rainfall differences ~~differences between scenarios~~ on December 16 are put in ~~the supplementary materials for reference (~~Figure S7~~32)~~. Distinct effects of aerosols appear~~ed~~ on~~during~~ the second day when the rainfall peaks~~ed~~ (Figure 3~~Figure 3Figure 3~~d), although aerosol concentration peaks occur ~~s lead to more cloud droplet number concentration associated with smaller radius~~ on the first day (Figure 4~~Figure 5~~a)~~but the aerosol concentration differences occurred on the first day, as shown in Figure 4b.;~~ T~~t~~his suggests that the ~~a time lag effects of~~ aerosol impact ~~s on precipitation~~ is~~are~~ modulated by other factors (e.g. meteorological conditions). On December 15, the domain-averaged precipitation increases~~d~~ by 1.4 mm. Interestingly, a dipole pattern is manifested by a~~A~~ reduction ~~of~~ up to 19.4 mm over ~~appearsed in~~ northern Guangdong P~~p~~rovince and~~, whereas~~ an increase ~~of~~ up to 33.7 mm over ~~occursred in~~ southern Guangdong P~~p~~rovince~~,~~ (particularly ~~in the region~~ near the Pearl River estuary)~~and land along the coast~~. This means ~~the~~ different responses of precipitation in the warm and cold sectors (Figure S3), ~~which~~ indicat~~ing~~es that the impact of aerosols on deep convective and stratiform clouds differs in this extreme rainfall case. To address this issue, two regions, R1 (22°–24° N and 112°–115° E) and R2 (24°–25° N and 110°–112° E), are selected for the following analysis which are denoted by red and green boxes, respectively (Figure 3). The average precipitation ~~The region 22°–24° N and 112°–115° E, denoted by red boxes in Figure 3Figure 3, is our focus for the following analysis, because it exhibits prominent rainfall~~ increases by 16.7%~~differences (+7.8 mm)~~ (+7.8 mm) over R1 while ~~on average and covers some of the most advanced city clusters in China including Hong Kong, Shenzhen, and Guangzhou.~~ decreases by 10.2 % (–4.4 mm) in R2. The contribution from ~~corresponding precipitation differences induced by~~ ARI and ACI over R1 (R2) a~~iswe~~re ~~–1.3 mm~~ (–1.3 mm (–0.7 mm)~~2.8%)~~ and ~~+9.3 mm (~~+9.3 mm (–3.7 mm)~~19.9%)~~, respectively. Positive (negative) indicates an increase~~, and negative indicates~~ (a decrease). It is evident that ~~from the pattern of precipitation changes that~~ the net aerosol effects a~~we~~re dominated by ACI ~~during this event~~for both convective and stratiform cloud regimes. The subsequent analysis of this study is focused on precipitation enhancement in the warm sector ~~where~~which covers most advanced city clusters including Hong Kong, Shenzhen, and Guangzhou. The responses of stratiform clouds to increased aerosols in cold sector are discussed in section 4. ~~The time series of average precipitation over the red box shows that the model simulations reproduced a rainfall amount comparable to the observation (Figure S43).~~ Compared with the CTL and ARIoff runs, the CLEAN run yields~~ed~~ an analogous time evolution, with less rainfall during the peak time from 06Z~~ 8:00 a.m.~~ on December 15 to 10Z~~:00 a.m.~~ on December 16 (Figure S8). The next question that arose i~~wa~~s how ACI can increase the rainfall amount in the warm side~~over the region~~.

Formatted: Font: 10 pt, (Asian) Chinese (PRC)

Formatted: Font: 10 pt, (Asian) Chinese (PRC)

Formatted: Font: 10 pt, (Asian) Chinese (PRC)

Formatted: Font: 10 pt, (Asian) Chinese (PRC)

Formatted: Font: 10 pt

Formatted: Font: 10 pt

Formatted: Font: 10 pt, (Asian) Chinese (PRC)

Figure 4~~Figure 4Figure 4~~a shows the time–~~-~~height cross section of cloud fraction (shading) and $PM_{2.5}$ concentration (contour) in the CTL run. The cloud fraction is calculated as sum of cloud water, cloud ice, and snow following Hong et al. (1998). Most cloud fraction concentrates below 8 km in the first day, associating with small amount of rainfall. Deep convection, with a cloud base at approximately 500 m and cloud top extending to~~ approximately~~ 16~~4~~ km, appears~~ed~~ during December 15–16 when peak rainfall occurs~~red~~. The $PM_{2.5}$ concentration~~s~~ in Figure 4~~Figure 4Figure 4~~a portrays a sharp contrast before and after the rainfall peak. After the rainfall peaks~~ed~~ at near 07Z in Figure S8~~3~~, aerosols a~~we~~re washed out dramatically~~ by precipitation~~. However, before the peak, $PM_{2.5}$ concentration~~s~~ decreases~~d~~ gradually from 40 μg m^{-3} near the surface to 5 μg m^{-3} near 7 km above the ground. With aerosols acting as cloud condensation nuclei, more cloud droplets are formed with smaller radius~~, particularly before the rainfall peak when aerosol concentration is high~~ (Figure 5a). Smaller cloud droplets evaporate associated with a reduction of cloud water (Figure 6a), resulting in cooling effect and weaker updraft (Figure 5~~Figure 5Figures 5~~g~~ and 5i~~). Thus, the cloud fraction decreases before the peak, particularly~~especially~~ below 2 km. By contrast,~~. These aerosols acted as cloud condensation nuclei to promote cloud droplet formation and invigorate convection (Figures 4b and 4c).~~ t~~T~~here ~~was~~ a prominent cloud fraction band appears ~~increase~~ near 4 km throughout the peak period~~ (~~Figure 4b)~~with aerosols~~. The increase of cloud fraction extends~~ed~~ to the upper troposphere, near 14 km, corresponding to the increase of ice cloud shown in Figure 5~~Figure 5Figures 5~~d~~ and 5f~~. As a result, the deep convection is enhanced associated with more rainfall during peak time. ~~By contrast, cloud reduction below 2 km from 06Z on December 14 to 12Z on December 15 may be linked to excessive aerosol concentrations and shallow clouds, which led small droplets to evaporate (Gunn and Phillips, 1957; Zhong et al., 2015). The evaporative cooling resulted in weaker updraft, as shown in Figures 5g and 5i.~~ The similarity of cloud fraction changes between Figure 4~~Figure 4Figure 4~~b and Figure 4~~Figure 4Figure 4~~c suggests that ACI dominated the total aerosol effect in this event, which is consistent with the previous discussion.

Figure 5~~Figure 5Figures 5~~a–5c present the aerosol effects on cloud droplet number concentration (CDNC; shading) and cloud effective radius (contour). With aerosols, CDNC increases~~d dramatically~~ by 5.5 times accompanied by reduced cloud effective radius near 2 km from 00Z on December 14 to 00Z on December 15, which reduces the efficiency of collision-coalescence between cloud droplets into raindrops (Rosenfeld, 2000; Twomey, 1977). This is characterized by less rain water formed in Figure 6c, indicating suppression of the warm rain. Figure 6a shows more cloud water formed at 2–6 km due to higher supersaturation. The consumption of moisture and energy limits the formation of low cloud below. When~~During~~ droplets nucleate~~ion~~ due to activating enormous aerosols, there are abundant latent heat release by enhanced condensation below the 0°C isotherm line. This is also reported in Fan et al. (2018) in which the mechanism responsible for ~~convection intensification is~~ latent heat release is from cloud water formation with ultrafine aerosols. This is called “warm-phase invigoration” in their study which is different from “cold-phase invigoration” via suppressing the warm rain. ~~Interestingly, U~~unlike their work, the warm rain is~~ still~~ suppressed before 15Z on December 15 (Figure 6c) even though with strong latent heat release through cloud water formation. This is because the conversion of cloud droplets into rain drops is inversely proportional to cloud droplet numbers with two-moment bulk scheme using autoconversion parameterization (Khairoutdinov and Kogan, 2000). Thus, ~~The~~

Formatted: Font: 10 pt, (Asian) Chinese (PRC)
Formatted: Font: 10 pt, (Asian) Chinese (PRC)
Formatted: Font: 10 pt, (Asian) Chinese (PRC)
Formatted: Font: 10 pt, (Asian) Chinese (PRC)
Formatted: Font: 10 pt, (Asian) Chinese (PRC), (Other) English (United States)
Formatted: Font: 10 pt, (Asian) Chinese (PRC)
Formatted: Font: 10 pt, (Asian) Chinese (PRC)
Formatted: Font: 10 pt
Formatted: Font: 10 pt, (Asian) Chinese (PRC)
Formatted: Font: 10 pt, (Asian) Chinese (PRC)
Formatted: Font: 10 pt, (Asian) Chinese (PRC)
Formatted: Font: 10 pt, (Asian) Chinese (PRC)
Formatted: Font: 10 pt, (Asian) Chinese (PRC)
Formatted: Font: 10 pt, (Asian) Chinese (PRC)
Formatted: Font: 10 pt, (Asian) Chinese (PRC)
Formatted: Font: 10 pt, (Asian) Chinese (PRC)
Formatted: Font: 10 pt, (Asian) Chinese (PRC), (Other) English (United States)
Formatted: Font: 10 pt, (Asian) Chinese (PRC), (Other) English (United States)
Formatted: Font: 10 pt, (Asian) Chinese (PRC)
Formatted: Font: 10 pt, (Asian) Chinese (PRC)
Formatted: Font: 10 pt, Font color: Auto, (Asian) Chinese (PRC)
Formatted: Font: 10 pt, (Asian) Chinese (PRC), (Other) English (United States)

~~rain water is not increased by accretion of added cloud droplets, which implement that~~ the precipitation increase is because of enhancement of cold rain. Both cloud ice number concentration and its effective radius increase~~are~~ significantly ~~increased~~ between 6Z and 15Z on 15 December. Moreover, the mass and number of ice particles~~crystals~~ including cloud ice, snow, and graupel increase drastically during this period~~. Note the magnitude of snow and graupel mass is ten times of that of rain water~~. A distinct latent heat release center appears above 0°C isotherm line, which is even stronger than the condensational heat below. These two peaks in aerosols induced diabatic heating are also discussed in Wang et al. (2014) for oceanic deep convection. However, the peaks ~~at 3 km and 7 km~~ are much higher at 3 km and 7 km~~. This may be~~ because the convection occurs over the land. The latent heat from these two peaks thus will intensify convective strength. These findings suggest that the cold-cloud process plays a dominant role in the precipitation increase before 15Z on 15 December. ~~To further analyze the source of this latent heat release, following Fan et al. (2018), T~~the latent heat released for~~from~~ each process, which is calculated as the product of mass conversion between different phases and its associate latent heat release rate in the model, ~~condensation, deposition, and freezing during cold and warm cloud processes~~ is~~are~~ further analyzed for both cold and warm clouds ~~diagnosed~~ (Figure S9~~Figure 7~~). ~~The rimming processes are included into the freezing. Cold-phase invigoration by aerosols has been shown in both observational (Andreas et al., 2004) and modeling (Khain et al., 2005; Fan et al., 2007) studies. Particularly, much attention is paid to mixed and cold process in which supercooled droplets are likely to freeze and release latent heat, further enhancing convection (Koren et al., 2008; Rosenfeld et al., 2008; Tao et al., 2007). Interestingly, the latent heat release due to freezing with aerosols is negligible compared with that due to condensation and deposition.~~ The salient ~~distinct~~ latent heat changes mentioned above in Figure 5g is caused ~~induced~~ by deposition in cold cloud (Figure S9~~Figure 7~~e). ~~-~~Figure S10~~8~~ shows the time-height distribution of mass and number concentration~~s~~ for different hydrometers in control run. It should be n~~N~~oted that the magnitude of snow and graupel mass is ten times of that of rain water. There are affluent snow and graupel before 15Z on 15 December located where the distinct changes in depositional heat appears.~~- Smaller cloud effective radius associated with more droplets is produced due to aerosols activation.~~ With aerosols~~s~~, the snow and graupel grow~~s~~ at the expenses of ice crystals and rain water via aggregation and riming, respectively (Figure 6c–e). The former refers to the collision and coalescence of ice crystals to form snow while the latter represents the accretion of cloud drops and rain drops by snow and graupel to form larger graupels. These are the main processes of converting liquid mass to solid phase, contributing to additional precipitating particles. However, the latent heat due to riming is relatively small (Figure S9f) because the latent heat release per unit for freezing (334 kJ kg^{-1}) is only 1/8 of that for deposition (2256 kJ kg^{-1}). The latent heat release due to deposition in cold cloud is stronger than that due to condensation in warm cloud even though the latter is also important (Figure S9a and S9e). In deep convection, the strong updraft usually makes the atmospheric condition saturated for water which is supersaturated with respect to ice. With the presence of snow and graupel (Figure S10), the formation of ice particles is enhanced accompanied by additional latent heat release due to deposition (Figure 6 and Figure S9). ~~The subsequent condensational growth lowers the water supersaturation, which is also reported in Fan et al. (2018). As this occurs, the environment becomes unsaturated to water, resulting in the evaporation of liquid water. This is known as the Bergeron-Findeisen-Wegener theory. With the presence of ice crystals, water vapor deposition is prior to happen on ice surface when~~

Formatted: Font: 10 pt, Font color: Auto, (Asian) Chinese (PRC)

Formatted: Font: 10 pt, Font color: Auto, (Asian) Chinese (PRC)

Formatted: Font: 10 pt, Font color: Auto, (Asian) Chinese (PRC)

Formatted: Font: 10 pt, Font color: Auto, (Asian) Chinese (PRC)

Formatted: Font: 10 pt, Font color: Auto, (Asian) Chinese (PRC)

Formatted: Font: 10 pt, Font color: Auto, (Asian) Chinese (PRC)

Formatted: Font: 10 pt, Font color: Auto, (Asian) Chinese (PRC)

Formatted: Font: 10 pt, (Asian) Chinese (PRC), (Other) English (United States)

Formatted: Font: 10 pt, Font color: Auto, (Asian) Chinese (PRC)

Formatted: Font: 10 pt, (Asian) Chinese (PRC)

Formatted: Font: 10 pt, (Asian) Chinese (PRC), (Other) English (United States)

Formatted: Font: 10 pt, Font color: Auto, (Asian) Chinese (PRC)

Formatted ...

Formatted ...

Formatted ...

Field Code Changed

Formatted: Font: 10 pt

Formatted ...

Formatted ...

Formatted ...

Formatted ...

Formatted ...

Formatted ...

Formatted ...

Formatted ...

Formatted ...

Formatted ...

Formatted ...

Formatted: Font: 10 pt

Formatted ...

Formatted ...

Formatted ...

~~the saturation with respect to water is supersaturation with respect to ice. Correspondingly, the ice crystals (i.e. cloud ice, snow, and graupel) increase at the expense of rain water (Figure 6c–e). The latent heat release due to deposition in cold cloud is stronger than that due to condensation in warm cloud though the latter is also very important.~~ After 15Z on December 15, most of the ~~ice crystals~~ snow and graupel sedimentate ~~fall as precipitation~~. Compared with depositional heating, the condensational heating plays a dominant role in intensifying convective strength. The rain water increases through accretion of added cloud droplets, leading to precipitation increases. These findings highlight two different processes and mechanisms in the precipitation increase before and after 15Z on December 15. The dominant source for latent heat release is depositional heating in the former case (cold rain enhancement) while condensational heating in the latter (warm rain enhancement). Due to latent heat release with aerosols, the vertical motion is boosted (Figure 5g) which further enhances the supersaturation and ~~associated with~~ latent heat release. Via microphysics–dynamics feedback, the convection is intensified, and precipitation increase~~d~~s. This feedback has been widely discussed in ACI effects on deep convection (Fan et al., 2018; Koren et al., 2015; Tao et al., 2012).~~, which reduced the efficiency of collision-coalescence between cloud droplets into raindrops (Rosenfeld, 2000; Twomey, 1977). Smaller cloud droplets are more likely to ascend to higher altitudes, where ice precipitation particles can form. Both the cloud ice number concentration (CINC) and ice cloud effective radius increased above the freezing level (approximately 4 km as calculated from CTL simulation, see dashed lines in Figure 4) from 18Z on December 14 (Figures 5d and 5f). The interim processes released substantial latent heat up to 24 K d^{-1} aloft and strengthened the updrafts (Figures 5g and 5i). These changes, in turn, invigorated greater convection (Storer and van den Heever, 2013; Zhong et al., 2015) and resulted in more precipitation in the estuary. Both observational and numerical studies have found this cloud invigoration effect (Altaratz et al., 2014). The effect refers to the processes that increases in aerosols reduce cloud droplet size and suppress coalescence and warm rain, leading to more freezing of cloud droplets associated with latent heat release and enhancing cold rain (Rosenfeld et al., 2008). The coupling between cloud microphysics and dynamics is at the core of this process (Koren et al., 2015). This feedback loop is driven by latent heat release and regulated by the size distribution of cloud droplets, which is related to the first indirect effect of aerosols (Tao et al., 2012).~~

To further delineate the mechanism of this microphysics–dynamics feedback, the moisture budget tool i~~wa~~s implemented based on the hourly model output. The atmospheric moisture balance is expressed as follows:

$$\frac{\partial Q}{\partial t} = E - P + MFC \quad (1)$$

where Q is the column-integrated water vapor in the atmosphere, t is time, E is evaporation, P is precipitation, and MFC is the vertically integrated moisture flux convergence.

Evaporation is small in areas of intense precipitation and saturation (Banacos and Schultz, 2005). The column-integrated water vapor changes are small (figure not shown), thus precipitation is balanced by MFC ~~the moisture flux convergence~~ as follows:

$$P \approx MFC \quad (2)$$

MFC can be further divided into two terms as

Formatted: Font: 10 pt, Font color: Auto, (Asian) Chinese (PRC)

Formatted: Font: 10 pt, (Asian) Chinese (PRC), (Other) English (United States)

Formatted: Font: 10 pt, Font color: Auto, (Asian) Chinese (PRC)

Formatted: Font: 10 pt, Font color: Auto, (Asian) Chinese (PRC)

Formatted: Font: 10 pt, (Asian) Chinese (PRC)

Formatted: Font color: Text 1

Formatted: Font color: Text 1

Formatted: Font color: Text 1

Formatted: Font color: Text 1

Formatted: Font color: Text 1

Formatted: Font color: Text 1

Formatted: Font color: Text 1

$$-\frac{1}{g}\int_0^{P_s}\nabla\cdot\left(q\overrightarrow{V_h}\right)dp = -\frac{1}{g}\int_0^{P_s} q\nabla\cdot\overrightarrow{V_h}\,dp - \frac{1}{g}\int_0^{P_s}\overrightarrow{V_h}\cdot\nabla q\,dp \quad (3)$$

where the first term on the right side is the horizontal moisture convergence (hereafter CON); the second term is the horizontal advection of water vapor (hereafter ADV). Thus, the precipitation is balanced by the sum of CON and ADV as

$$P \approx MFC = CON + ADV \quad (4)$$

The spatial distributions of column-integrated MFC (shading) and moisture flux (vector) between CTL and CLEAN on December 15 are displayed in Figure 7~~Figure 7Figure 8Figure 8Figure 6~~a. The MFC pattern i~~wa~~s in good agreement with precipitation differences in Figure 3~~Figure 3Figure 3Figure 3~~d, suggesting the validity of the derivation of Equation (2). The ~~average~~ MFC change averaged over R1 ~~the analysis region~~ i~~wa~~s +8.1 mm, which is comparable to +7.8 mm in precipitation difference. ~~The vertically integrated moisture flux changes in Figure 8a followed the wind pattern, as shown in Figure 20, SFigure 15Figure 13d.~~ The moisture flux is enhanced over R1 ~~the analysis region~~ driven by strong convergence~~, which is consistent with microphysics-dynamics feedback discussed above~~~~The moisture was transported by northerly wind over the northeast of Guangdong province and southerly wind over the sea~~. These flows converged in the estuary and near the coast with a magnitude of approximate~~ly~~ 25 kg m^{-1} s^{-1}. The overall pattern of CON is broadly consistent with that of MFC, which indicates that the MFC changes are mainly driven by CON changes (Figure S11~~-9Figure 9~~a). The ADV changes contribute about 35% of MFC changes over the analysis region but are much more scattered than CON changes (Figure S11~~9Figure 9~~c). ~~The pattern of differences between CTL and CLEAN resembles that between ARIoff and CLEAN (Figure 9Figure 9Figure 6), which suggest the dominant effect of ACI. The magnitude of changes over the analysis region~~ i~~was smaller in the former case, indicating the compensation effect between ARI and ACI in this case, as noted in section 3.1.~~

These findings reveal the prominent effects of aerosols on rainfall amount over the estuary and near the coast in this extreme rainfall event. The pattern of precipitation and associated cloud-related variables in ~~CTL minus CLEAN (~~total effects~~)~~ bears~~ore~~ a resemblance to that in ~~ARIoff minus CLEAN (~~ACI effects~~)~~, which allows~~ed~~ us to ascertain that ACI dominates~~d the total effects~~. By applying the moisture budget tool, we confirm~~ed~~ the microphysical-~~–~~dynamic feedback of ACI effects on invigorating convection. ~~Cloud invigoration is the consequence of the following chain of processes. (1) Larger concentrations of cloud droplets with smaller radii are induced by increased aerosols. (2) Collision–coalescence processes slow, and water clouds ascend to freeze into ice clouds. (3) Additional latent heat release enhances horizontal convergence and strengthens upward motion. (4) More vigorous latent heat is released aloft in response to stronger convection. These feedback processes enhance cold rain and result in greater precipitation.~~

3.3 Local versus remote aerosol emission effects

~~A crucial question is the extent to which increased anthropogenic aerosols from either local (i.e., domain 2, which denotes Guangdong~~ P~~p~~~~rovince) or remote (i.e., domain 1, which denotes outside Guangdong~~ P~~p~~~~rovince) sources result in precipitation changes.~~ ~~Previous studies have reported different roles of local and remote aerosol sources in affecting tropical precipitation~~

Formatted: Font: Not Italic

Formatted: Font: 10 pt, (Asian) Chinese (PRC)

Formatted: Font: 10 pt, (Asian) Chinese (PRC)

Formatted: Font: 10 pt, (Asian) Chinese (PRC)

Formatted: Font: 10 pt, (Asian) Chinese (PRC)

Formatted: Font: 10 pt, (Asian) Chinese (PRC)

Formatted: Font: 10 pt, (Asian) Chinese (PRC)

Formatted: Font: 10 pt, (Asian) Chinese (PRC)

Formatted: Font: 10 pt, (Asian) Chinese (PRC)

Formatted: Font: 10 pt, (Asian) Chinese (PRC), (Other) English (United States)

Formatted: Font: 10 pt, (Asian) Chinese (PRC)

Formatted: Font: 10 pt, (Asian) Chinese (PRC)

Formatted: Font: 10 pt, (Asian) Chinese (PRC), (Other) English (United States)

Formatted: Font: 10 pt, (Asian) Chinese (PRC), (Other) English (United States)

Formatted: Font: 10 pt, (Asian) Chinese (PRC), (Other) English (United States)

~~(Chou et al., 2005) and monsoons associated with precipitation (Bollasina et al., 2014; Cowan and Cai, 2011) from a climate perspective. However, the differing effects of local and remote aerosols on weather, such as extreme rainfall, are rarely explored.~~ ~~In this section, w~~We disentangle ~~examine~~ the roles and relative importance of local (i.e., domain 2, which denotes Guangdong Province) and remote (i.e., domain 1, which denotes outside Guangdong Province) aerosols~~s~~ in the precipitation increase in the estuary during this extreme rainfall event.

Figure 8~~Figure 8Figure 9~~a and 8~~9~~b show t~~T~~he differences in time-~~–~~height cross section of cloud fraction (shading) and $PM_{2.5}$ concentration (contour) induced by the effects of local and remote emissions ~~are shown in Figure 9Figure 10a Figures 7a and 9107b~~, respectively. With local emissions, the aerosol concentration~~s~~ mainly increases~~d~~ within the PBL below 2 km before 12Z on December 15 (Figure 8~~Figure 10Figure 7~~b). The accumulated aerosols a~~we~~re washed out quickly after the rainfall initiated. By contrast, with remote emissions, ~~a~~ higher aerosol concentration extends~~ed~~ to approximately 8 km after 03Z on December 14 (Figure 8~~Figure 10Figure 7~~a). Two peaks near 0.5 km and 5 km above ground a~~we~~re centered near 10Z and 18Z on December 14, respectively, indicating a strong transportation of aerosols. The earlier peak, near 5 km, i~~wa~~s caused by stronger wind speed in the free atmosphere compared with that within the PBL. Moreover, the aerosol concentration~~s~~ lasts for~~ed~~ longer before decreasing dramatically until the peak rainfall starts~~ed~~ at 07Z on December 15, because aerosols a~~we~~re transported continuously from the north~~remote area~~. The cloud fraction reduction i~~wa~~s coherent with aerosol concentration peaks, indicating that increased aerosols lead small cloud droplets to evaporate. Moreover, more deep cloud formation consuming moisture and energy. The similar ~~Comparing patterns of~~ cloud fraction changes between Figure 8~~Figure 10 Figures 7~~a ~~and 107b~~ and Figure 4~~Figure 4Figure 4~~b indicates~~s~~ the dominant effects of aerosols from remote areas. The CDNC (shading) increases~~d~~ in both D1 and D2 runs compared with the CLEAN run before the rainfall peak (Figure S12~~Figure 11~~a ~~Figures 8a~~ and S12~~18~~b). However, the discernible cloud effective radius (contours) decrease appears~~ed~~ only in the D1 run and i~~wa~~s attributed to a stronger CDNC increase. Correspondingly, the CINC and ice cloud effective radius show~~ed~~ more remarkable increases in the D1 run during the rainfall peak time (Figure S12~~Figure 11Figures 8~~c and S12~~18~~d). The associated latent heat and vertical velocity a~~we~~re much stronger in the D1 run compared with that in the D2 run (Figure S12~~Figure 11Figure 11Figures 8~~e and S12~~18~~f). Interestingly, most of latent heat release with local emissions ~~are~~ occurs~~happened~~ below the 0°C isotherm line. Figure 9~~Figure 9Figure 12~~ shows the changes in mass and number of different hydrometeors with remote aerosol~~s~~ emissions. There are plenty of snow and graupel formations at the expense of rain water when precipitation increases before 15Z on 15 December, indicating an intensified cold rain process. The corresponding latent heat release is dominated by deposition in cold cloud (Figure S13). By contrast, after 15Z on ~~15~~ December 15, rain water increases significantly during precipitation enhancement, representing stronger warm rain process. The associated latent heat release is due to condensational heating in warm cloud concentrated below the 0°C isotherm line. The patterns of changes in hydrometeors and latent heat in D1 assembles that in CTL run, ~~which~~ further confirming the driving factor ~~dominant role~~ of remote aerosol~~s~~ emissions. The distribution of time-height changes in hydrometeors and latent heat between D2 and CLEAN runs are shown in Figure S14~~9~~ and Figure S15~~0~~, respectively. As aerosols from local emissions are concentrated near the surface and are washed out dramatically once the rain initiated, much less cloud water formed than that in D1 run. ~~Thus, the supersaturation is lowered as~~

Formatted: Font: 10 pt
Formatted: Font: 10 pt
Formatted: Font: 10 pt
Formatted: Font: 10 pt, (Asian) Chinese (PRC), (Other) English (United States)
Field Code Changed
Formatted: Font: 10 pt
Formatted: Font: 10 pt
Formatted: Font: 10 pt
Formatted: Font: 10 pt
Formatted: Font: 10 pt
Formatted: Font: 10 pt
Formatted: Font: 10 pt, (Asian) Chinese (PRC)
Formatted: Font: 10 pt, (Asian) Chinese (PRC)
Formatted: Font: 10 pt
Formatted: Font: 10 pt
Formatted: Font: 10 pt
Field Code Changed
Formatted: Font: 10 pt
Formatted: Font: 10 pt
Formatted: Font: 10 pt

~~strongly as that in D1 simulation.~~ More rain water is formed by accretion of cloud droplets which indicates that intensified warm rain is the only reason for the precipitation increase with local aerosol emissions. As a result, the average precipitation increase over R1 ~~the analysis region~~ on December 15 i~~wa~~s 7.3 mm with remote aerosol emissions, much greater than that with local aerosol emissions (3.1 mm, Figure 10~~Figure 10Figure 14~~c a~~ Figures 9c a~~nd 10~~49~~d). These findings suggest that both the effects of local and, to a much greater extent, remote aerosol emissions contribute to precipitation increases~~ over the analysis region~~.

3.4 Tenfold anthropogenic emissions and chemical ICs and BCs

~~An optimal aerosol loading should exist theoretically in which the convection is the most vigorous (Rosenfeld et al., 2008). For aerosol concentrations below the optimum, the convection is invigorated by smaller droplets; thus, stronger updraft releases larger latent release (Dagan et al., 2015b). By contrast, suppression effects dominate above the optimum (Small et al., 2009). The optimum value is determined by environmental conditions (e.g., relative humidity, see Dagan et al., 2015a). In this section, a tenfold aerosol emission simulation (10×) iwas conducted to examine the sensitivity of precipitation and associated cloud properties to aerosol concentrations.~~

The $PM_{2.5}$ concentration~~s~~ (contours) in the tenfold aerosol emission simulation (10×)~~10×~~ increase~~s~~~~d~~ significantly to approximately ten times that in CTL, indicating a linear relationship from emissions to aerosol concentration (Figure S16~~Figure 15Figure 10~~). ~~The associated boundary layer cloud formation (shading) iwas further suppressed below 2 km, which is consistent with the result in Figure 4Figure 4b.~~ The ~~change~~ pattern~~s~~ changes in cloud fraction and aerosol concentration in Figure S16 ~~Figure 15. DFigure 10~~ are similar to that in Figure 4~~Figure 4Figure 4~~b, but with ~~Figure 15 Figure 10 shows~~ a much greater magnitude. The CDNC (shading) increase and cloud effective radius (contour~~s~~) reduction in Figure S17~~Figure 16Figure 11~~a are also more pronounced than those in Figure 5~~Figure 5Figure 5~~a. CDNC noticeably decrease~~sd~~ below 1.5 km but increase~~sd~~ substantially from 1.5 km to 4 km before 04Z~~4:00 a.m.~~ on December 14, associating with smaller radius. Smaller cloud droplet tends to evaporate. In addition, more cloud droplets are produced due to higher supersaturation upward. The consumption of water and energy leads to a further reduction ~~of~~in low cloud (Figure S18~~Figure 17~~a). ~~This finding suggests the ascent of cloud droplets, which is attributed to the smaller effective radius induced by excessive aerosols in 10× compared with that in CTL. The smaller cloud droplets favored the formation of deeper convection manifested by more CINC and larger ice cloud effective radii (Figure 11b).~~ The involved latent heat and vertical velocity during the rainfall peak time (from 08Z on December 15 to 10Z on December 16) in Figure S17~~Figure 16~~c ~~Figure 11c~~ exhibit a stronger increase associated with a higher altitude above the freezing level than th~~ose~~~~at~~ in Figure 5~~Figure 5Figure 5~~c. Besides, a distinct weaker latent heat release associated with negative vertical velocity anomaly appears below freezing level between 10Z and 22Z on 15 December. ~~This indicate a more important role of cold related processes in latent heat release. The ice crystals also increase drastically with bigger radius. Figure 17~~ shows the changes in mass and number concentration~~s~~ of different hydrometeors in 10× simulation. Compared with the CTL run, the snow and graupel are also increased with a ~~stronger~~larger magnitude, particularly before 15Z

Formatted: Font: 10 pt
Formatted: Font: 10 pt
Formatted: Font: 10 pt
Formatted: Font: 10 pt
Formatted: Font: 10 pt, (Asian) Chinese (PRC)
Formatted: Font: 10 pt, (Asian) Chinese (PRC), (Other) English (United States)
Formatted: Font: 10 pt, (Asian) Chinese (PRC)
Formatted: Font: 10 pt, (Asian) Chinese (PRC)
Formatted: Font: 10 pt
Formatted: Font: 10 pt
Formatted: Font: 10 pt, (Asian) Chinese (PRC)
Formatted: Font: 10 pt, (Asian) Chinese (PRC)
Formatted: Font: 10 pt
Formatted: Font: 10 pt
Formatted: Font: 10 pt, (Asian) Chinese (PRC)
Formatted: Font: 10 pt, (Asian) Chinese (PRC)
Formatted: Font: 10 pt, (Asian) Chinese (PRC), (Other) English (United States)

on 15 December, indicating enhanced cold rain. However, rain water shows decrease during all the time instead of an increase after 15Z when precipitation increases in the CTL run. This means the warm rain is suppressed much stronger in 10× simulation. ~~As w~~With ten times of aerosols emissions, the aerosols~~s~~ lower the supersaturation much stronger by activation to form much smaller cloud droplets. The rain water evaporates rather than increases by accretion of additional cloud droplet, associating with strong condensational cooling in warm cloud (Figure S19~~Figure 18~~a). ~~This means that water ascended higher and froze before precipitating, which led to additional latent heat release. A more salient negative anomaly of latent heat and vertical velocity arose below 4 km from 06Z to 22Z on December 15 and below 10 km from 06Z to 18Z on December 16. This should relate to stronger cloud evaporation and ice melting, as discussed by Rosenfeld et al. (2008). The greater cooling below and greater heating above suggest the intensified upward energy transport. This configuration should enhance updraft above and downdraft below induced by additional warming and cooling respectively, which could further invigorate convection and produce more precipitation (Rosenfeld, 2006).~~ Precipitation on December 15 i~~wa~~s suppressed up to 39.6 mm over the upstream region of aerosol sources ~~up to 39.6 mm in the northwest of Guangdong province~~ but substantially enhanced up to 59.7 mm over the downstream region near the coastal region (Figure 11~~Figure 19~~b~~Figure 12b~~). ~~A similar finding iwas reported by Zhong et al. (2015).~~ T~~T~~he delay of early rain in the upstream area resultes~~d~~ in more rainfall with a ~~and~~ stronger ~~rain~~ intensity within ~~the downstream area and~~ a more narrowed region in the downstream area~~compared with the red box in Figure 3Figure 3b~~. The average precipitation over~~in~~ Guangdong P~~p~~rovince on December 15 decreases~~d~~ by 1.0 mm in 10×, whereas it increases~~d~~ by 1.4 mm in CTL. Tenfold aerosol emissions produce~~d~~ a more polluted environment, with $PM_{2.5}$ concentration~~s~~ of approximately 300 μg m^{-3}. Although abundant moisture i~~wa~~s transported from the ~~Bay of Bengal and the~~ South China Sea (Figure 1b~~Figure S1b~~), the aerosol loading may still ~~have~~ surpass~~ed~~ the optimal value for convective~~cloud~~ invigoration and thus suppress~~ed~~ precipitation over Guangdong P~~p~~rovince. Moreover, aside from suppressing the rainfall amount, excessive aerosols also have the potential to redistribute precipitation and increase its range in spatial distribution. ~~With tenfold aerosol emissions, the experiment showed a similar pattern to the CTL run, but the signal was much stronger, implying that the mechanism was consistent with what we discussed before.~~

4 Summary and discussion

~~In this study, we~~This study fin~~oun~~ds that aerosols significantly affect local extreme weather (i.e., torrential rainfall), invigorating deep convection, via ACI effects. This ~~Deep convection~~ invigoration effect by aerosols has been discussed in both observation (Andreae et al., 2004; Koren et al., 2004) and model simulations (Khain et al., 2005; Storer et al., 2013). Most of these studies are focused on mixed and cold processes, ~~. Increasing aerosolss can suppress warm rain because of smaller cloud droplets. These smaller cloud droplets are likely lifted upward to freeze. The latent heat due to freezing will further enhance convection (Rosenfeld et al., 2008).~~ which~~This~~ is referred to as cold-phase invigoration. ~~A recent interesting study conducted by~~ Fan et al. (2018) found that additional nucleation of cloud droplet can release abundant condensational heat below freezing level. More cloud water will form via condensation on the additional cloud droplets. This process will increase both warm rain

Formatted: Font: 10 pt

Formatted: Font: 10 pt

Formatted: Font: 10 pt

Formatted: Font: 10 pt, (Asian) Chinese (PRC)

Formatted: Font: 10 pt

and supercooled cloud water. Furthermore, the ice-related processes are enhanced~~ with latent heat release~~, resulting in ~~further~~ intensifi~~ed~~ying the convection.~~ In their study, the source of latent heat is dominated by condensational heating, accompanied by enhanced warm rain. In contrast to cold-phase invigoration, the concept of warm-phased invigoration is proposed in this work.~~

In response to increased~~With~~ aerosol~~s~~s, the precipitation is enhanced ~~increased~~in the warm side between 03Z on December 15 to 10Z on December 16. ~~by suppressing warm rain and invigorating deep convection induced by the effects of remote emissions through ACI. With aerosols,~~ CDNC increases remarkably, reducing the size of cloud droplets~~, which lowers supersaturation significantly through condensation enhancement~~. Additional cloud water form~~s~~ed with intensified condensational heating, leading to enhanced convection and increased precipitation. However, rain water decrease~~s~~d substantially before 15Z on 15 December, indicating ~~suppressed~~ warm rain is suppressed, which is different to Fan et al. (2018). The source of enhanced latent heat release is dominated by deposition in cold cloud associated with an increase ~~of~~in snow and graupel, representing cold rain enhancement. ~~There are abundant ice crystals including snow and graupel at 4–6 km from 00Z to 15Z on 15 December. As aerosols activation decreases the supersaturation, with presence of ice crystals, water vapor deposition on ice is more likely to happen because the saturation with respect to water is supersaturation with respect to ice. The environment become unsaturated to water when this situation occurs, resulting in evaporation of rain water. This process is known as the Bergeron-Findeisen-Wegener theory. As a result, the mass and number of ice crystals increase drastically at the expense of rain water, suggesting a dominant role of cold rain before 15Z on 15 December.~~ Most of snow and graupel fall as precipitation when the peak rainfall occurs after 15Z. By contrast, the warm rain is enhanced characterized by an increase ~~of~~in rain water associat~~ing~~ed with condensational heating in warm cloud via accretion of cloud droplet, which is consistent with Fan et al. (2018). The enhanced latent heat boosts the vertical motion, leading to higher supersaturation accompanied by stronger latent heat release. ~~Smaller cloud droplets are unfavorable to collision–coalescence, which is an essential process for initiating warm rain (Tao et al., 2012). Thus, more cloud water ascends to a higher altitude below the 0°C isotherm to freeze; this is associated with more latent heat release, and convection is invigorated (Rosenfeld et al., 2008). Moreover, additional latent heat release induced by freezing further enhances the upward motion.~~ This feedback between microphysical and dynamic processes results in more rainfall (Tao et al., 2007) up to 33.7 mm in our simulation. On average, ACI enhance~~s~~d precipitation over R1~~the analysis region~~. Conversely, ARI partially compensate~~s~~d for the precipitation increase by 14%. The analysis of the moisture budget suggests that the precipitation increase i~~was~~s caused ~~manifested~~ by strengthening ~~the column-integrated~~ MFC via increased~~. Further decomposition of MFC suggest the importance of horizontal~~ moisture convergence.~~ Our finding confirms that microphysical–dynamic feedback is at the core of the effects of ACI on convection invigoration.~~

It is critical to explain ~~An interesting question is~~ why the precipitation increases ~~induced by ACI~~ appear ~~over the~~on land near the Pearl River estuary and along the coast. Khain et al. (2008) found that aerosols generally suppress (invigorate) convection ~~cloud formation~~ in relatively dry (moist) conditions~~, whereas they invigorate convection in moist environments~~. Fan et al. (2009) suggested that ~~wind shear may take a dominant role in regulating the effects of aerosols on deep convection. i~~Increased aerosols suppress (invigorate) convection under strong (weak) wind shear. These findings highlight the crucial roles of

Formatted: Font: 10 pt, Font color: Auto, (Asian) Chinese (PRC)

Formatted: Font: 10 pt, Font color: Auto, (Asian) Chinese (PRC)

Formatted: Font: 10 pt, Font color: Auto, (Asian) Chinese (PRC)

Formatted: Font: 10 pt, Font color: Auto, (Asian) Chinese (PRC) humidity and wind shear in modulating the convective~~loud~~ invigoration effects in response to ~~induced by~~ aerosols. ~~Strong wind shear enhances the entrainment of dry air into clouds and transports cloud liquid to unsaturated regions; this leads to greater evaporation and sublimation of cloud particles. These processes are associated with cooling, downdrafts, and convergence, especially at high aerosol concentrations (Khain, 2009; Lee et al., 2008). The convergence thus fosters secondary cloud formation and contributes to an increase in precipitation. However, Fan et al. (2009) stressed that the net latent heat release, as an energy source for convection, is greater under weak wind shear than under strong wind shear. Aerosols enhance convection under weak wind shear until an optimal aerosol concentration is reached at which the net latent heat release equilibrates. This mechanism may only be applicable to isolated storms rather than to cloud systems. Note that the previous studies have used different wind components (zonal component, meridional component, or total wind) at different heights with different thresholds (e.g., upper limits vary from 10 m s^{-1} to 20 m s^{-1}). These different standards may only suitable for specific environmental conditions, because previous studies have been based on limited cases. In our work,~~ T~~t~~he wind shear i~~wa~~s estimated as the difference between the maximum and minimum total wind speeds at 0–10 km. We choose 10 km because the latent heat release, a key factor determining convection intensity and partly depends on wind shear, extends up to approximately 10 km (Figure 5~~Figure 5~~g). Figure S20 shows t~~T~~he spatial distribution of wind shear ~~(first row)~~ and column-integrated water vapor ~~(second row) are presented in Figure 20~~ ~~Figure~~ Figure S15~~13~~. The wind shear increases~~d~~ with the southeast–northwest tilt ranging from 35 m s^{-1} to 80 m s^{-1} ~~(Figure 20aFigures 13a and 2013b)~~. ~~Our definition of wind shear iwas different from other studies (e.g., Lee et al. 2008; Fan et al. 2009; Li et al. 2011; Guo et al., 2016a), with a higher altitude. We chose 10 km because the latent heat release, which is a key factor determining convection intensity and partly depends on wind shear, extends up to approximately 10 km (Figure 5Figure 5g). Although the wind shear in our work iwas stronger than that in other studies with magnitudes lower than 10 m s^{-1},~~ T~~t~~he aerosol-induced convective invigoration effect appears~~ed~~ over the region with relatively weak wind shear and high humidity ~~on the land along the coast, as presented in Figure 20Figure 13~~. This invigoration effect under weak wind shear for cloud systems i~~wa~~s described in ~~a recent work (~~Li et al.~~,~~ ~~(~~(2011)~~, whereas it iwas to some extent contradicted by the results of Lee et al. (2008)~~. ~~Conversely, precipitation was suppressed to the northwest of Guangdong, with relatively strong wind shear and low humidity, as shown in Figure 20Figures 13b and 2013d. The gradients of wind shear and humidity increased between the southeast and northwest of domain 2 on December 15 when peak rainfall occurred. The results confirm that the effect of aerosols on precipitation is related to relative humidity and wind shear. However, this relationship remains dependent on the situation and may be affected by other meteorological variables, such as convective available potential energy (Khain et al., 2005), cloud phase (Lin et al., 2006), and cloud type (Koren et al., 2008). The relative importance of different meteorological variables in regulating the aerosol-induced precipitation effect requires both long-term observation and model sensitivity tests to provide a more comprehensive picture.~~

Aerosol emissions a~~we~~re separated into those from Guangdong Province and those from elsewhere, named experiments D2 and D1, respectively, to represent the effects of aerosol concentration~~s~~ from local and remote emissions on this extreme rainfall event. The surface aerosol concentration~~s~~ from local emissions dilute~~s~~ ~~accumulated~~ quick~~slow~~ly ~~from local emissions if the rainfall system coames~~ with strong northerlies. Instead, aerosols ~~,~~ from remote areas are imported~~transported~~ ~~from remote~~

Formatted: Font: 10 pt, (Asian) Chinese (PRC)

Formatted: Font: 10 pt

Formatted: Font: 10 pt

Formatted: Font: 10 pt, (Asian) Chinese (PRC)

Formatted: Font: 10 pt

Formatted: Font: 10 pt

~~areas~~ persistently~~,~~ extending~~ed~~ to higher altitudes~~ ,~~ up to 8 km. The aerosol concentration~~s~~ ~~thus a~~~~were~~is thus maintained at a relatively high level in the D1, ~~and~~ invigorating~~ed~~ convection. The resemblance of changes in different hydrometeors and latent heat between D1 and CTL further suggest the dominant role of remote aerosols~~ in the convection invigoration~~. Interestingly, with local emissions, the precipitation enhancement is ~~mainly~~ through intensified warm rain only. This is because much less aerosols stay in the atmosphere with only local aerosol~~s~~ emissions once the rainfall is initiated. The effect of nucleated cloud droplets on reducing supersaturation and size of droplets is much weaker~~ than that with remote aerosol emissions~~. Thus, the rain water is increased by accretion of cloud droplets, enhancing the warm rain. The precipitation averaged over R1 ~~the analysis region~~ on December 15 increases~~d~~ by 7.3 mm from the effects of remote aerosol emissions but only 3.1 mm from local aerosol emissions. These results ~~suggest that the effects of remote aerosol emissions played a dominant role in the intensification of precipitation in the estuary, which~~ imply~~ies~~ the potential influence of remote aerosol emissions on extreme synoptic weather events. However, this crucial issue remains insufficiently explored.

~~Previous studies have suggested an optimal aerosol loading in which condensational heating and evaporative cooling are balanced, leading to the most vigorous convection (Fan et al., 2007, 2009; Rosenfeld et al., 2008; Wang, 2005).~~ A tenfold emission experiment shows~~ed~~ a similar pattern with CTL but with a much stronger signal. Our ~~Fu~~further analysis of hydrometeors and latent heat reveals that the main reason for the precipitation increase is ~~via~~due to the intensified cold rain. The warm rain is suppressed almost all the time~~ because the reduction of supersaturation due to cloud droplet nucleation is much stronger than that in CTL run~~. ~~As a result, only the ice-related processes are intensified based on the Bergeron-Findeisen-Wegener theory. Instead, the increase of rain water by accretion of droplets is suppressed.~~ ~~The greater cooling below and heating above led to enhanced upward heat transport, which could further invigorate convection and result in more precipitation later (Rosenfeld et al., 2008).~~ Excessive aerosols lead to more precipitation increases, up to 59.7 mm, which is much larger than the 33.7 mm from CTL. However, the precipitation increase i~~wa~~s limited to a more narrowed region along the coast in the downwind area~~; this may be related to the adequate supply of water vapor from onshore wind, as shown in Figure 20Figure 13d~~. The average precipitation over Guangdong P~~p~~rovince decreases~~d~~ by 1.0 mm in 10× but increases~~d~~ by 1.4 mm in CTL. These results indicate that aerosol concentration~~s~~ in 10× exceeds~~ed~~ the optimal aerosol loading for convective~~on~~ invigoration and ~~instead~~ suppresses~~ed~~ the rainfall amount instead. ~~The retribution for spatial distribution of precipitation with a sharper contrast implies that air pollution may increase the possibility of both flood and drought.~~

The effects of ACI on clouds is strongly regime based (Gryspeerdt and Stier, 2012). The mechanism of the precipitation ~~decreases~~reduction over R2 (cold sector) ~~another region, in 24°–25°N, 110°–112°E,~~ is also discussed~~investigated~~. Figure S2~~11~~ shows the distribution of time-height mass and number concentration~~s~~ of different hydrometeors ~~averaged over this region~~ from CTL run. There are lots of ice particles~~crystals with cloud ice~~ extending up to 16 km, indicating ~~strong~~ deep stratiform clouds~~convection~~, which is consistent with low cloud top temperature in Figure S1b. The cloud base is higher than that over R1, characterized by smaller low-level cloud water on December 15 when strong aerosol impact occurs. This can also be suggested from low convective available potential energy (not shown) and surface temperature (Figure S3). With aerosols, more cloud droplets nucleated on which water can condensate. Additional cloud water is subsequently formed near

Formatted: Font: 10 pt

Formatted: Font: (Default) Times New Roman, 10 pt

Formatted: Font: 10 pt, (Asian) Chinese (PRC)

Formatted: Font: 10 pt, (Asian) Chinese (PRC)

Formatted: Font: 10 pt, (Asian) Chinese (PRC)

Formatted: Font: 10 pt, (Asian) Chinese (PRC)

Formatted: Font: 10 pt, (Asian) Chinese (PRC)

Formatted: Font: 10 pt, (Asian) Chinese (PRC)

to 4 km (Figure S22~~12~~a), accompanied by reduced supersaturation. The reduction in~~of~~ rain water and ~~ice crystals (particularly in~~ graupel~~)~~ suggests that both the warm rain and cold rain are suppressed~~,~~ associated~~ing~~ with less condensational and depositional heat release, respectively (Figure S23). The typical response~~process~~ of deep stratiform clouds to aerosols is~~is~~ via collision processes (Fan et al., 2016). Before 06Z on December 15, the warm rain is inhabited because of slower autoconversion which is caused by smaller cloud droplet. The riming efficiency is weakened in the later time, resulting in less graupel and suppressed precipitation.~~Less latent heat is released dominated by condensation in warm cloud and deposition in cold cloud. There could be two reasons for this. The first one is that the mass of water vapor is small over this region in the northwest corner of the domain, so that not enough water supply for convection invigoration effect with aerosols. The other one is related to the very strong wind shear over this region with maximum value up to 80 m s~~$^{-1}$~~. This condition is unfavored for latent heat to accumulate, which is key factor to convection strength (Fan et al., 2009). Thus, the precipitation is suppressed over this region with aerosols.~~ With ten times of aerosol emissions, the mass and number of rain water and graupel~~ice crystals~~ are further reduced, accompanied by a weaker latent heat release (Figure S24~~14~~ and S25~~15~~). As a result, the precipitation is further suppressed (Figure 11~~Figure 19b~~).

One may wonder whether the precipitation differences over Guangdong are driven by meteorological fields changes in domain 1 or by transport of aerosols because the atmospheric conditions of domain 1 also change~~s~~ in response to increased aerosols. The changes in meteorology in turn may affect the precipitation. Figure S26 shows the aerosol effects on 2-m temperature and column water vapor in domain 1. With aerosols, the moisture change is small over the whole China. The surface temperature decrease~~s~~ up to about 1 K is seen over northeastern China, Sichuan, and northeastern Indo-China Peninsula. However, the temperature over Guangdong Province show~~s~~ marginal changes as the aerosol ~~concentration~~ is concentrated to the north of Guangdong and incident solar radiation is weak in rainy days. The relatively small changes in meteorological fields over Guangdong may indicate a dominant role of transboundary aerosols~~s~~. Figure S27 shows the precipitation differences over Guangdong on 15 December based on domain 1 output. The pattern of precipitation changes is very different from that calculated based on domain 2 output, suggesting that the atmospheric condition changes in domain 1 cannot account for the precipitation differences in Figure 3d. Moreover, the importance of ACI discussed above works for both D1 and D2 experiment which may further confirm the precipitation changes are driven by transboundary aerosols rather than changes in meteorology in domain 1. Note the cumulus scheme is used in domain 1 but not in domain 2 which may result in different response of precipitation to atmospheric circulation changes in domain 1. To completely disentangle the meteorology impact from that of transboundary aerosols, the possible solution could be to apply~~ication of~~ nudging to constrain the meteorology as same as CTL and scale the emissions in domain 1. This could be conducted in future sensitivity studies.

We note that uncertainties exist in aerosol emission and the representation of ACI. Although ice nucleation may have little effect on the spatial distribution and temporal evolution of surface precipitation (Deng et al., 2018), this factor is not yet considered in the WRF-Chem model. This may explain negligible differences in results between simulations with and without dust and sea salt emissions. Additionally, dust sources are far from our analysis region and the prevailing wind is northerly; these produce low dust and sea salt concentration~~s~~, respectively. It is noteworthy that we assume the ARI and ACI effects are

Formatted: Superscript
Formatted: Font: 10 pt
Formatted: Font: 10 pt
Formatted: Font: 10 pt, Not Bold, Not Italic, English (United Kingdom)
Formatted: Font: 10 pt, Not Bold, Not Italic, English (United Kingdom)
Formatted: Font: 10 pt, Not Bold, Not Italic, English (United Kingdom)
Formatted: Font: 10 pt, Not Bold, Not Italic, English (United Kingdom)
Formatted: Font: 10 pt, Not Bold, Not Italic, English (United Kingdom)
Formatted: Font: 10 pt, Not Bold, Not Italic, English (United Kingdom)
Formatted: Font: 10 pt, Not Bold, Not Italic, English (United Kingdom)
Formatted: Font: 10 pt, Not Bold, Not Italic, English (United Kingdom)
Formatted: Font: 10 pt, Not Bold, Not Italic, English (United Kingdom)
Formatted: Font: 10 pt, Not Bold, Not Italic, English (United Kingdom)
Formatted: Font: 10 pt, Not Bold, Not Italic, English (United Kingdom)
Formatted: Font: 10 pt, Not Bold, Not Italic, English (United Kingdom)
Formatted: Font: 10 pt, Not Bold, Not Italic, English (United Kingdom)
Formatted: Font: 10 pt, Not Bold, Not Italic, English (United Kingdom)
Formatted: Font: 10 pt, Not Bold, Not Italic, English (United Kingdom)
Formatted: Font: 10 pt, Not Bold, Not Italic, English (United Kingdom)
Formatted: Font: 10 pt, Not Bold, Not Italic, English (United Kingdom)
Formatted: Font: 10 pt, Not Bold, Not Italic, English (United Kingdom)
Formatted: Font: 10 pt, Not Bold, Not Italic, English (United Kingdom)
Formatted: Font: 10 pt, Not Bold, Not Italic, English (United Kingdom)
Formatted: Font: 10 pt, Not Bold, Not Italic, English (United Kingdom)
Formatted: English (United Kingdom)

linear additive as previous studies (Fan et al., 2015; Zhong et al., 2015), so that the ACI effect is derived by subtracting ARI from total aerosol effects. To ~~We cannot~~ check the nonlinearity between ARI and ACI effects ~~because it~~ is difficult by ~~not easy to~~ turning off ACI effect. The problem is how to set the background concentration of cloud droplet number while keep the ARI as same in control run. This means that we could only prescribe the CDNC ~~cloud droplet number concentration~~ rather than adjust the emission or aerosol concentration. However, the ACI effect is very sensitive to the number we set (Gustafson et al., 2007).

~~Although o~~Our findings are limited to a case study;~~,~~ ~~Nevertheless~~nevertheless, this case is~~, nevertheless,~~ representative of the remarkable aerosol effect on an extreme rainfall event~~s~~ through ACI (both convective and stratiform clouds). This finding provides more evidence of the importance of considering aerosols in extreme weather forecasting (i.e., torrential rainfall) ~~forecasting~~. More ~~interestingly~~importantly, aerosol~~s~~s from remote emission sources exhibit~~ed~~ the potential to modify extreme weather through transboundary air pollution. It ~~hints~~pinpoints that we need to be careful about the spatial scale when looking at the effect of aerosols on extreme weather event. ~~This case clearly demonstrates the complicated feedback between the dynamic and microphysical processes induced by aerosols.~~ Aerosol~~s~~s substantially redistribut~~ed~~e the rainfall amount, ~~a finding~~ with crucial implications for the availability and usability of water resources in different regions of the world (Li et al., 2011). High aerosol concentration~~s~~ may therefore intensify both flood and drought by invigorating convection.

Acknowledgment. We thank the two anonymous reviewers whose insightful comments lead to a significant improvement of the manuscript. This work was jointly supported by the Early Career Scheme of Research Grants Council of Hong Kong (grant CUHK24301415), the National Key Basic Research Program of China (grant 2015CB954103), the Ministry of Science and Technology of China (grant 2017YFC1501401), the Improvement on Competitiveness in Hiring New Faculties Fund (2013/2014) of The Chinese University of Hong Kong (CUHK, grant 4930059), and the Vice-Chancellor's Discretionary Fund of the Chinese University of Hong Kong (grant 4930744). The appointment of NCL at the CUHK is supported by the AXA Research Fund. We would also like to acknowledge Met Office Climate Science for Service Partnership China as part of the Newton Fund for supporting Zhen Liu and Massimo Bollasina on the paper revision effort. Model simulations were conducted on computer clusters at Geophysical Fluid Dynamics Laboratory (GFDL). Larry Horowitz and Maofeng Liu provided helpful comments. We acknowledge the Global Scholarship Program for Research Excellence 2017–18 at the CUHK for supporting Zhen Liu's exchange visit to Princeton University. Chun Zhao is supported by the Thousand Talents Plan for Young Professionals, the Fundamental Research Funds for the Central Universities, and the National Natural Science Foundation of China (grant 41775146).

References

Altaratz, O., Koren, I., Remer, L. A. and Hirsch, E.: Review: Cloud invigoration by aerosols-Coupling between microphysics

Formatted: Font: 10 pt

Formatted: Font: 10 pt

and dynamics, Atmos. Res., 140–141, 38–60, doi:10.1016/j.atmosres.2014.01.009, 2014.

Andreae, M. O., Rosenfeld, D., Artaxo, P., Costa, A. A., Frank, G. P., Longo, K. M. and Silva-Dias, M. A. F.: Smoking rain clouds over the Amazon, Science, 303(5662), 1337–1342, doi:10.1126/science.1092779, 2004.

Banacos, P. C. and Schultz, D. M.: The use of moisture flux convergence in forecasting convective initiation: historical and operational perspectives, Weather Forecast., 20(3), 351–366, doi:10.1175/WAF858.1, 2005.

Bell, T. L., Rosenfeld, D., Kim, K. M., Yoo, J. M., Lee, M. I. and Hahnenberger, M.: Midweek increase in U.S. summer rain and storm heights suggests air pollution invigorates rainstorms, J. Geophys. Res. Atmos., 113(2), doi:10.1029/2007JD008623, 2008.

~~Binkowski, F. S. and Shankar, U.: The regional particulate matter model: 1. Model description and preliminary results, J. Geophys. Res., 100(D12), 26191, doi:10.1029/95JD02093, 1995.~~

Bollasina, M. A., Ming, Y. and Ramaswamy, V.: Anthropogenic aerosols and the weakening of the South Asian summer monsoon, Science, 334(6055), 502–505, doi:10.1126/science.1204994, 2011.

Bollasina, M. A., Ming, Y., Ramaswamy, V., Schwarzkopf, M. D. and Naik, V.: Contribution of local and remote anthropogenic aerosols to the twentieth century weakening of the South Asian Monsoon, Geophys. Res. Lett., 41(2), 680–687, doi:10.1002/2013GL058183, 2014.

Chang, C.-P., Z. Wang, and H. Hendon: The Asian winter monsoon, The Asian Monsoon, B. Wang, Ed., Springer, 89–127, 2006.

Chang, W., Zhan, J., Zhang, Y., Li, Z., Xing, J. and Li, J.: Emission-driven changes in anthropogenic aerosol concentrations in China during 1970–2010 and its implications for $PM_{2.5}$ control policy, Atmos. Res., doi:10.1016/j.atmosres.2018.05.008, 2018.

~~Chapman, E. G., Gustafson, W. I., Easter, R. C., Barnard, J. C., Ghan, S. J., Pekour, M. S. and Fast, J. D.: Coupling aerosol-cloud-radiative processes in the WRF-Chem model: Investigating the radiative impact of elevated point sources, Atmos. Chem. Phys., 9(3), 945–964, doi:10.5194/acp-9-945-2009, 2009.~~

~~Chen, F. and Dudhia, J.: Coupling an advanced land surface–hydrology model with the Penn State–NCAR MM5 modeling system. Part I: Model implementation and sensitivity, Mon. Weather Rev., 129(4), 569–585, doi:10.1175/1520-0493(2001)129<0569:CAALSH>2.0.CO;2, 2001.~~

Chen, T., Guo, J., Li, Z., Zhao, C., Liu, H., Cribb, M., Wang, F. and He, J.: A CloudSat perspective on the cloud climatology and its association with aerosol perturbations in the vertical over Eastern China, J. Atmos. Sci., 73(9), 3599–3616, doi:10.1175/JAS-D-15-0309.1, 2016.

Chen X. C., Jahn H. J., Engling G., Ward T. J., Kraemer A., Ho K. F., Yim S. H. L., Chan C. Y.: Chemical characterization and sources of personal exposure to fine particulate matter ($PM_{2.5}$) in the megacity of Guangzhou, China., Environ. Pollut., 231, 871–881, 2017.

Chou, C., Neelin, J. D., Lohmann, U. and Feichter, J.: Local and remote impacts of aerosol climate forcing on tropical precipitation, J. Clim., 18(22), 4621–4636, doi:10.1175/JCLI3554.1, 2005.

Formatted: Font: (Default) Times New Roman, (Asian) Times New Roman, 10 pt, Font color: Auto

Formatted: Font: (Default) Times New Roman, (Asian) Times New Roman, 10 pt, Font color: Auto, Subscript

Formatted: Font: (Default) Times New Roman, (Asian) Times New Roman, 10 pt, Font color: Auto

Cohen A J, Brauer M, Burnett R, et al.: Estimates and 25-year trends of the global burden of disease attributable to ambient air pollution: an analysis of data from the Global Burden of Diseases Study, The Lancet, 2017, 389 (10082), 1907-1918, 2015.

Cowan, T. and Cai, W.: The impact of Asian and non-Asian anthropogenic aerosols on 20th century Asian summer monsoon, Geophys. Res. Lett., 38(11), doi:10.1029/2011GL047268, 2011.

Cui, Z. Q., Carslaw, K. S., Yin, Y. and Davies, S.: A numerical study of aerosol effects on the dynamics and microphysics of a deep convective cloud in a continental environment, J. Geophys. Res., 111(D5), D05201, doi:10.1029/2005JD005981, 2006.

~~Dagan, G., Koren, I. and Altaratz, O.: Aerosol effects on the timing of warm rain processes, Geophys. Res. Lett., 42(11), 4590–4598, doi:10.1002/2015GL063839, 2015a.~~

~~Dagan, G., Koren, I. and Altaratz, O.: Competition between core and periphery-based processes in warm convective clouds – from invigoration to suppression, Atmos. Chem. Phys., 15(5), 2749–2760, doi:10.5194/acp-15-2749-2015, 2015b.~~

Dee, D. P., Uppala, S. M., Simmons, A. J., Berrisford, P., Poli, P., Kobayashi, S., … Vitart, F.: The ERA-Interim reanalysis: Configuration and performance of the data assimilation system. Q. J. Royal Meteorol. Soc., 137(656), 553–597. https://doi.org/10.1002/qj.828, 2011.

Deng, W. J., Wu, N. G., Lin, L. X., and Zhang, H., L.: Causal analysis of an unusual continuous torrential rainfall event in Guangdong in the winter of 2013, Meteor. Sci. Technol., 43(2), 276-282, doi:10.19517/j.1671-6345.2015.02.019, 2015.

Deng, X., Xue, H. and Meng, Z.: The effect of ice nuclei on a deep convective cloud in South China, Atmos. Res., 206, 1–12, doi:10.1016/j.atmosres.2018.02.013, 2018.

Ding, A., Wang, T., Xue, L., Gao, J., Stohl, A., Lei, H., Jin, D., Ren, Y., Wang, X., Wei, X., Qi, Y., Liu, J. and Zhang, X.: Transport of north China air pollution by midlatitude cyclones: Case study of aircraft measurements in summer 2007, J. Geophys. Res. Atmos., 114(8), doi:10.1029/2008JD011023, 2009.

Ding, A. J., Fu, C. B., Yang, X. Q., Sun, J. N., Petäjä, T., Kerminen, V. M., Wang, T., Xie, Y., Herrmann, E., Zheng, L. F., Nie, W., Liu, Q., Wei, X. L. and Kulmala, M.: Intense atmospheric pollution modifies weather: A case of mixed biomass burning with fossil fuel combustion pollution in eastern China, Atmos. Chem. Phys., 13(20), 10545–10554, doi:10.5194/acp-13-10545-2013, 2013.

Dutot, A. L., Rynkiewicz, J., Steiner, F. E. and Rude, J.: A 24-h forecast of ozone peaks and exceedance levels using neural classifiers and weather predictions, Environ. Model. Softw., 22(9), 1261–1269, doi:10.1016/j.envsoft.2006.08.002, 2007.

~~Easter, R. C., Ghan, S. J., Zhang, Y., Saylor, R. D., Chapman, E. G., Laulainen, N. S., Abdul-Razzak, H., Leung, L. R., Bian, X. and Zaveri, R. A.: MIRAGE: Model description and evaluation of aerosols and trace gases, J. Geophys. Res. D Atmos., 109(20), doi:10.1029/2004JD004571, 2004.~~

Emmons, L. K., Walters, S., Hess, P. G., Lamarque, J.-F., Pfister, G. G., Fillmore, D., Granier, C., Guenther, A., Kinnison, D., Laepple, T., Orlando, J., Tie, X., Tyndall, G., Wiedinmyer, C., Baughcum, S. L. and Kloster, S.: Description and evaluation of the Model for Ozone and Related chemical Tracers, version 4 (MOZART-4), Geosci. Model Dev., 3(1), 43–67,

Formatted: Font: (Default) Times New Roman, (Asian) Times New Roman, 10 pt, Font color: Auto

Formatted: Font: (Default) Times New Roman, (Asian) Times New Roman, 10 pt, Font color: Auto

Formatted: Font: (Default) Times New Roman, (Asian) Times New Roman, 10 pt, Not Italic, Font color: Auto

Formatted: Font: (Default) Times New Roman, (Asian) Times New Roman, 10 pt, Not Italic, Font color: Auto

Formatted: Font: (Default) Times New Roman, (Asian) Times New Roman, 10 pt, Not Italic, Font color: Auto

Formatted: Font: (Default) Times New Roman, (Asian) Times New Roman, 10 pt, Not Italic, Font color: Auto

Formatted: Font: (Default) Times New Roman, (Asian) Times New Roman, 10 pt, Font color: Auto

Formatted: Font: (Default) Times New Roman, (Asian) Times New Roman, 10 pt, Not Italic, Font color: Auto

Formatted: Font: (Default) Times New Roman, (Asian) Times New Roman, 10 pt, Font color: Auto

Field Code Changed

Formatted: Hyperlink, Font: (Default) Times New Roman, (Asian) Times New Roman, 10 pt, Font color: Auto, English (United Kingdom)

doi:10.5194/gmd-3-43-2010, 2010.

Fan, J., Zhang, R., Li, G. and Tao, W. K.: Effects of aerosols and relative humidity on cumulus clouds, J. Geophys. Res. Atmos., 112(14), doi:10.1029/2006JD008136, 2007.

Fan, J., Zhang, R., Tao, W.-K. and Mohr, K. I.: Effects of aerosol optical properties on deep convective clouds and radiative forcing, J. Geophys. Res., 113(D8), D08209, doi:10.1029/2007JD009257, 2008.

Fan, J., Yuan, T., Comstock, J. M., Ghan, S., Khain, A., Leung, L. R., Li, Z., Martins, V. J. and Ovchinnikov, M.: Dominant role by vertical wind shear in regulating aerosol effects on deep convective clouds, J. Geophys. Res. Atmos., 114(22), doi:10.1029/2009JD012352, 2009.

Fan, J., Rosenfeld, D., Ding, Y., Leung, L. R. and Li, Z.: Potential aerosol indirect effects on atmospheric circulation and radiative forcing through deep convection, Geophys. Res. Lett., 39(9), doi:10.1029/2012GL051851, 2012.

Fan, J., Leung, L. R., Rosenfeld, D., Chen, Q., Li, Z., Zhang, J. and Yan, H.: Microphysical effects determine macrophysical response for aerosol impacts on deep convective clouds, Proc. Natl. Acad. Sci., 110(48), E4581–E4590, doi:10.1073/pnas.1316830110, 2013.

Fan, J., Rosenfeld, D., Yang, Y., Zhao, C., Leung, L. R. and Li, Z.: Substantial contribution of anthropogenic air pollution to catastrophic floods in Southwest China, Geophys. Res. Lett., n/a-n/a, doi:10.1002/2015GL064479, 2015.

Fan, J., Wang, Y., Rosenfeld, D. and Liu, X.: Review of Aerosol–Cloud Interactions: Mechanisms, Significance, and Challenges, J. Atmos. Sci., 73(11), 4221–4252, doi:10.1175/JAS-D-16-0037.1, 2016.

Fan, J., Rosenfeld, D., Zhang, Y., Giangrande, S. E., Li, Z., Machado, L. A. T., Martin, S. T., Yang, Y., Wang, J., Artaxo, P., Barbosa, H. M. J., Braga, R. C., Comstock, J. M., Feng, Z., Gao, W., Gomes, H. B., Mei, F., Pöhlker, C., Pöhlker, M. L., Pöschl, U. and De Souza, R. A. F.: Substantial convection and precipitation enhancements by ultrafine aerosol particles, Science (80-.)., doi:10.1126/science.aan8461, 2018.

~~Fast, J. D., Gustafson, W. I., Easter, R. C., Zaveri, R. A., Barnard, J. C., Chapman, E. G., Grell, G. A. and Peckham, S. E.: Evolution of ozone, particulates, and aerosol direct radiative forcing in the vicinity of Houston using a fully coupled meteorology-chemistry-aerosol model, J. Geophys. Res. Atmos., 111(21), 1–29, doi:10.1029/2005JD006721, 2006.~~

Fu, G., Yu, J., Yu, X., Ouyang, R., Zhang, Y., Wang, P., Liu, W. and Min, L.: Temporal variation of extreme rainfall events in China, 1961-2009, J. Hydrol., 487, 48–59, doi:10.1016/j.jhydrol.2013.02.021, 2013.

~~Graf, H. F.: The complex interaction of aerosols and clouds, Science, 303(5662), 1309–1311, doi:10.1126/science.1094411, 2004.~~

Grell, G., Freitas, S. R., Stuefer, M. and Fast, J.: Inclusion of biomass burning in WRF-Chem: Impact of wildfires on weather forecasts, Atmos. Chem. Phys., 11(11), 5289–5303, doi:10.5194/acp-11-5289-2011, 2011.

Grell, G. A., Peckham, S. E., Schmitz, R., McKeen, S. A., Frost, G., Skamarock, W. C. and Eder, B.: Fully coupled “online” chemistry within the WRF model, Atmos. Environ., 39(37), 6957–6975, doi:10.1016/j.atmosenv.2005.04.027, 2005.

Gryspeerdt, E. and Stier, P.: Regime-based analysis of aerosol-cloud interactions, Geophys. Res. Lett., doi:10.1029/2012GL053221, 2012.

Formatted: Font: 10 pt, English (United States)

Formatted: Font: Times New Roman, 10 pt, Check spelling and grammar

Formatted: Font: (Default) Times New Roman, (Asian) Times New Roman, 10 pt, Font color: Auto

Gu, Y. and Yim, S. H. L.: The air quality and health impacts of domestic trans-boundary pollution in various regions of China, Environ. Int., 97, 117–124, doi:10.1016/j.envint.2016.08.004, 2016.

Gunn, R. and Phillips, B. B.: An experimental investigation of the effect of air pollution on the Initiation of rain, J. Meteorol., 14, 272–279, 1957.

Guo, J., Deng, M., Lee, S. S., Wang, F., Li, Z., Zhai, P., Liu, H., Lv, W., Yao, W. and Li, X.: Delaying precipitation and lightning by air pollution over the pearl river delta. Part I: Observational analyses, J. Geophys. Res. Atmos., 121(11), 6472–6488, doi:10.1002/2015JD023257, 2016a.

Guo, L., Turner, A. G. and Highwood, E. J.: Local and remote impacts of aerosol species on indian summer monsoon rainfall in a GCM, J. Clim., 29(19), 6937–6955, doi:10.1175/JCLI-D-15-0728.1, 2016b.

Guo J., Lou M., Miao Y., Wang Y., Zeng Z., Liu H., He J., Xu H., Wang F., Min M., and Zhai P.: Trans-Pacific transport of dust aerosol originated from East Asia: Insights gained from multiple observations and modeling, Environ. Poll., 230, 1030–1039, 10.1016/j.envpol.2017.07.062, 2017.

Gustafson, W. I., Chapman, E. G., Ghan, S. J., Easter, R. C. and Fast, J. D.: Impact on modeled cloud characteristics due to simplified treatment of uniform cloud condensation nuclei during NEAQS 2004, Geophys. Res. Lett., 34(19), L19809, doi:10.1029/2007GL030021, 2007.

~~Hansen, J., Sato, M. and Ruedy, R.: Radiative forcing and climate response, J. Geophys. Res., 102(D6), 6831–6864, doi:10.1029/96JD03436, 1997.~~

He, K., Huo, H. and Zhang, Q.: Urban air pollution in China: Current status, characteristics, and progress, Annu. Rev. Energy Environ., 27(1), 397–431, doi:10.1146/annurev.energy.27.122001.083421, 2002.

Hong, S.-Y., Juang, H.-M. H., Zhao, Q., Hong, S.-Y., Juang, H.-M. H. and Zhao, Q.: Implementation of Prognostic Cloud Scheme for a Regional Spectral Model, Mon. Weather Rev., 126(10), 2621–2639, doi:10.1175/1520-0493(1998)126<2621:IOPCSF>2.0.CO;2, 1998.

~~Hong, S.-Y., Noh, Y. and Dudhia, J.: A new vertical diffusion package with an explicit treatment of entrainment processes., Mon. Weather Rev., 134(9), 2318–2341, doi:10.1175/MWR3199.1, 2006.~~

Hu, Z., Zhao, C., Huang, J., Leung, L. R., Qian, Y., Yu, H., Huang, L. and Kalashnikova, O. V.: Trans-Pacific transport and evolution of aerosols: Evaluation of quasi-global WRF-Chem simulation with multiple observations, Geosci. Model Dev., 9(5), 1725–1746, doi:10.5194/gmd-9-1725-2016, 2016.

~~Iacono, M. J., Delamere, J. S., Mlawer, E. J., Shephard, M. W., Clough, S. A. and Collins, W. D.: Radiative forcing by long-lived greenhouse gases: Calculations with the AER radiative transfer models, , 113, 2–9, doi:10.1029/2008JD009944, 2008.~~

Ilotoviz, E., Khain, A. P., Benmoshe, N., Phillips, V. T. J. and Ryzhkov, A. V.: Effect of Aerosols on Freezing Drops, Hail, and Precipitation in a Midlatitude Storm, J. Atmos. Sci., doi:10.1175/JAS-D-14-0155.1, 2016.

IPCC, 2013: Climate Change 2013: The physical science basis. Contribution of working Group I to the fifth assessment report of the Intergovernmental Panel on Climate Change [Stocker, T.F., D. Qin, G.-K. Plattner, M. Tignor, S.K. Allen, J.

Formatted: Font: (Default) Times New Roman, (Asian) Times New Roman, 10 pt, Font color: Auto

Boschung, A. Nauels, Y. Xia, V. Bex and P.M. Midgley (eds.)]. Cambridge University Press, Cambridge, United Kingdom and New York, NY, USA, 1535 pp, doi:10.1017/CBO9781107415324.

Janssens-Maenhout, G., Crippa, M., Guizzardi, D., Dentener, F., Muntean, M., Pouliot, G., Keating, T., Zhang, Q., Kurokawa, J., Wankmüller, R., Denier Van Der Gon, H., Kuenen, J. J. P., Klimont, Z., Frost, G., Darras, S., Koffi, B. and Li, M.: HTAP-v2.2: A mosaic of regional and global emission grid maps for 2008 and 2010 to study hemispheric transport of air pollution, Atmos. Chem. Phys., 15(19), 11411–11432, doi:10.5194/acp-15-11411-2015, 2015.

Jiang, J. H., Su, H., Huang, L., Wang, Y., Massie, S., Zhao, B., Omar, A. and Wang, Z.: Contrasting effects on deep convective clouds by different types of aerosols, Nat. Commun., doi:10.1038/s41467-018-06280-4, 2018.

Jiang, Q., Li, W., Wen, J., Qiu, C., Sun, W., Fang, Q., Xu, M. and Tan, J.: Accuracy evaluation of two high-resolution satellite-based rainfall products: TRMM 3B42V7 and CMORPH in Shanghai, Water (Switzerland), 10(1), doi:10.3390/w10010040, 2018.

Jin, Q., Yang, Z. L. and Wei, J.: Seasonal responses of Indian summer monsoon to dust aerosols in the middle East, India, and China, J. Clim., 29(17), 6329–6349, doi:10.1175/JCLI-D-15-0622.1, 2016.

Joyce, R. J., Janowiak, J. E., Arkin, P. A. and Xie, P.: CMORPH: A method that produces global precipitation estimates from passive microwave and infrared data at high spatial and temporal resolution, J. Hydrometeorol., 5(3), 487–503, doi:10.1175/1525-7541(2004)005<0487:CAMTPG>2.0.CO;2, 2004.

~~Kain, J. S. and J. M. Fritsch: A one-dimensional entraining/detraining plume model and its application in convective parameterization, J. Atmos. Sci., 47, 2784–2802, doi.org/10.1175/1520-0469(1990)047<2784:AODEPM>2.0.CO;2, 1990.~~

~~Kaufman, Y. J. and Koren, I.: Smoke and pollution aerosol effect on cloud cover, Science, 313(5787), 655–658, doi:10.1126/science.1126232, 2006.~~

Khain, A., Rosenfeld, D. and Pokrovsky, A.: Aerosol impact on the dynamics and microphysics of deep convective clouds, Q. J. R. Meteorol. Soc., 131(611), 2639–2663, doi:10.1256/qj.04.62, 2005.

Khain, A. P.: Notes on state-of-the-art investigations of aerosol effects on precipitation: A critical review, Environ. Res. Lett., 4(1), doi:10.1088/1748-9326/4/1/015004, 2009.

Khain, A. P., BenMoshe, N. and Pokrovsky, A.: Factors determining the impact of aerosols on surface precipitation from clouds: An attempt at classification, J. Atmos. Sci., 65(6), 1721–1748, doi:10.1175/2007JAS2515.1, 2008.

Khairoutdinov, M. and Kogan, Y.: A new cloud physics parameterization in a large-eddy simulation model of marine stratocumulus, Mon. Weather Rev., doi:10.1175/1520-0493(2000)128<0229:ancppi>2.0.co;2, 2000.

Koren, I., Kaufman, Y. J., Remer, L. A. and Martins, J. V.: Measurement of the effect of amazon smoke on inhibition of cloud formation, Science, 303(5662), 1342–1345, doi:10.1126/science.1089424, 2004.

Koren, I., Vanderlei Martins, J., Remer, L. A. and Afargan, H.: Smoke invigoration versus inhibition of clouds over the amazon, Science, 321(5891), 946–949, doi:10.1126/science.1159185, 2008.

Koren, I., Feingold, G. and Remer, L. A.: The invigoration of deep convective clouds over the Atlantic: Aerosol effect,

Formatted: Font: 10 pt, English (United States)

Formatted: Font: 10 pt, English (United States)

Formatted: Font: 10 pt, English (United States)

Formatted: Font: 10 pt, English (United States)

Formatted: Font: 10 pt, English (United States)

Formatted: Font: 10 pt, English (United States)

Formatted: Font: 10 pt, English (United States)

Formatted: Font: 10 pt, English (United States)

Formatted: Font: 10 pt, English (United States)

Formatted: Font: 10 pt, English (United States)

Formatted: Font: 10 pt, English (United States)

meteorology or retrieval artifact?, Atmos. Chem. Phys., 10(18), 8855–8872, doi:10.5194/acp-10-8855-2010, 2010.

Koren, I., Dagan, G. and Altaratz, O.: From aerosol-limited to invigoration of warm convective clouds, Science, 344(6188), 1143–1146, doi:10.1126/science.1252595, 2014.

Koren, I., Altaratz, O. and Dagan, G.: Aerosol effect on the mobility of cloud droplets, Environ. Res. Lett., 10(10), doi:10.1088/1748-9326/10/10/104011, 2015.

Lau, K. M. and Kim, K. M.: Observational relationships between aerosol and Asian monsoon rainfall, and circulation, Geophys. Res. Lett., 33(21), 1–5, doi:10.1029/2006GL027546, 2006.

Lee, S. S., Donner, L. J., Phillips, V. T. J. and Ming, Y.: The dependence of aerosol effect on clouds and precipitation on cloud-system organization, shear and stability, J. Geophys. Res. Atmos., 113(16), doi:10.1029/2007JD009224, 2008.

Li, G., Wang, Y. and Zhang, R.: Implementation of a two-moment bulk microphysics scheme to the WRF model to investigate aerosol-cloud interaction, J. Geophys. Res. Atmos., 113(15), doi:10.1029/2007JD009361, 2008.

Li, Z., Niu, F., Fan, J., Liu, Y., Rosenfeld, D. and Ding, Y.: Long-term impacts of aerosols on the vertical development of clouds and precipitation, Nat. Geosci., 4(12), 888–894, doi:10.1038/ngeo1313, 2011.

Li Z., W.K.-M. Lau, V. Ramanathan, G. Wu, Y. Ding, M.G. Manoj, J. Liu, Y. Qian, J. Li, T. Zhou, J. Fan, D. Rosenfeld, Y. Ming, Y. Wang, J. Huang, B. Wang, X. Xu, S.-S., Lee, M. Cribb, F. Zhang, X. Yang, Takemura, K. Wang, X. Xia, Y. Yin, H. Zhang, J. Guo, P.M. Zhai, N. Sugimoto, S. S. Babu, G.P. Brasseur: Aerosol and monsoon climate interactions over Asia, Rev. Geophys., 54(4): 866–929, doi: 10.1002/2015RG000500, 2016.

~~Lin, J. C., Matsui, T., Pielke, S. A. and Kummerow, C.: Effects of biomass-burning-derived aerosols on precipitations and clouds in the Amazon Basin: A satellite-based empirical study, J. Geophys. Res. Atmos., 111(19), doi:10.1029/2005JD006884, 2006.~~

Lin, Y., Wang, Y., Pan, B., Hu, J., Liu, Y. and Zhang, R.: Distinct Impacts of Aerosols on an Evolving Continental Cloud Complex during the RACORO Field Campaign, J. Atmos. Sci., doi:10.1175/JAS-D-15-0361.1, 2016.

Liu, H., Jacob, D. J., Bey, I. and Yantosca, R. M.: Constraints from 210 Pb and 7 Be on wet deposition and transport in a global three-dimensional chemical tracer model driven by assimilated meteorological fields, J. Geophys. Res. Atmos., 106(D11), 12109–12128, doi:10.1029/2000JD900839, 2001.

Liu, H., J. Guo, I. Koren, O. Altaratz, G. Dagan, Y. Wang, J. H. Jiang, P. Zhai, and Y. Yung: Non-monotonic aerosol effect on precipitation in convective clouds over tropical oceans, Scientific Reports, 9: 1-7. doi: 10.1038/s41598-019-44284-2, 2019a

Liu, L., J. Guo, H. Gong, Z. Li, W. Chen, R. Wu, L. Wu, L. Wang, H. Xu, J. Li, D. Chen, and P. Zhai: Contrasting influence of Gobi and Taklimakan deserts on the dust aerosols in western North America. Geophysical Research Letters, doi: 10.1029/2019GL083508, 2019b.

Liu, Z., Yim, S. H. L., Wang, C. and Lau, N. C.: The impact of the aerosol direct radiative forcing on deep convection and air quality in the Pearl River Delta Region, Geophys. Res. Lett., doi:10.1029/2018GL077517, 2018.

Liu, Z., Ming, Y., Wang, L., Bollasina M. A., Luo, M., Lau, N. C., and Yim, S. H. L.: A model investigation of aerosol-induced

Formatted: Font: 10 pt, English (United States)

Formatted: Font: 10 pt, Not Bold, Not Italic, English (United States)

Formatted: Font: 10 pt, Not Bold, Not Italic, Font color: Auto, English (United States)

Formatted: Font: 10 pt, English (United States)

Formatted: Font: 10 pt, Not Bold, Not Italic, English (United States)

Formatted: Font: 10 pt, English (United States)

Formatted: Font: 10 pt, Font color: Auto, English (United States), Pattern: Clear

Formatted: Font: Times New Roman, 10 pt, English (United States)

Formatted: Font: 10 pt, English (United States)

Formatted: Font: 10 pt, Not Bold, Not Italic, English (United States)

Formatted: Font: 10 pt, English (United States)

Formatted: Font: 10 pt, Not Bold, Not Italic, English (United States)

Formatted: Font: 10 pt, English (United States)

Formatted: Font: 10 pt, English (United States)

changes in the East Asian winter monsoon, Geophys. Res. Lett., doi: 10.1029/2019GL084228, 2019c.

Madronich, S.: Photodissociation in the atmosphere: 1. Actinic flux and the effects of ground reflections and clouds, J. Geophys. Res., 92(D8), 9740, doi:10.1029/JD092iD08p09740, 1987.

~~Morrison, H., Thompson, G. and Tatarskii, V.: Impact of cloud microphysics on the development of trailing stratiform precipitation in a simulated squall line: Comparison of one- and two-moment schemes, Mon. Weather Rev., 137(3), 991–1007, doi:10.1175/2008MWR2556.1, 2009.~~

~~Myhre, G., Myhre, C. E. L., Samset, B. H. and Storelvmo, T.: Aerosols and their relation to global climate and climate sensitivity, Nat. Educ. Knowl., 4(5):7, 1-15 [online] Available from: http://www.nature.com/scitable/knowledge/library/aerosols-and-their-relation-to-global-climate-102215345, 2013.~~

Otte, T. L., Pouliot, G., Pleim, J. E., Young, J. O., Schere, K. L., Wong, D. C., Lee, P. C. S., Tsidulko, M., McQueen, J. T., Davidson, P., Mathur, R., Chuang, H.-Y., DiMego, G. and Seaman, N. L.: Linking the eta model with the community multiscale air quality (CMAQ) modeling system to build a national air quality forecasting system, Weather Forecast., 20(3), 367–384, doi:10.1175/WAF855.1, 2005.

Qin, Y., Chen, Z., Shen, Y., Zhang, S. and Shi, R.: Evaluation of satellite rainfall estimates over the Chinese Mainland, Remote Sens., 6(11), 11649–11672, doi:10.3390/rs61111649, 2014.

Rosenfeld, D.: Suppression of rain and snow by urban and industrial air pollution, Science, 287(5459), 1793–1796, doi:10.1126/science.287.5459.1793, 2000.

Rosenfeld, D.: Aerosol-cloud interactions control of earth radiation and latent heat release budgets, Space Sci. Rev., 125(1–4), 149–157, doi:10.1007/s11214-006-9053-6, 2006.

Rosenfeld, D. and Woodley, W.: Deep convective clouds with sustained supercooled liquid water down to -37.5 degrees C, Nature, 405(6785), 440–2, doi:10.1038/35013030, 2000.

Rosenfeld, D., Kaufman, Y. J. and Koren, I.: Switching cloud cover and dynamical regimes from open to closed Benard cells in response to the suppression of precipitation by aerosols, Atmos. Chem. Phys., 6(9), 2503–2511, doi:10.5194/acp-6-2503-2006, 2006.

Rosenfeld, D., Lohmann, U., Raga, G. B., O'Dowd, C. D., Kulmala, M., Fuzzi, S., Reissell, A. and Andreae, M. O.: Flood or drought: How do aerosols affect precipitation?, Science, 321(5894), 1309–1313, doi:10.1126/science.1160606, 2008.

~~Skamarock, W. C., Klemp, J. B., Dudhia, J., Gill, D. O., Barker, D. M., Duda, M. G., Huang, X.-Y., Wang, W. and Powers, J. G.: A description of the advanced research WRF version 3. [online] Available from: https://pdfs.semanticscholar.org/ace5/4d4d1d6c9914997ad8f4e410044fdeb95b9d.pdf (Accessed 15 May 2018), 2008.~~

~~Small, J. D., Chuang, P. Y., Feingold, G. and Jiang, H.: Can aerosol decrease cloud lifetime?, Geophys. Res. Lett., 36(16), doi:10.1029/2009GL038888, 2009.~~

Storer, R. L. and van den Heever, S. C.: Microphysical processes evident in aerosol forcing of tropical deep convective clouds, J. Atmos. Sci., 70(2), 430–446, doi:10.1175/JAS-D-12-076.1, 2013.

Tao, W. K., Li, X., Khain, A., Matsui, T., Lang, S. and Simpson, J.: Role of atmospheric aerosol concentration on deep convective precipitation: Cloud-resolving model simulations, J. Geophys. Res. Atmos., 112(24), doi:10.1029/2007JD008728, 2007.

Tao, W. K., Chen, J. P., Li, Z., Wang, C. and Zhang, C.: Impact of aerosols on convective clouds and precipitation, Rev. Geophys., 50(2), doi:10.1029/2011RG000369, 2012.

Twomey, S.: The Influence of pollution on the shortwave albedo of clouds, J. Atmos. Sci., 34(7), 1149–1152, doi:10.1175/1520-0469(1977)034<1149:TIOPOT>2.0.CO;2, 1977.

Wang, C.: A modeling study of the response of tropical deep convection to the increase of cloud condensation nuclei concentration: 1. Dynamics and microphysics, J. Geophys. Res. Atmos., 110(21), 1–16, doi:10.1029/2004JD005720, 2005.

Wang, Y., Wan, Q., Meng, W., Liao, F., Tan, H. and Zhang, R.: Long-term impacts of aerosols on precipitation and lightning over the Pearl River Delta megacity area in China, Atmos. Chem. Phys., 11(23), 12421–12436, doi:10.5194/acp-11-12421-2011, 2011.

Wang, Y., Lee, K. H., Lin, Y., Levy, M. and Zhang, R.: Distinct effects of anthropogenic aerosols on tropical cyclones, Nat. Clim. Chang., doi:10.1038/nclimate2144, 2014.

Wang, Y., Ma, P. L., Jiang, J. H., Su, H. and Rasch, P. J.: Toward reconciling the influence of atmospheric aerosols and greenhouse gases on light precipitation changes in Eastern China, J. Geophys. Res., doi:10.1002/2016JD024845, 2016.

Wang, Y., Vogel, J. M., Lin, Y., Pan, B., Hu, J., Liu, Y., Dong, X., Jiang, J. H., Yung, Y. L. and Zhang, R.: Aerosol microphysical and radiative effects on continental cloud ensembles, Adv. Atmos. Sci., doi:10.1007/s00376-017-7091-5, 2018.

Wiedinmyer, C., Akagi, S. K., Yokelson, R. J., Emmons, L. K., Al-Saadi, J. A., Orlando, J. J. and Soja, A. J.: The Fire INventory from NCAR (FINN) – a high resolution global model to estimate the emissions from open burning, Geosci. Model Dev. Discuss., 3(4), 2439–2476, doi:10.5194/gmdd-3-2439-2010, 2010.

Wu, D., Tie, X., Li, C., Ying, Z., Lau, A. K. H., Huang, J., Deng, X. and Bi, X.: An extremely low visibility event over the Guangzhou region: A case study, Atmos. Environ., 39(35), 6568–6577, doi:10.1016/j.atmosenv.2005.07.061, 2005.

Xie, P., Joyce, R., Wu, S., Yoo, S.-H., Yarosh, Y., Sun, F. and Lin, R.: Reprocessed, bias-corrected CMORPH global high-resolution precipitation estimates from 1998, J. Hydrometeorol., 18(6), 1617–1641, doi:10.1175/JHM-D-16-0168.1, 2017.

~~Yang, Q., Gustafson, W. I., Fast, J. D., Wang, H., Easter, R. C., Morrison, H., Lee, Y. N., Chapman, E. G., Spak, S. N. and Mena-Carrasco, M. A.: Assessing regional scale predictions of aerosols, marine stratocumulus, and their interactions during VOCALS-REx using WRF-Chem, Atmos. Chem. Phys., 11(23), 11951–11975, doi:10.5194/acp-11-11951-2011, 2011.~~

~~Zaveri, R. A. and Peters, L. K.: A new lumped structure photochemical mechanism for large-scale applications, J. Geophys. Res. Atmos., 104(D23), 30387–30415, doi:10.1029/1999JD900876, 1999.~~

~~Zaveri, R. A., Easter, R. C., Fast, J. D. and Peters, L. K.: Model for simulating aerosol interactions and chemistry (MOSAIC), J. Geophys. Res. Atmos., 113(13), doi:10.1029/2007JD008782, 2008.~~

Zhang, Y. L., and F. Cao: Fine particulate matter ($PM_{2.5}$) in China at a city level. Sci. Rep., 5, 14884, https://doi.org/10.1038/srep14884, 2015.

~~Zhao, C., Wang, Y., Choi, Y. and Zeng, T.: Summertime impact of convective transport and lightning NOx production over North America: Modeling dependence on meteorological simulations, Atmos. Chem. Phys., 9(13), 4315–4327, doi:10.5194/acp-9-4315-2009, 2009.~~

Zhao, C., Liu, X., Leung, L. R., Johnson, B., Mcfarlane, S. A., Jr, W. I. G., Fast, J. D. and Easter, R.: The spatial distribution of mineral dust and its shortwave radiative forcing over North Africa: modeling sensitivities to dust emissions and aerosol size treatments, Atmos. Chem. Phys., 10, 8821–8838, doi:10.5194/acp-10-8821-2010, 2010.

~~Zhao, C., Liu, X., Leung, L. R. and Hagos, S.: and Physics Radiative impact of mineral dust on monsoon precipitation variability over West Africa, (2007), 1879–1893, doi:10.5194/acp-11-1879-2011, 2011.~~

Zhao, C., Leung, L. R., Easter, R., Hand, J. and Avise, J.: Characterization of speciated aerosol direct radiative forcing over California, J. Geophys. Res. Atmos., 118(3), 2372–2388, doi:10.1029/2012JD018364, 2013~~a~~.

~~Zhao, C., Chen, S., Leung, L. R., Qian, Y., Kok, J. F., Zaveri, R. A. and Huang, J.: Uncertainty in modeling dust mass balance and radiative forcing from size parameterization, Atmos. Chem. Phys., 13(21), 10733–10753, doi:10.5194/acp-13-10733-2013, 2013b.~~

Zhao, C., Hu, Z., Qian, Y., Ruby Leung, L., Huang, J., Huang, M., Jin, J., Flanner, M. G., Zhang, R., Wang, H., Yan, H., Lu, Z. and Streets, D. G.: Simulating black carbon and dust and their radiative forcing in seasonal snow: A case study over North China with field campaign measurements, Atmos. Chem. Phys., 14(20), 11475–11491, doi:10.5194/acp-14-11475-2014, 2014.

Zhao, C., Huang, M., Fast, J. D., Berg, L. K., Qian, Y., Guenther, A., Gu, D., Shrivastava, M., Liu, Y., Walters, S., Pfister, G., Jin, J., Shilling, J. E. and Warneke, C.: Sensitivity of biogenic volatile organic compounds to land surface parameterizations and vegetation distributions in California, Geosci. Model Dev., 9(5), 1959–1976, doi:10.5194/gmd-9-1959-2016, 2016.

Zhao, C., Lin, Y., Wu, F., Wang, Y., Li, Z., Rosenfeld, D. and Wang, Y.: Enlarging Rainfall Area of Tropical Cyclones by Atmospheric Aerosols, Geophys. Res. Lett., doi:10.1029/2018GL079427, 2018.

Zhong, S., Qian, Y., Zhao, C., Leung, R. and Yang, X. Q.: A case study of urbanization impact on summer precipitation in the greater Beijing metropolitan area: Urban heat island versus aerosol effects, J. Geophys. Res., 120(20), 10,903-10,914, doi:10.1002/2015JD023753, 2015.

Zhong, S., Qian, Y., Zhao, C., Leung, R., Wang, H., Yang, B., Fan, J., Yan, H., Yang, X. Q. and Liu, D.: Urbanization-induced urban heat island and aerosol effects on climate extremes in the Yangtze River Delta region of China, Atmos. Chem. Phys., 17(8), 5439–5457, doi:10.5194/acp-17-5439-2017, 2017.

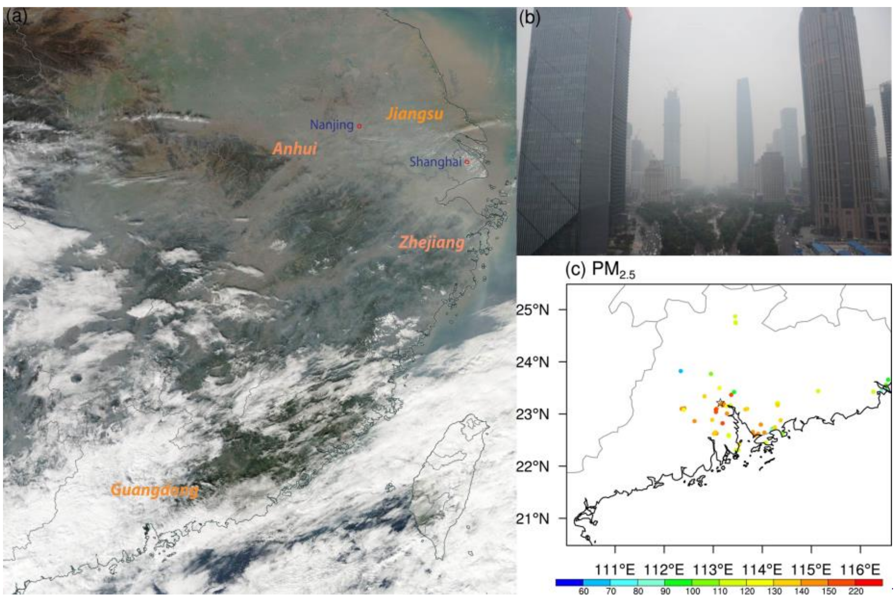
(a)
Nanjing
Jiangsu
Anhui
Shanghai
Zhejiang
Guangdong
(b)
(c) PM2.5
25°N
24°N
23°N
22°N
21°N
111°E 112°E 113°E 114°E 115°E 116°E
60 70 80 90 100 110 120 130 140 150 220

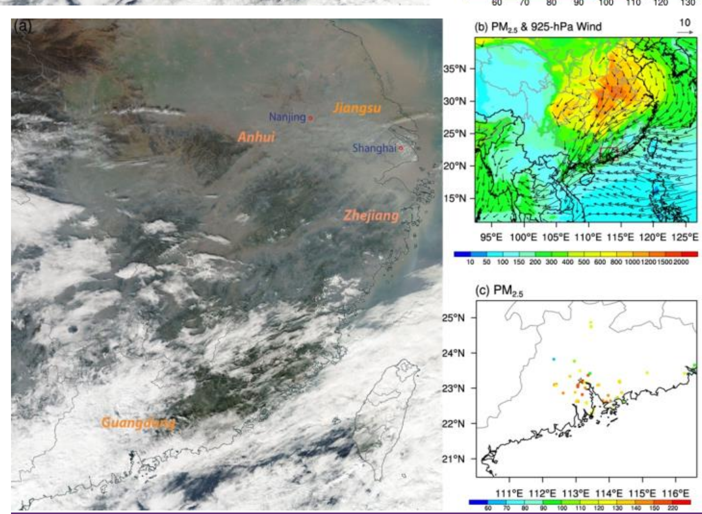
(a)
Nanjing
Jiangsu
Anhui
Shanghai
Zhejiang
Guangdong
(b) PM2.5 & 925-hPa Wind
10
35°N
30°N
25°N
20°N
15°N
95°E 100°E 105°E 110°E 115°E 120°E 125°E
(c) PM2.5
25°N
24°N
23°N
22°N
21°N
111°E 112°E 113°E 114°E 115°E 116°E

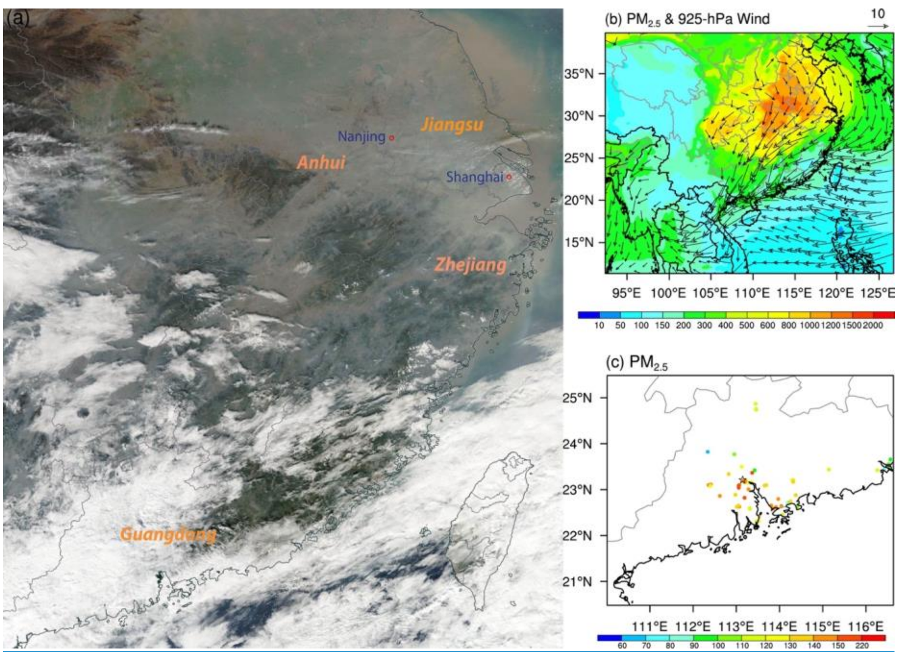

Figure 1. (a) Terra satellite true-color image of east China on December 13, 2013 (UTC), provided by NASA's Worldview (source: https://worldview.earthdata.nasa.gov/). Red circles denote city locations, blue fonts denote cities, and orange fonts in bold italic denote provinces. (b) Spatial distribution of 3-day averaged column-integrated $PM_{2.5}$ concentrations (shading; ~~unit:~~ μg m^{-2}) and 925-hPa wind (vector; ~~unit:~~ m s^{-1}) during December 14–16, 2013, in control run. The red box denotes the analysis region~~Photo of Canton Tower taken by Lin Longyong in the afternoon of December 13, 2013 (source: https://3g.163.com/fashion/article/9HJVQL9C00264MP0.html)~~. (c) Hourly-averaged $PM_{2.5}$ (~~unit:~~ μg m^{-3}) concentration on December 13, 2013, observed in Guangdong P~~p~~rovince. Colored circles denote in situ station locations, and black star denotes Guangzhou.

Formatted: Caption

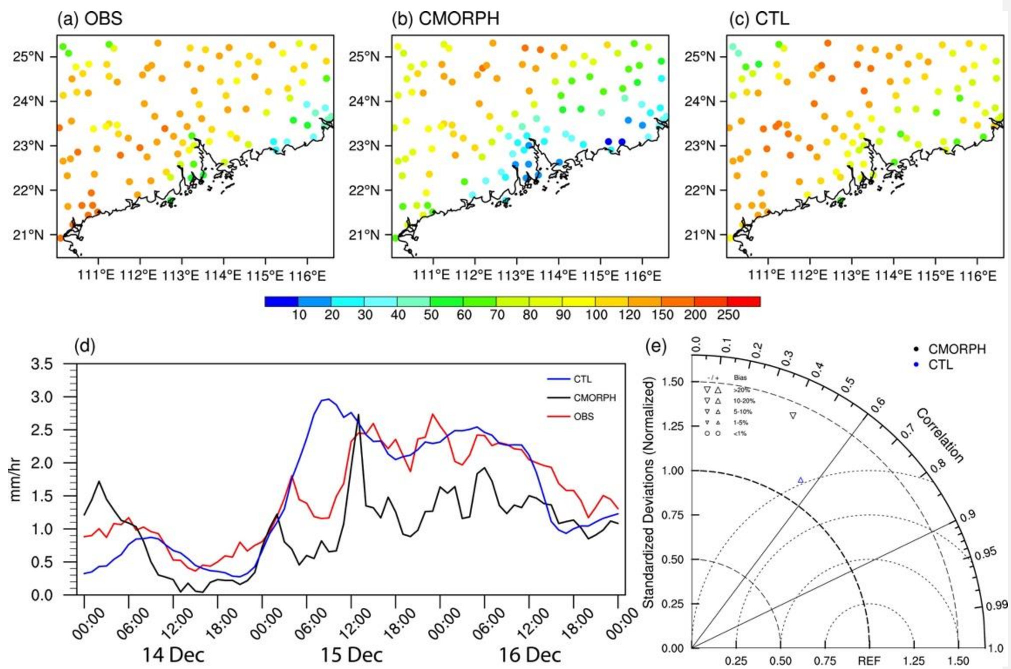
(a) OBS
(b) CMORPH
(c) CTL
25°N
24°N
23°N
22°N
21°N
111°E 112°E 113°E 114°E 115°E 116°E
10 20 30 40 50 60 70 80 90 100 120 150 200 250
(d)
mm/hr
CTL
CMORPH
OBS
00:00 06:00 12:00 18:00
14 Dec
15 Dec
16 Dec
(e)
CMORPH
CTL
Standardized Deviations (Normalized)
Correlation
REF

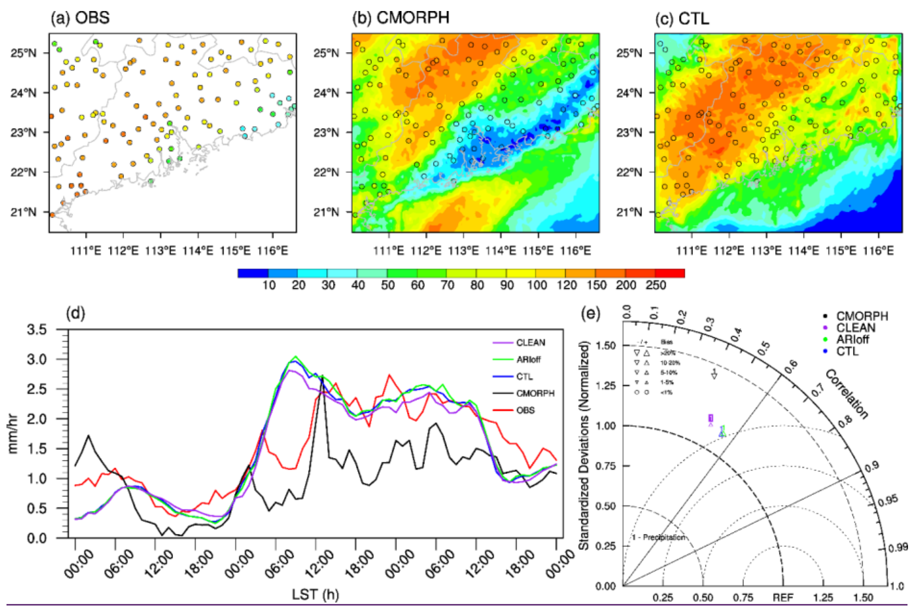

Figure 2. Spatial distribution of accumulated precipitation (~~unit:~~ mm) from 00Z on December 14, 2013~~,~~ to 00Z on December 17, 2013 (local standard time [LST]) from (a) station observations (OBS), (b) CMORPH satellite, (c) control simulation (CTL). Circles denote locations of in situ observations. (d) Time series of station average of rain rate (~~unit:~~ mm h^{-1}) over the entire domain 2 for OBS (red), CMORPH (black)~~, and~~ CTL (blue), ARIoff (green), and CLEAN (purple). (e) Taylor diagrams for 3-day accumulated precipitation in CTL (blue), ARIoff (green), CLEAN (purple), and CMORPH (black) compared with OBS. Triangles and circles at top-left corner in (e) denote bias. Sizes of triangles indicate magnitude of bias. Inverted (upright) triangles represent a negative (positive) bias. ARIoff run refers to simulation with aerosol-radiation interactions off.

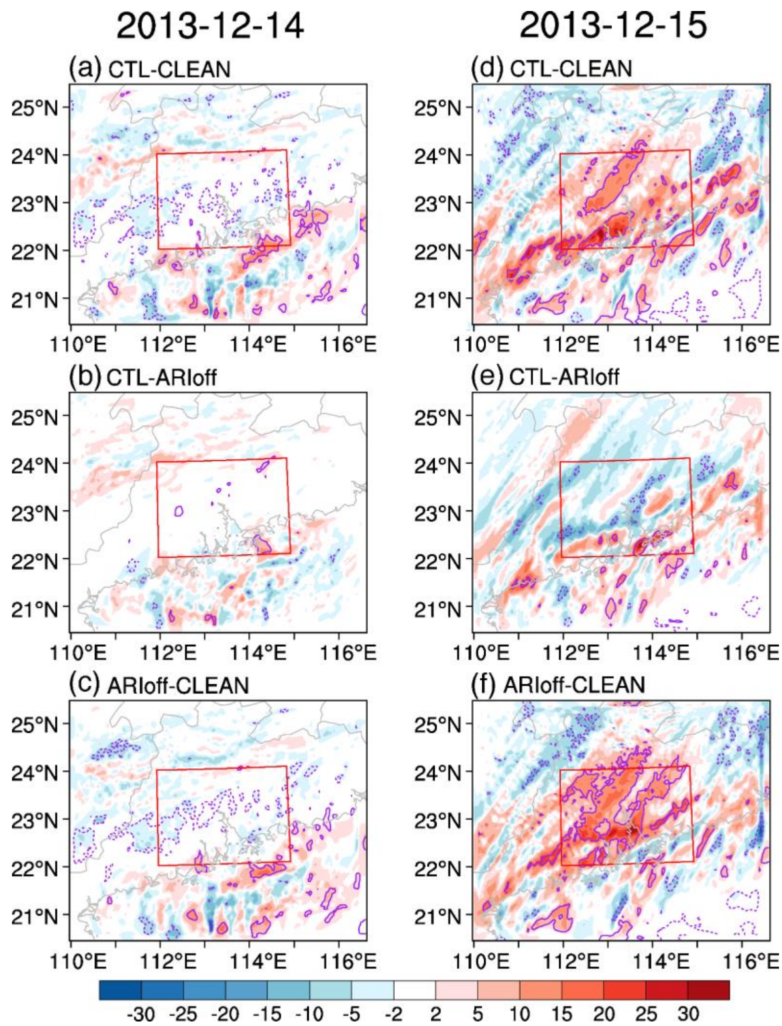
2013-12-14
2013-12-15
(a) CTL-CLEAN
(b) CTL-ARIoff
(c) ARIoff-CLEAN
(d) CTL-CLEAN
(e) CTL-ARIoff
(f) ARIoff-CLEAN
25°N
24°N
23°N
22°N
21°N
110°E
112°E
114°E
116°E
-30 -25 -20 -15 -10 -5 -2 2 5 10 15 20 25 30

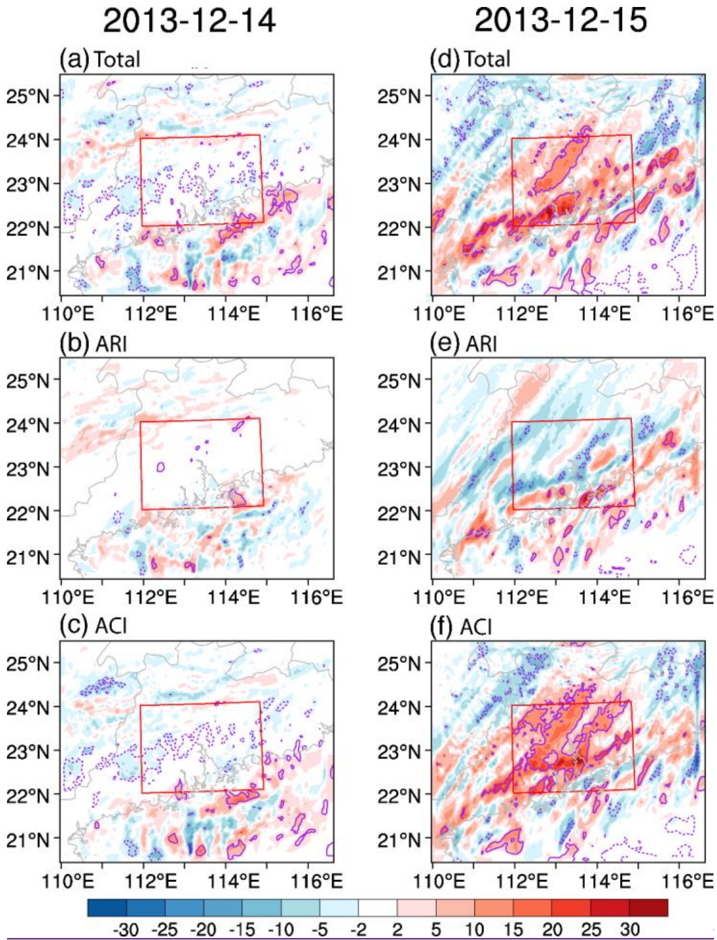
2013-12-14
2013-12-15
(a) Total
(b) ARI
(c) ACI
(d) Total
(e) ARI
(f) ACI
25°N
24°N
23°N
22°N
21°N
110°E
112°E
114°E
116°E
-30 -25 -20 -15 -10 -5 -2 2 5 10 15 20 25 30

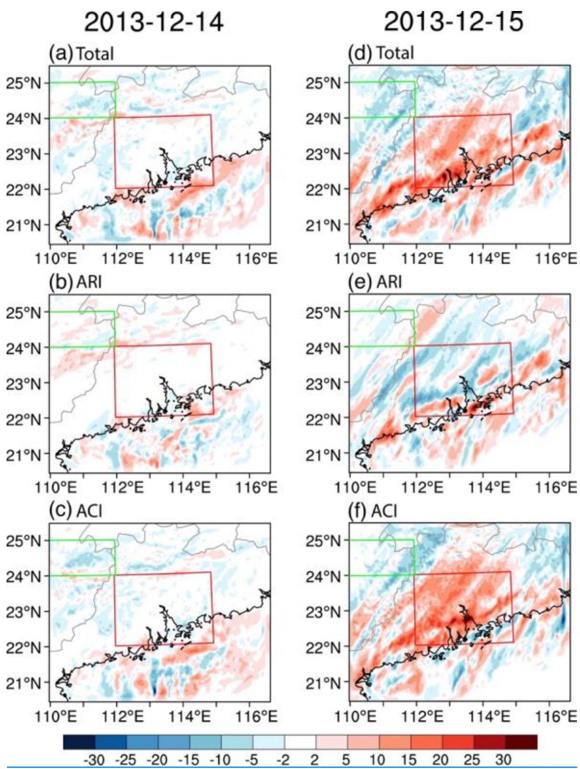

Figure 3. Differences in precipitation (~~unit:~~ mm) (a) between CTL and CLEAN ~~(i.e., CTL minus CLEAN; first row)~~, (b) CTL and ARIoff ~~(i.e., CTL minus ARIoff; second row)~~, and (c) ARIoff and CLEAN ~~(i.e., ARIoff minus CLEAN; third row)~~ on December 14. (c–f) Same as (a–c) but for ~~(left column) and~~ December 15 ~~(right column)~~. ~~Solid (dashed) purple contour lines indicate positive (negative) differences at the 90% significance level according to two-tailed Student's *t* test.~~ Red boxes (22°–24° N, 112°–115° E) and green boxes (24°–25° N, 110°–112° E) denote the ~~analysis~~ region R1 and R2, respectively. ~~ARIoff run refers to simulation with aerosol-radiation interactions off.~~

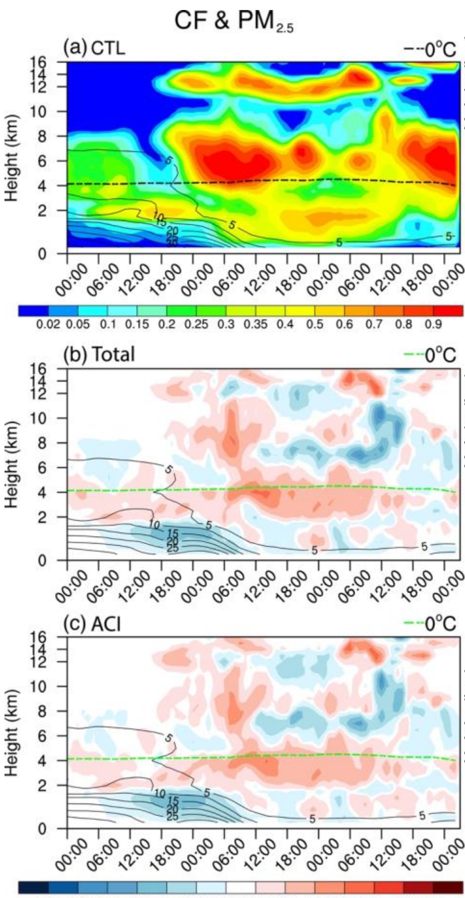
CF & PM2.5
(a) CTL
--0°C
(b) Total
--0°C
(c) ACI
--0°C
Height (km)
0.02 0.05 0.1 0.15 0.2 0.25 0.3 0.35 0.4 0.5 0.6 0.7 0.8 0.9
-0.3 -0.25 -0.2 -0.15 -0.1 -0.05 -0.01 0.01 0.05 0.1 0.15 0.2 0.25 0.3

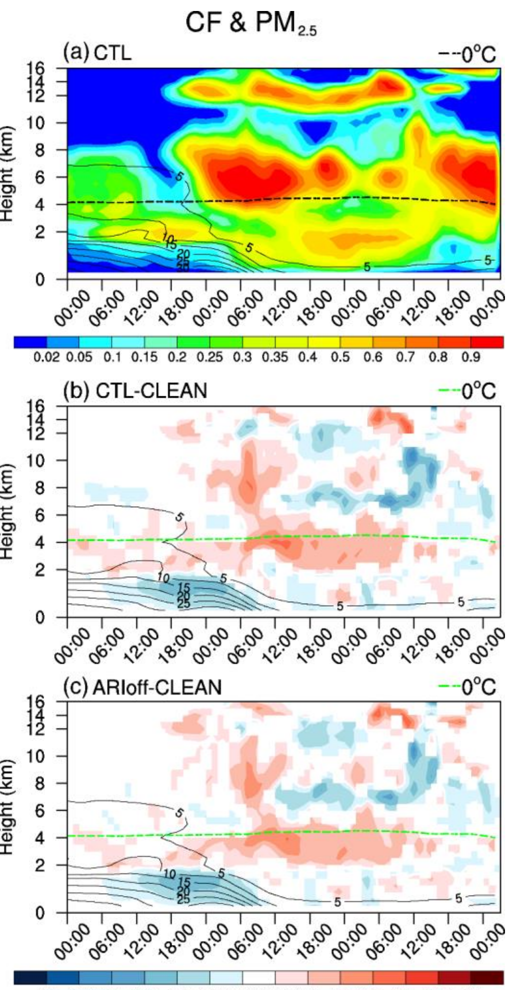
CF & PM2.5
(a) CTL
--0°C
(b) CTL-CLEAN
--0°C
(c) ARIoff-CLEAN
--0°C
Height (km)
0.02 0.05 0.1 0.15 0.2 0.25 0.3 0.35 0.4 0.5 0.6 0.7 0.8 0.9
-0.3 -0.25 -0.2 -0.15 -0.1 -0.05 -0.01 0.01 0.05 0.1 0.15 0.2 0.25 0.3

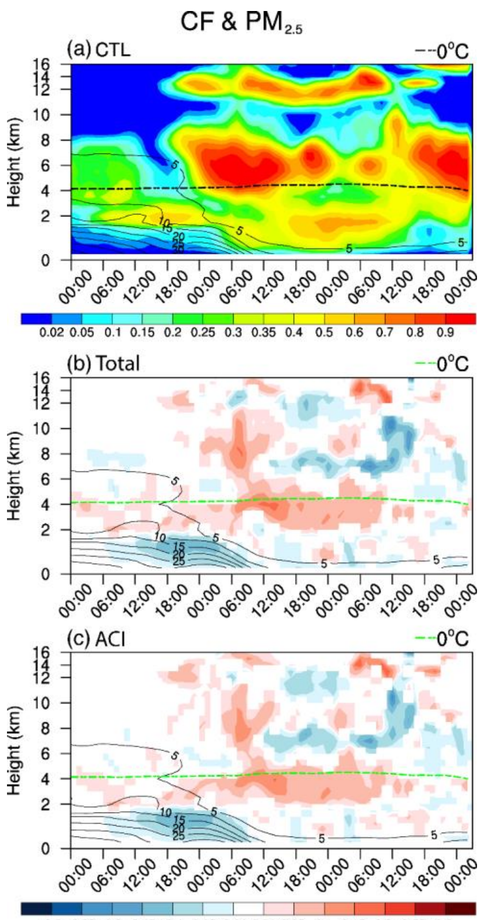

Figure 4. (a) Time-~~–~~height cross section of cloud fraction (CF; shading; ~~unit:~~ unitless) and $PM_{2.5}$ concentrations (contour; unit~~contour interval [CI]: 5~~ μg m^{-3}) averaged over R1 ~~the red box shown in Figure 3Figure 3~~ in CTL run. Differences in the time-~~–~~height cross section of CF (shading; ~~unit:~~ unitless) and $PM_{2.5}$ concentration (contour; unit~~CI: 5~~ μg m^{-3}) averaged over R1 ~~the red box~~ shown in Figure 3~~Figure 3Figure 3Figure 3~~ between (b) CTL and CLEAN ~~(i.e., CTL minus CLEAN)~~ and (c) ARIoff and CLEAN ~~(i.e., ARIoff minus CLEAN)~~. The cloud fraction is calculated as sum of cloud water, cloud ice and snow. ~~In (b) and (c), only CF and $PM_{2.5}$ concentrations anomalies that exceed the 90% significance level are depicted with shading and contour, respectively.~~ Dashed lines denote 0°C isotherm calculated as the averaged zero-layer height over R1~~the red box in Figure 3Figure 3~~.

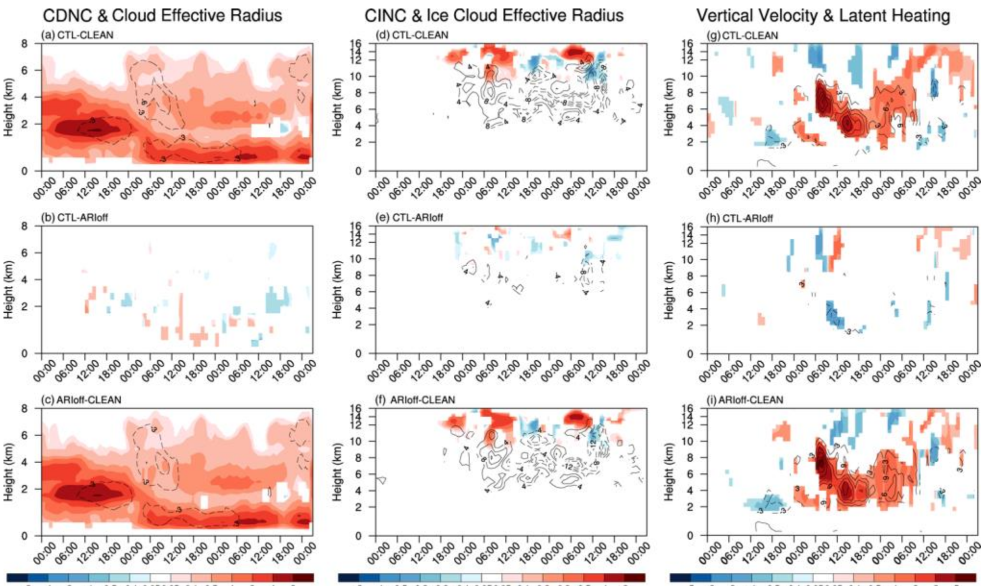

CDNC & Cloud Effective Radius
CINC & Ice Cloud Effective Radius
Vertical Velocity & Latent Heating
(a) CTL-CLEAN
(b) CTL-ARIoff
(c) ARIoff-CLEAN
(d) CTL-CLEAN
(e) CTL-ARIoff
(f) ARIoff-CLEAN
(g) CTL-CLEAN
(h) CTL-ARIoff
(i) ARIoff-CLEAN
Height (km)
00:00 06:00 12:00 18:00 00:00 06:00 12:00 18:00 00:00 06:00 12:00 18:00 00:00
-8 -4 -2 -1 -0.5 -0.1 -0.05 0.05 0.1 0.5 1 2 4 8
-2 -1 -0.5 -0.3 -0.2 -0.1 -0.05 0.05 0.1 0.2 0.3 0.5 1 2
-5 -3 -2 -1 -0.5 -0.1 -0.05 0.05 0.1 0.5 1 2 3 5

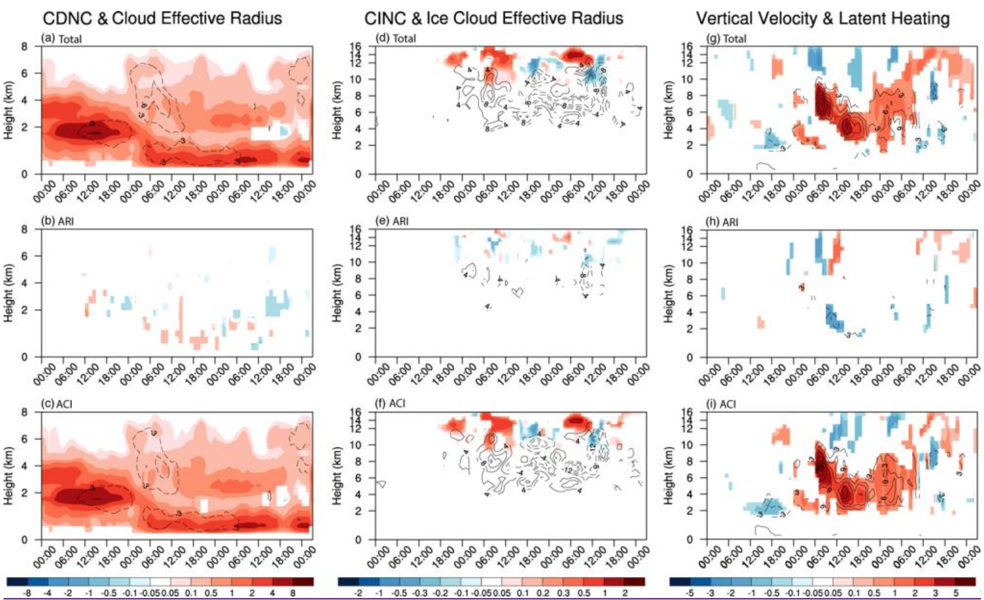

CDNC & Cloud Effective Radius
CINC & Ice Cloud Effective Radius
Vertical Velocity & Latent Heating
(a) Total
(b) ARI
(c) ACI
(d) Total
(e) ARI
(f) ACI
(g) Total
(h) ARI
(i) ACI
Height (km)
00:00 06:00 12:00 18:00 00:00 06:00 12:00 18:00 00:00 06:00 12:00 18:00 00:00
-8 -4 -2 -1 -0.5 -0.1 -0.05 0.05 0.1 0.5 1 2 4 8
-2 -1 -0.5 -0.3 -0.2 -0.1 -0.05 0.05 0.1 0.2 0.3 0.5 1 2
-5 -3 -2 -1 -0.5 -0.1 -0.05 0.05 0.1 0.5 1 2 3 5

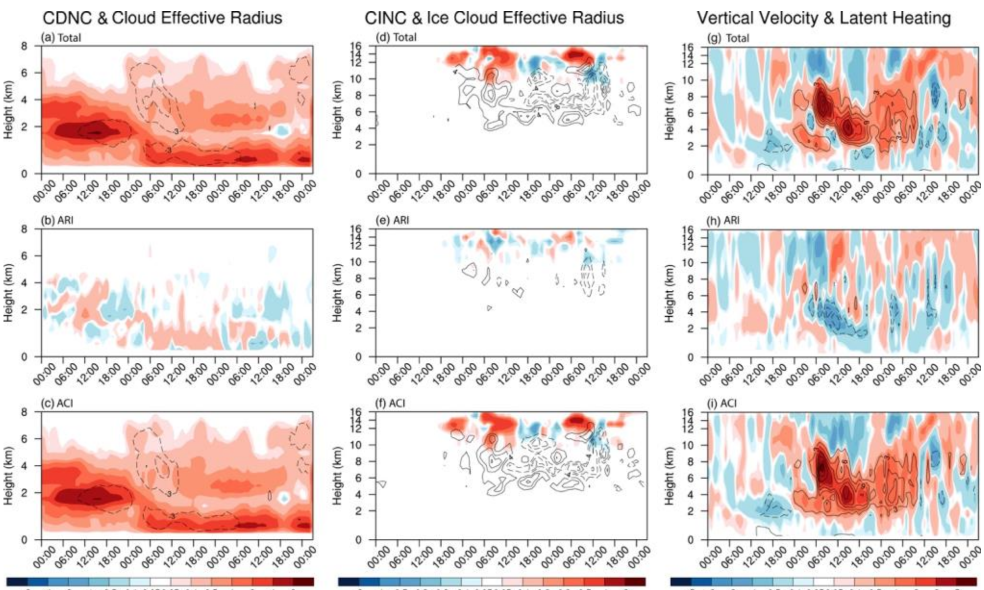

Figure 5. Differences with time (abscissa; from 00Z on December 14 to 02Z on December 17) and height (ordinate) in (a~~left column~~) cloud droplet number concentration (CDNC, shading; ~~unit:~~ 10^7 kg^{-1}) and cloud effective radius (contour; unit~~CI: 3~~ μm), (d~~middle column~~) cloud ice number concentration (CINC, shading; ~~unit:~~ 10^5 kg^{-1}) and ice cloud effective radius (contour; unit~~CI: 4~~ μm), and (g~~right column~~) vertical velocity (shading; ~~unit:~~ cm s^{-1}) and latent heating (contour; unit~~CI: 3~~ K d^{-1}) averaged over R1 ~~the red box shown in Figure 3Figure 3~~ between CTL and CLEAN ~~(i.e., CTL minus CLEAN; first row)~~. (b, e, h)~~,~~ Same as (a, d, g) but for differences between CTL and ARIoff ~~(i.e., CTL minus ARIoff; second row)~~. ~~,~~ (c, f, i) Same as (a, d, g) but for differences between ~~and~~ ARIoff and CLEAN ~~(i.e., ARIoff minus CLEAN; third row)~~. For CINC and ice cloud effective radius, only cloud ice is considered. ~~Only anomalies that exceed the 90% significance level are depicted with shading or contour.~~ Zero-value contour lines are omitted, and negative values are dashed.

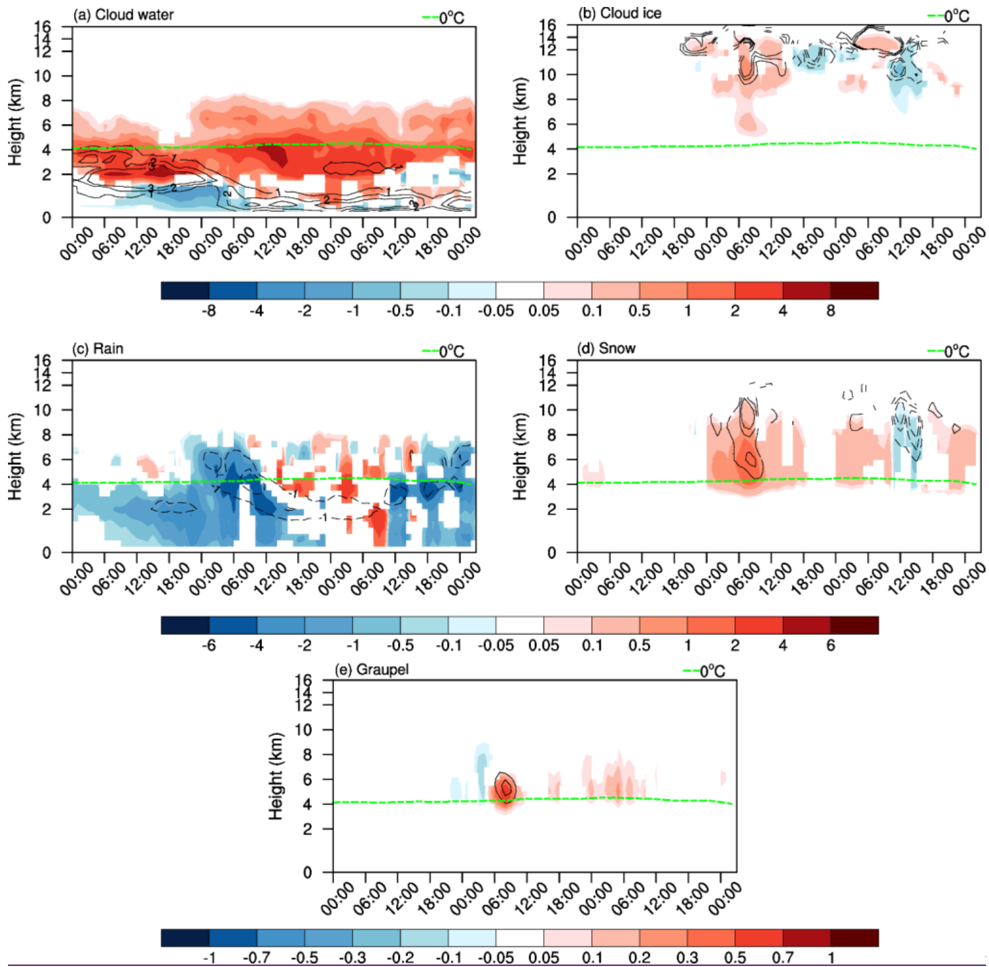
(a) Cloud water
(b) Cloud ice
(c) Rain
(d) Snow
(e) Graupel
0°C
Height (km)
00:00 06:00 12:00 18:00 00:00 06:00 12:00 18:00 00:00 06:00 12:00 18:00 00:00
-8 -4 -2 -1 -0.5 -0.1 -0.05 0.05 0.1 0.5 1 2 4 8
-6 -4 -2 -1 -0.5 -0.1 -0.05 0.05 0.1 0.5 1 2 4 6
-1 -0.7 -0.5 -0.3 -0.2 -0.1 -0.05 0.05 0.1 0.2 0.3 0.5 0.7 1

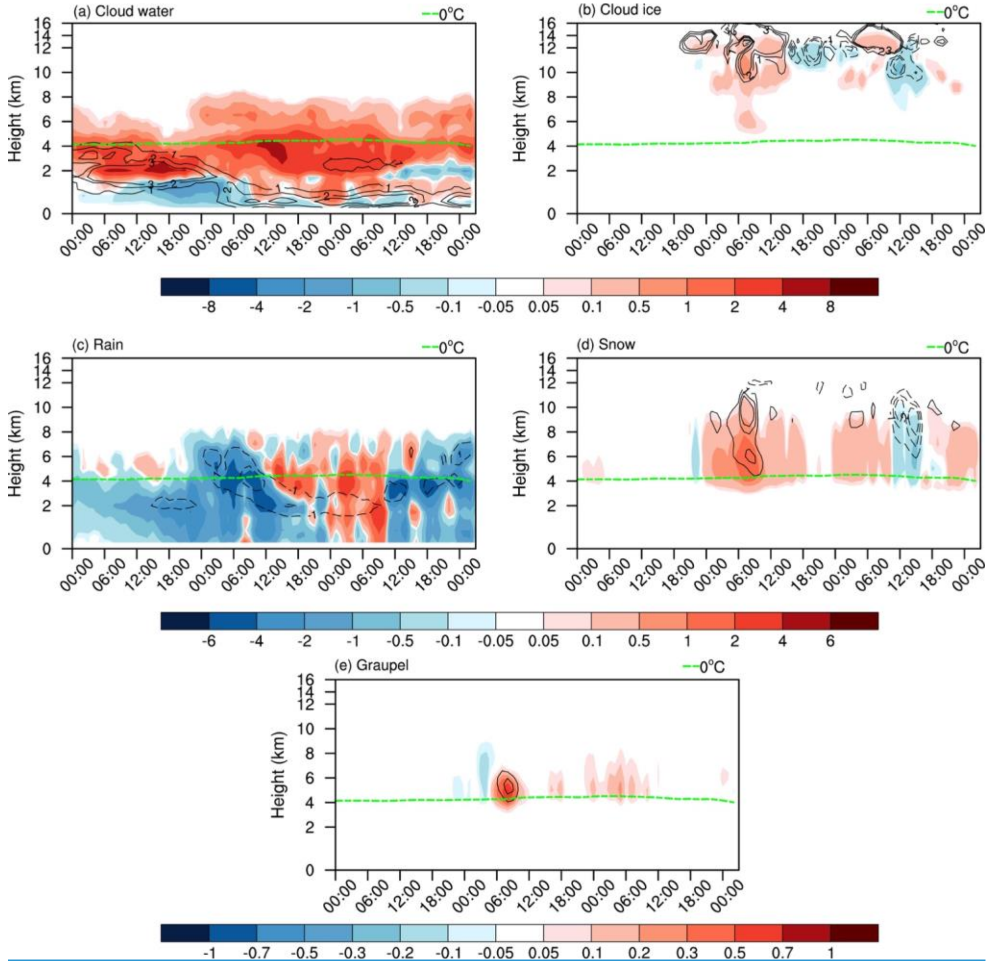

Figure 6. Differences with time (abscissa) and height (ordinate) in (a) cloud water (shading; ~~unit:~~ 10^{-5} kg kg^{-1}) and CDNC (contour; ~~unit:~~ 10^{7} kg^{-1}), (b) cloud ice (shading; ~~unit:~~ 10^{-5} kg kg^{-1}) and CINC (contour; ~~unit:~~ 10^{4} kg^{-1}), (c) rain (shading; ~~unit:~~ 10^{-5} kg kg^{-1}) and rain number concentration (contour; ~~unit:~~ 10^{5} kg^{-1}), (d) snow (shading; ~~unit:~~ 10^{-4} kg kg^{-1}) and snow number concentrations (contour; ~~unit:~~ 10^{3} kg^{-1}), and (e) graupel (shading; ~~unit:~~ 10^{-4} kg kg^{-1}) and graupel number concentration (contour; ~~unit:~~ 10^{3} kg^{-1}) between CTL and CLEAN ~~(i.e. CTL minus CLEAN)~~ averaged over R1~~the red box. Only anomalies that exceed 90% significance level are depicted with shading and contour.~~

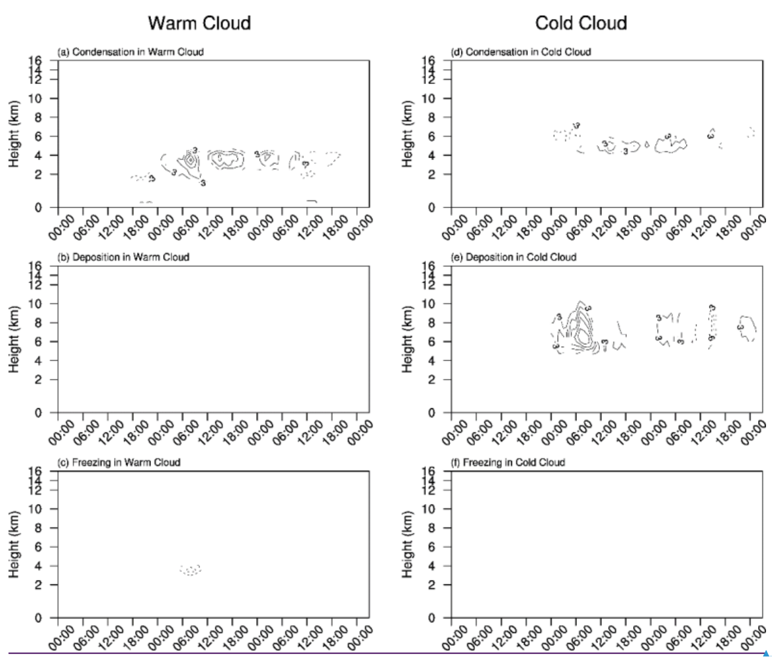

~~Figure . Differences with time (abscissa) and height (ordinate) in latent heat release (unit: K d^{-1}) from (a) condensation, (b) deposition, and (c) freezing processes between CTL and CLEAN (i.e. CTL minus CLEAN) averaged over the red box for the warm cloud. (d–f) Same as (a–c) but from cold cloud. Only anomalies that exceed 90% significance level are depicted with and contour. Zero-value contour lines are omitted, and negative values are dashed. The contour interval is 3 K d^{-1}. Note the blank represent the values are within 3 K d^{-1}.~~

Formatted: English (United States)

Formatted: English (United Kingdom)

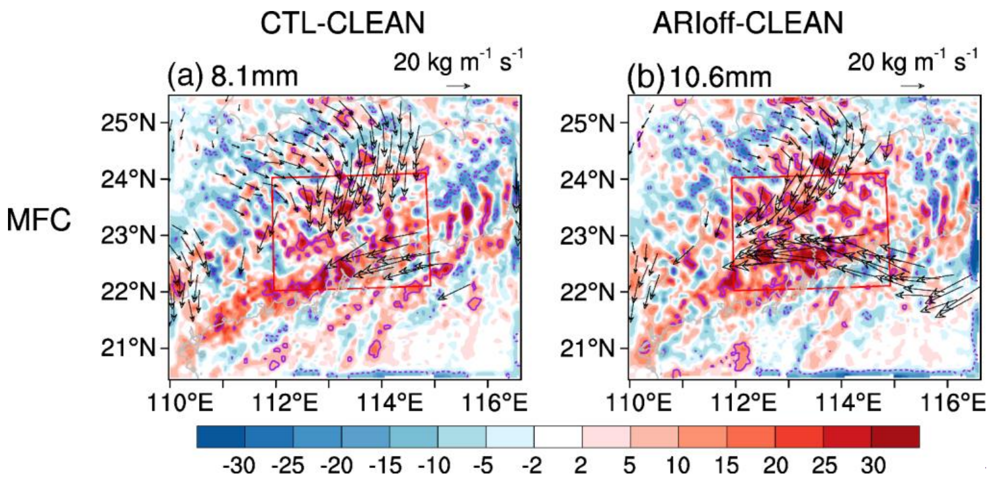
CTL-CLEAN
ARIoff-CLEAN
(a) 8.1mm
(b) 10.6mm
20 kg m-1 s-1
MFC
25°N
24°N
23°N
22°N
21°N
110°E
112°E
114°E
116°E
-30 -25 -20 -15 -10 -5 -2 2 5 10 15 20 25 30

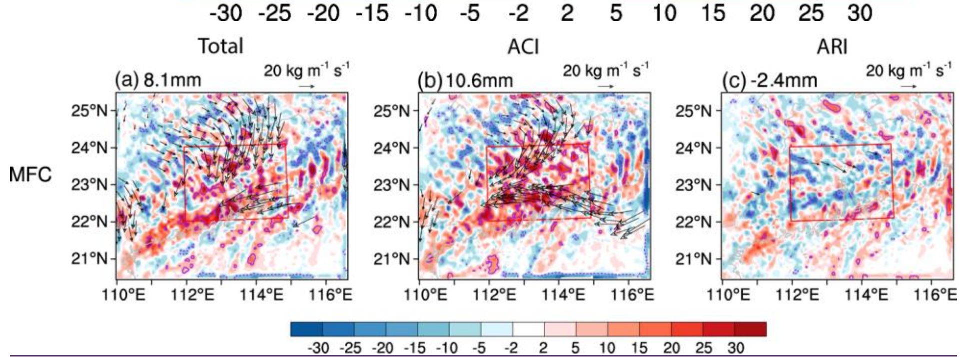
Total
ACI
ARI
(a) 8.1mm
(b) 10.6mm
(c) -2.4mm
20 kg m-1 s-1
MFC
25°N
24°N
23°N
22°N
21°N
110°E
112°E
114°E
116°E
-30 -25 -20 -15 -10 -5 -2 2 5 10 15 20 25 30

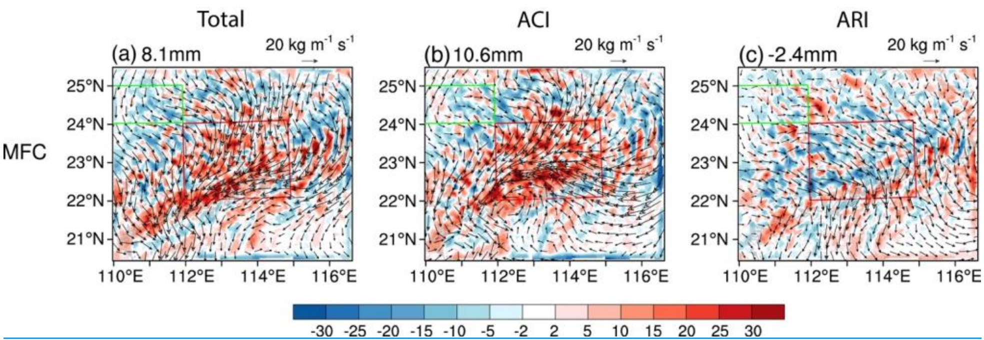

Figure ~~7~~7~~8~~86. Differences in column-integrated flux convergence (MFC; shading; ~~unit:~~ mm) and moisture flux (vector; ~~unit:~~ kg m^{-1} ~~s~~S^{-1}) between (a) CTL and CLEAN ~~(i.e., CTL minus CLEAN; left column)~~, ~~and~~ (b) ARIoff and CLEAN ~~(i.e., ARIoff minus CLEAN; right column)~~, and (c) CTL and ARIoff ~~(i.e. CTL minus ARIoff)~~ on December 15. ~~Solid (dashed) purple contour lines indicate positive (negative) differences (shading) at the 90% significance level according to two-tailed Student's *t* test. Only moisture flux anomalies that exceed the 90% significance level are depicted with black vectors.~~ Numbers at top-left corner of each panel represent values averaged over R1~~red boxes~~. ~~Red boxes (22°–24° N, 112°–115° E) denote the analysis region.~~

Formatted: Not Superscript/ Subscript

Formatted: Caption, Left

~~**Figure 9. Differences in column-moisture convergence (CON; unit: integrated mm) between (a) CTL and CLEAN (i.e. CTL minus CLEAN) and (b) ARIoff and CLEAN (i.e., ARIoff minus CLEAN) on December 15. (c, d) Same as (a, b) but for column-integrated advection of water vapor (ADV; unit: mm). The numbers at the top-left corner of each panel represent the values averaged over the red boxes. The red boxes denote the analysis region.**~~

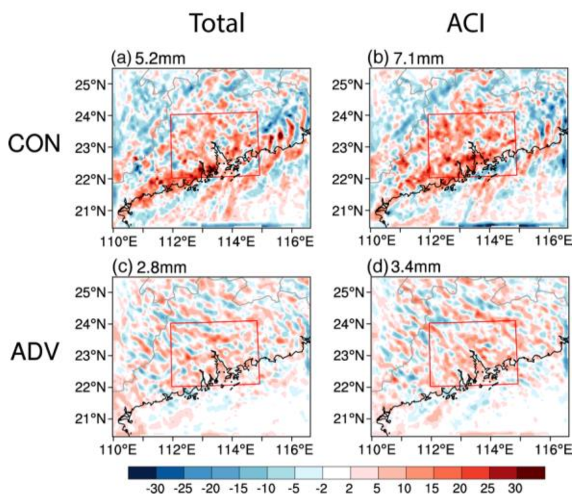

Formatted: Caption

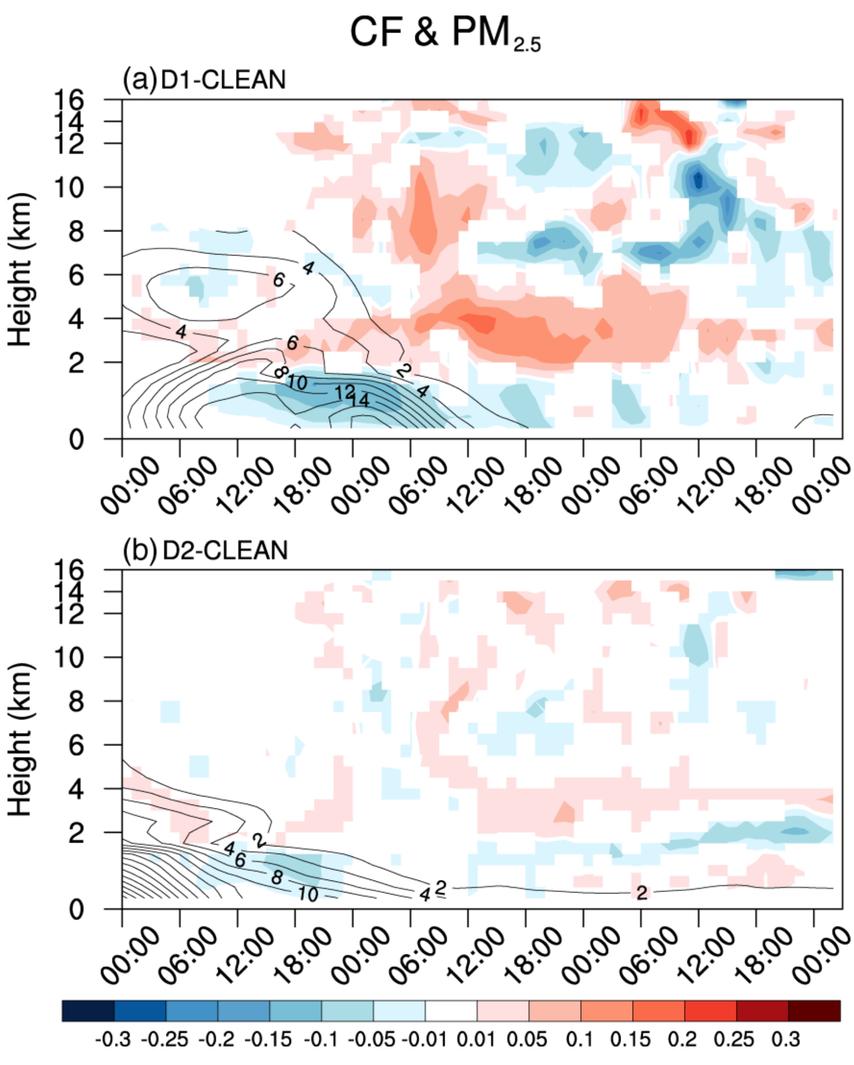
CF & PM2.5
(a) D1-CLEAN
(b) D2-CLEAN
Height (km)
16
14
12
10
8
6
4
2
0
00:00 06:00 12:00 18:00 00:00 06:00 12:00 18:00 00:00 06:00 12:00 18:00 00:00
-0.3 -0.25 -0.2 -0.15 -0.1 -0.05 -0.01 0.01 0.05 0.1 0.15 0.2 0.25 0.3

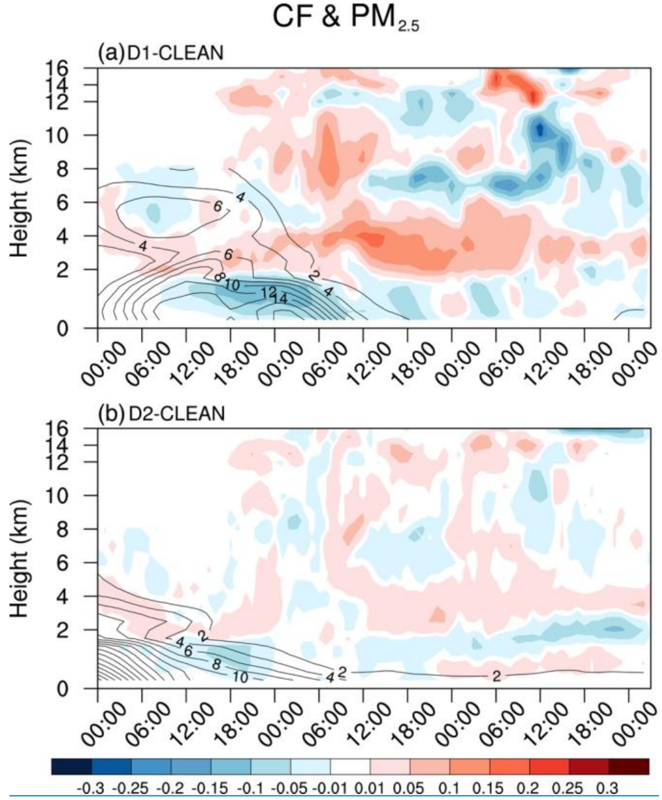

Figure 8. Differences~~Figure 10. Di fferences~~ in time-height cross section of CF (shading; ~~unit:~~ unitless) and $PM_{2.5}$ concentration (contour; ~~unit:~~ μg m^{-3}) averaged over R1 ~~the red box shown in Figure 3Figure 3~~ between (a) D1 and CLEAN ~~(i.e., D1 minus CLEAN)~~ and (b) D2 and CLEAN ~~(i.e., D2 minus CLEAN). Only CF and $PM_{2.5}$ concentrations anomalies that exceed the 90% significance level are depicted with shading and contour, respectively.~~

Formatted: English (United States)

~~**Figure 7. Differences in time–height cross section of CF (shading; unit: unitless) and $PM_{2.5}$ concentration (contour; CI: 2 μg m^{-3}) averaged over the red box shown in Figure 3 between (a) D1 and CLEAN (i.e., D1 minus CLEAN) and (b) D2 and CLEAN (i.e., D2 minus CLEAN). Only CF and $PM_{2.5}$ concentrations anomalies that exceed the 90% significance level are depicted with shading and contour, respectively.**~~

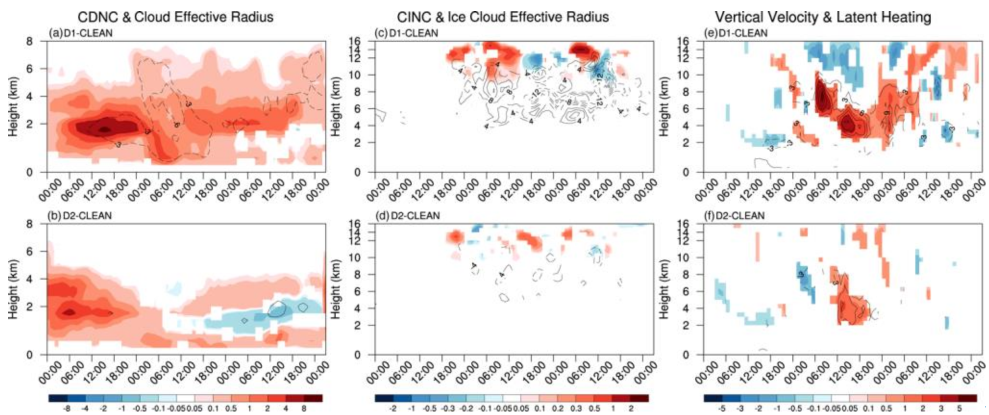

Figure 11Figure 8. Differences with time (abscissa; from 00Z on December 14 to 02Z on December 17) and height (ordinate) in (aleft column) CDNC (shading; unit: 10^7 kg^{-1}) and cloud effective radius (contour; unitCI: 3 μm), (cmiddle column) CINC (shading; unit: 10^5 kg^{-1}) and ice cloud effective radius (contour; unitCI: 4 μm), and (eright column) vertical velocity (shading; unit: cm s^{-1}) and latent heating (contour; unitCI: 3 K d^{-1}) averaged over the red box shown in Figure 3Figure 3 between D1 and CLEAN (i.e., D1 minus CLEAN; first row), (b, d, f) same as (a, c, e) but for differences between and D2 and CLEAN (i.e., D2 minus CLEAN; second row). Only anomalies that exceed the 90% significance level are depicted with shading or contour. Zero-value contour lines are omitted, and negative values are dashed.

Formatted: English (United Kingdom)

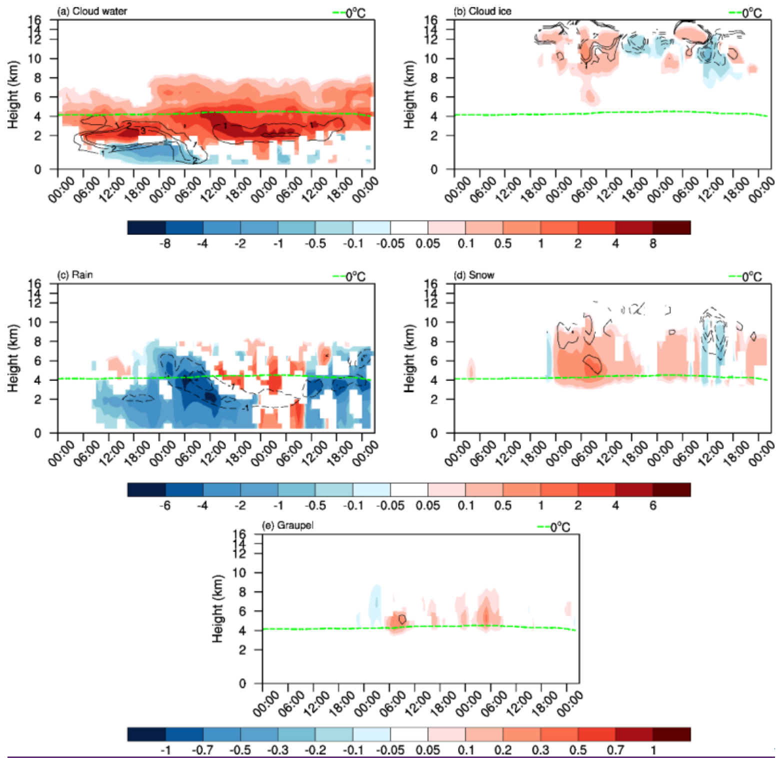
(a) Cloud water
(b) Cloud ice
(c) Rain
(d) Snow
(e) Graupel
0°C
Height (km)
00:00 06:00 12:00 18:00 00:00 06:00 12:00 18:00 00:00 06:00 12:00 18:00 00:00
-8 -4 -2 -1 -0.5 -0.1 -0.05 0.05 0.1 0.5 1 2 4 8
-6 -4 -2 -1 -0.5 -0.1 -0.05 0.05 0.1 0.5 1 2 4 6
-1 -0.7 -0.5 -0.3 -0.2 -0.1 -0.05 0.05 0.1 0.2 0.3 0.5 0.7 1

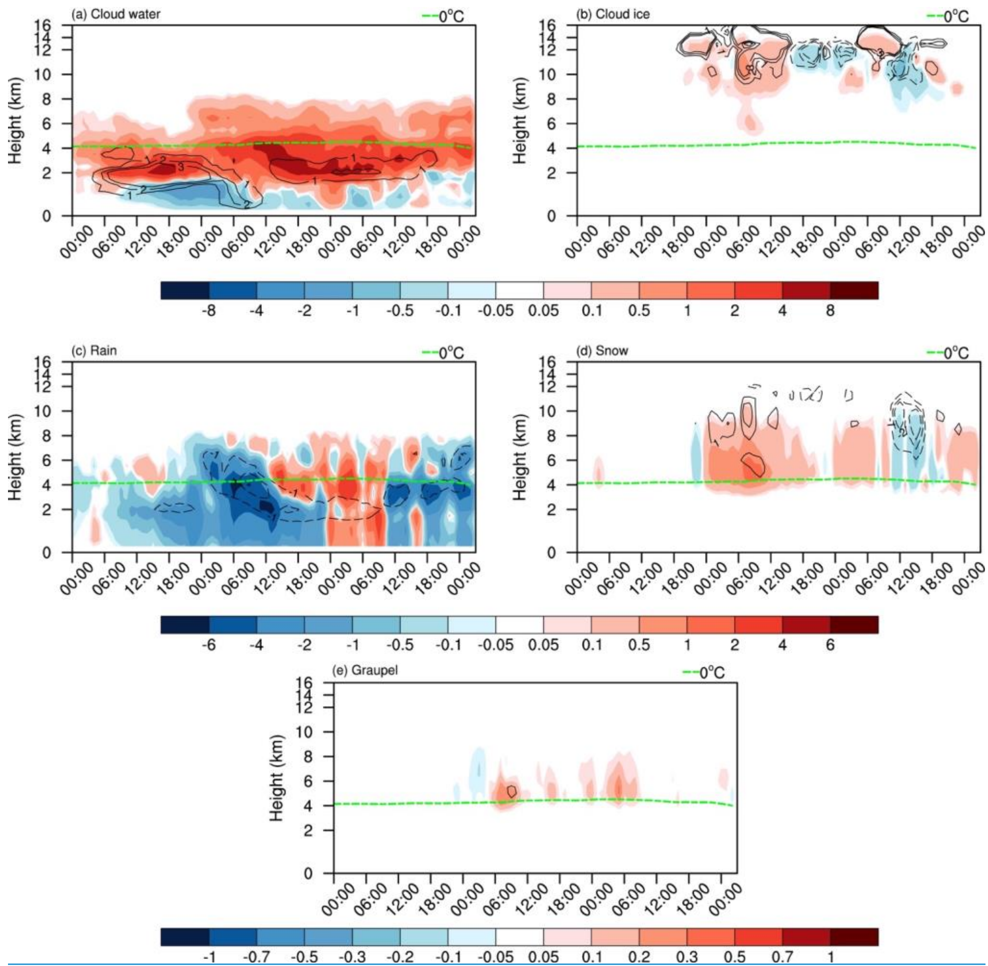

Figure 99~~12~~. Differences with time (abscissa) and height (ordinate) in (a) cloud water (shading; ~~unit:~~ 10^{-5} kg kg^{-1}) and CDNC (contour; ~~unit:~~ 10^{7} kg^{-1}), (b) cloud ice (shading; ~~unit:~~ 10^{-5} kg kg^{-1}) and CINC (contour; ~~unit:~~ 10^{4} kg^{-1}), (c) rain (shading; ~~unit:~~ 10^{-5} kg kg^{-1}) and rain number concentration (contour; ~~unit:~~ 10^{5} kg^{-1}), (d) snow (shading; ~~unit:~~ 10^{-4} kg kg^{-1}) and snow number concentrations (contour; ~~unit:~~ 10^{3} kg^{-1}), and (e) graupel (shading; ~~unit:~~ 10^{-4} kg kg^{-1}) and graupel number concentration (contour; ~~unit:~~ 10^{3} kg^{-1}) between D1 and CLEAN ~~(i.e. D1 minus CLEAN)~~ averaged over R1~~the red box~~. ~~Only anomalies that exceed 90% significance level are depicted with shading and contour.~~

Formatted: No underline

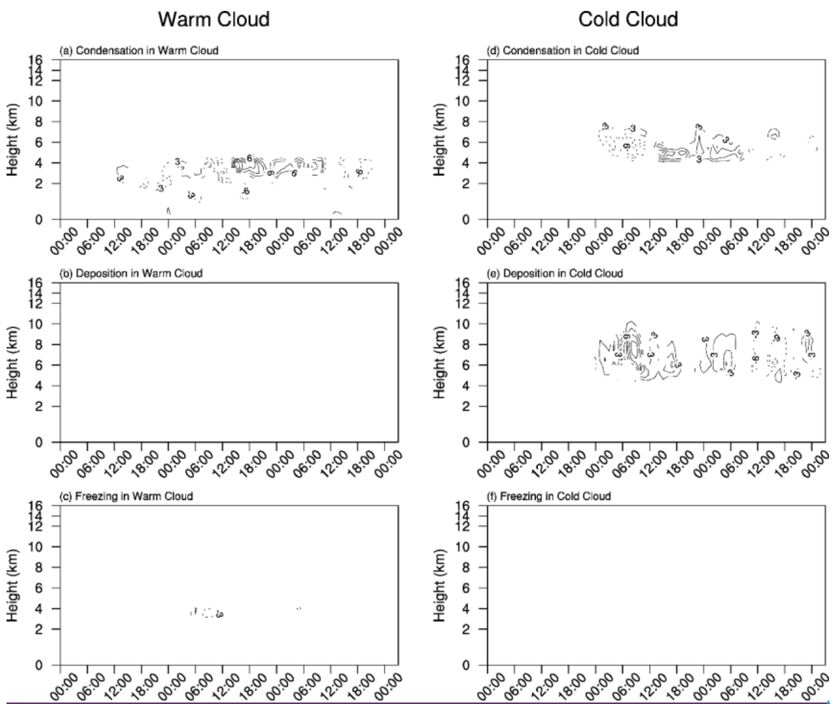

~~**Figure 13. Differences with time (abscissa) and height (ordinate) in (a) cloud water (shading; unit: 10^{-5} kg kg^{-1}) and CDNC (contour; unit: 10^{7} kg^{-1}), (b) cloud ice (shading; unit: 10^{-5} kg kg^{-1}) and CINC (contour; unit: 10^{4} kg^{-1}), (c) rain (shading; unit: 10^{-5} kg kg^{-1}) and rain number concentration (contour; unit: 10^{5} kg^{-1}), (d) snow (shading; unit: 10^{-4} kg kg^{-1}) and snow number concentrations (contour; unit: 10^{3} kg^{-1}), and (e) graupel (shading; unit: 10^{-4} kg kg^{-1}) and graupel number concentration (contour; unit: 10^{3} kg^{-1}) between D1 and CLEAN (i.e. D1 minus CLEAN) averaged over the red box. Only anomalies that exceed 90% significance level are depicted with shading and contour.**~~

Formatted: (Asian) Chinese (PRC), (Other) English (United States)

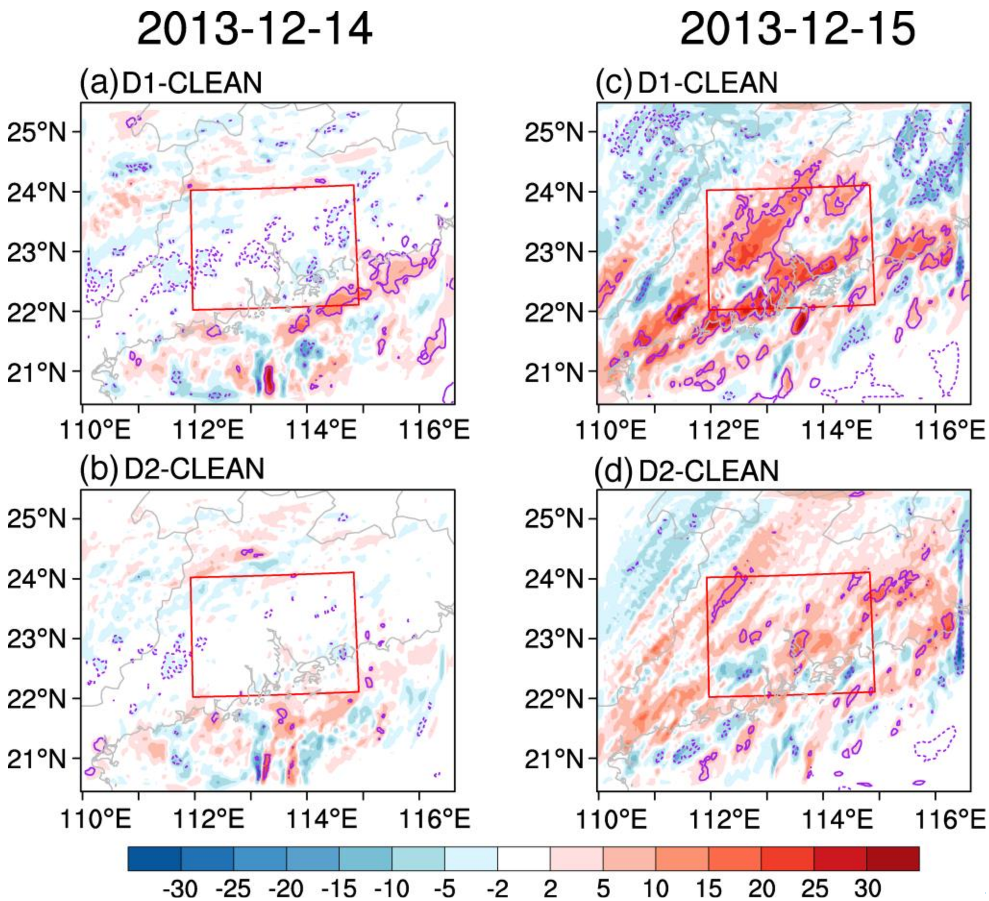
2013-12-14
2013-12-15
(a) D1-CLEAN
(b) D2-CLEAN
(c) D1-CLEAN
(d) D2-CLEAN
25°N
24°N
23°N
22°N
21°N
110°E
112°E
114°E
116°E
-30 -25 -20 -15 -10 -5 -2 2 5 10 15 20 25 30

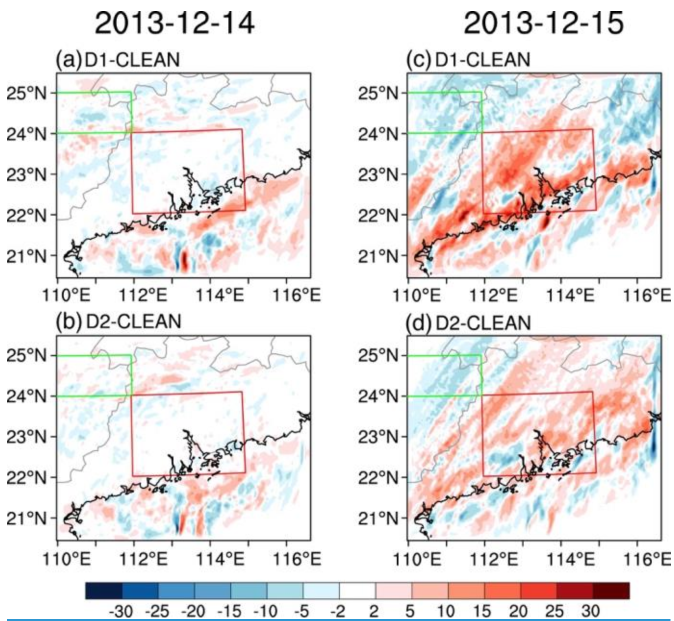

Figure 10~~10~~14~~Figure 9~~. Differences in precipitation (~~unit:~~ mm) between (a) D1 and CLEAN ~~(i.e., D1 minus CLEAN; first row)~~ and (b) D2 and CLEAN ~~(i.e., D2 minus CLEAN; second row)~~ on December 14. ~~(left column)~~ (c, d)~~and~~ Same as (a, b) but for December 15 ~~(right column)~~. ~~Solid (dashed) purple contour lines indicate positive (negative) differences at the 90% significance according to two-tailed Student's *t* test. Red boxes (22°–24° N, 112°–115° E) denote the analysis region.~~

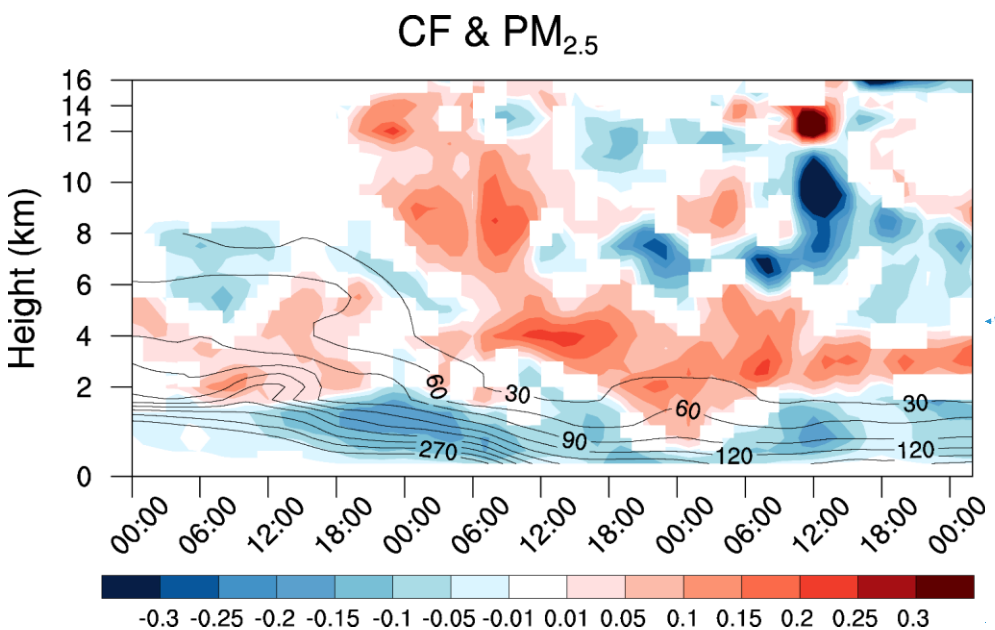

~~Figure 15. DFigure 10. Differences in the time- height cross section of cloud factor CF (shading; unit: unitless) and $PM_{2.5}$ concentrations (contour; unitCI: 30 μg m^{-3}) averaged over the red box shown in Figure 3Figure 3 between 10× and CLEAN (i.e., 10× minus CLEAN). Only CF and $PM_{2.5}$ concentrations anomalies that exceed the 90% significance level are depicted with shading and contour, respectively.~~

Formatted: Caption, Left

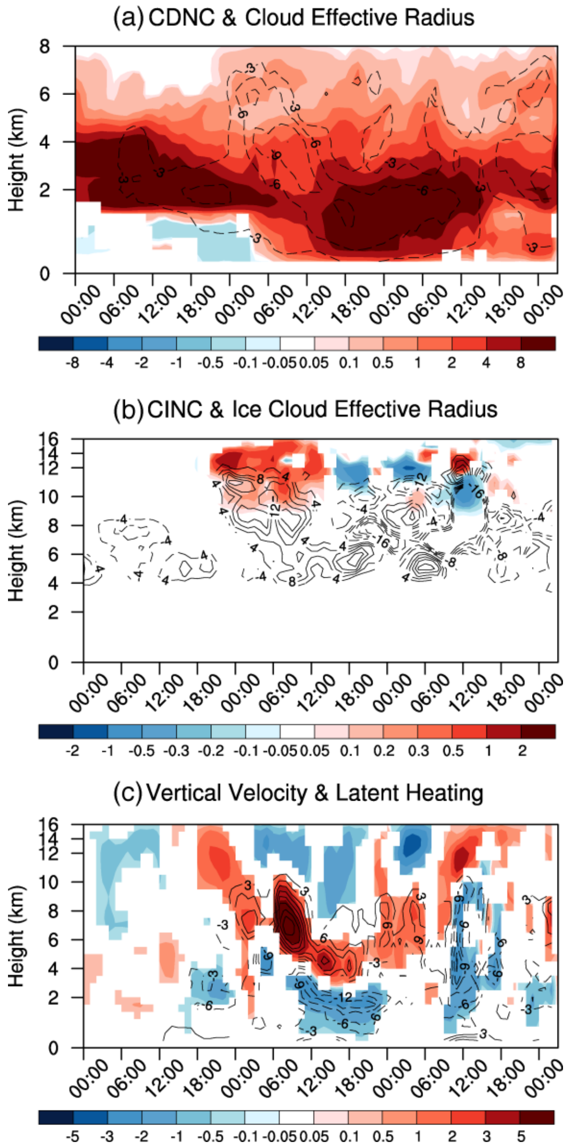

Formatted: Caption, Left

Figure 16. ~~Figure 11. Differences with time (abscissa; from 00Z on December 14 to 02Z on December 17) and height (ordinate) in (a) CDNC (shading; unit: 10^7 kg^{-1}) and cloud effective radius (unitCI: 3 μm), (b) CINC (shading; unit: 10^5 kg^{-1}) and ice cloud effective radius (contour; unitCI: 4 μm), and (c) vertical velocity (shading; unit: cm s^{-1}) and latent heating (contour; unitCI: 3 K d^{-1}) averaged over the red box shown in Figure 3Figure 3 between 10× and CLEAN (i.e., 10× minus CLEAN). Only anomalies that exceed the 90% significance level are depicted with shading or contour. Zero-value contour lines are omitted, and negative values are dashed.~~

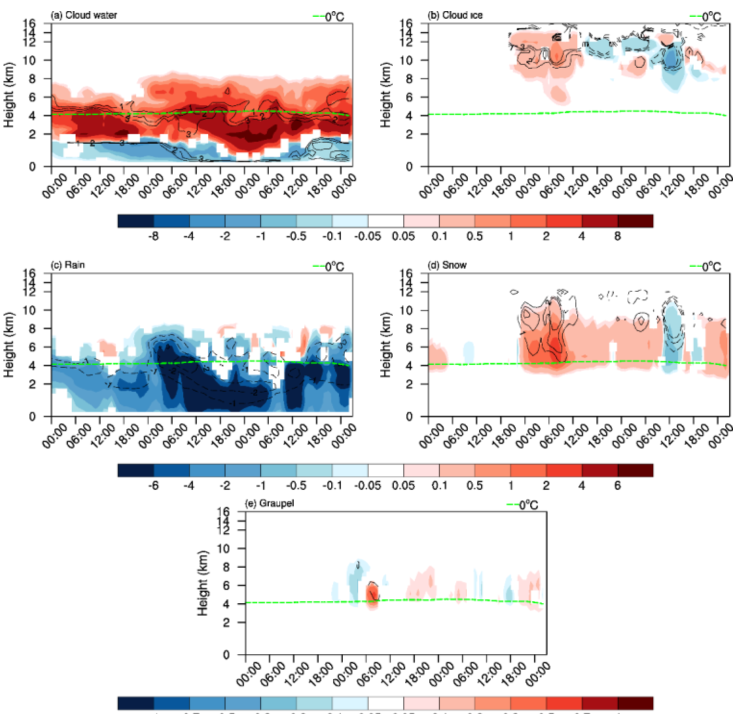

~~Figure 17. Differences with time (abscissa) and height (ordinate) in (a) cloud water (shading; unit: 10^{-5} kg kg^{-1}) and CDNC (contour; unit: 10^7 kg^{-1}), (b) cloud ice (shading; unit: 10^{-5} kg kg^{-1}) and CINC (contour; unit: 10^4 kg^{-1}), (c) rain (shading; unit: 10^{-5} kg kg^{-1}) and rain number concentration (contour; unit: 10^5 kg^{-1}), (d) snow (shading; unit: 10^{-4} kg kg^{-1}) and snow number concentrations (contour; unit: 10^3 kg^{-1}), and (e) graupel (shading; unit: 10^{-4} kg kg^{-1}) and graupel number concentration (contour; unit: 10^3 kg^{-1}) between 10× and CLEAN (i.e. 10× minus CLEAN) averaged over the red box. Only anomalies that exceed 90% significance level are depicted with shading and contour.~~

Formatted: Caption, Left

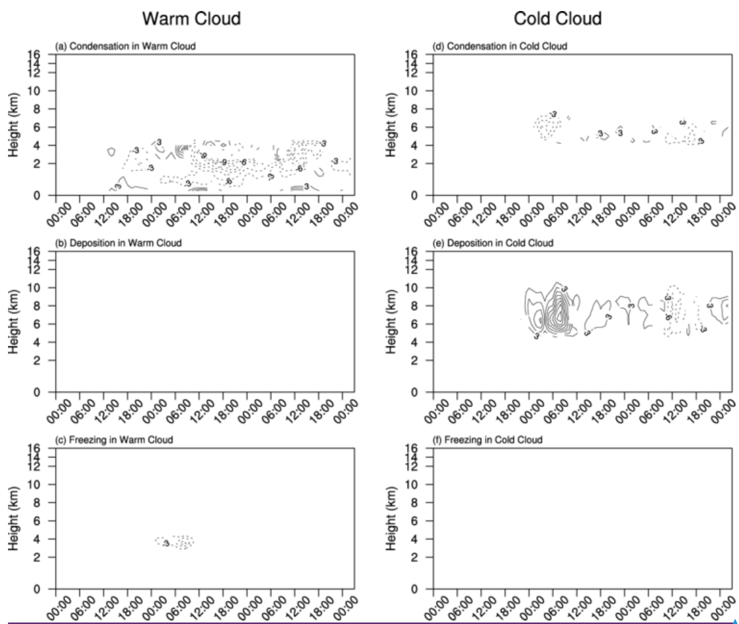

~~Figure 18. Differences with time (abscissa) and height (ordinate) in latent heat release (unit: K d^{-1}) from (a) condensation, (b) deposition, and (c) freezing processes between 10× and CLEAN (i.e. 10× minus CLEAN) averaged over the red box for the warm cloud. (d–f) Same as (a–c) but from cold cloud. Only anomalies that exceed 90% significance level are depicted with and contour. Zero-value contour lines are omitted, and negative values are dashed. The contour interval is 3 K d^{-1}. Note the blank represent the values are within 3 K d^{-1}.~~

Formatted: Font: 12 pt, Not Bold, English (United States)

Formatted: English (United Kingdom)

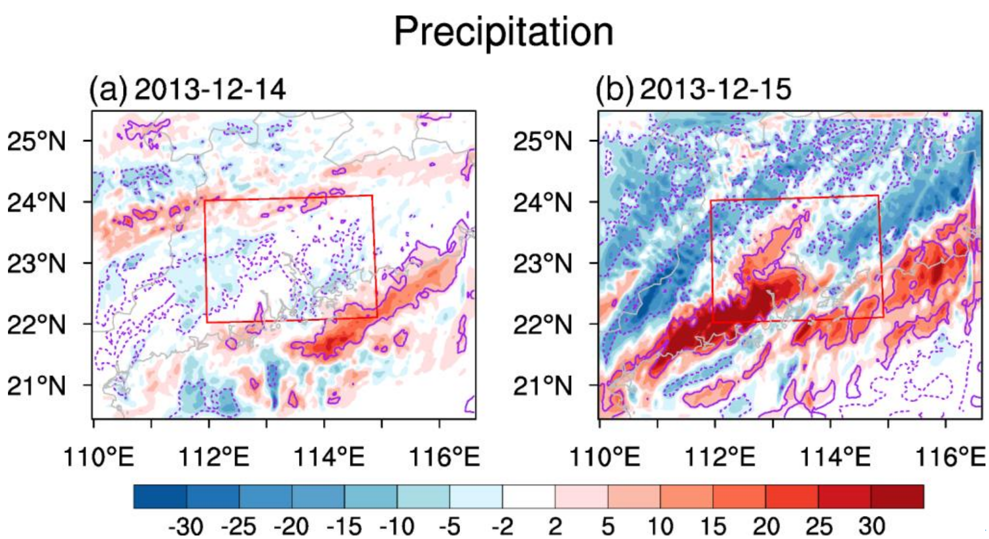

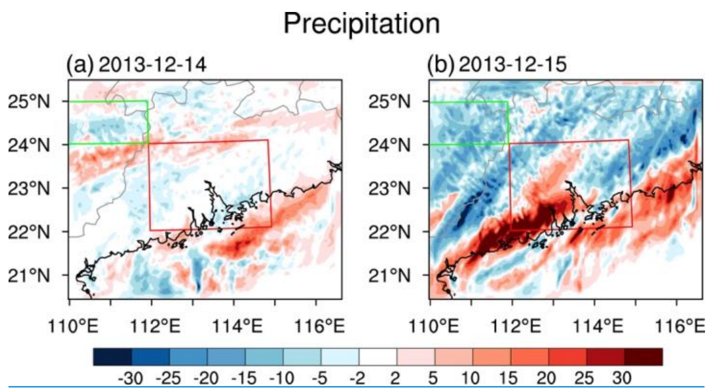

Figure 11~~11~~~~19~~. D~~Figure 12. D~~ifferences in precipitation (~~unit: ~~mm) between 10× and CLEAN~~ (i.e., 10× minus CLEAN)~~ on (a) December 14~~ (left)~~ and (b) December 15~~ (right)~~.~~ Solid (dashed) purple contour lines indicate positive (negative) differences at the 90% significance according to two-tailed Student's t test. Red boxes (22°–24° N, 112°–115° E) denote the analysis region.~~

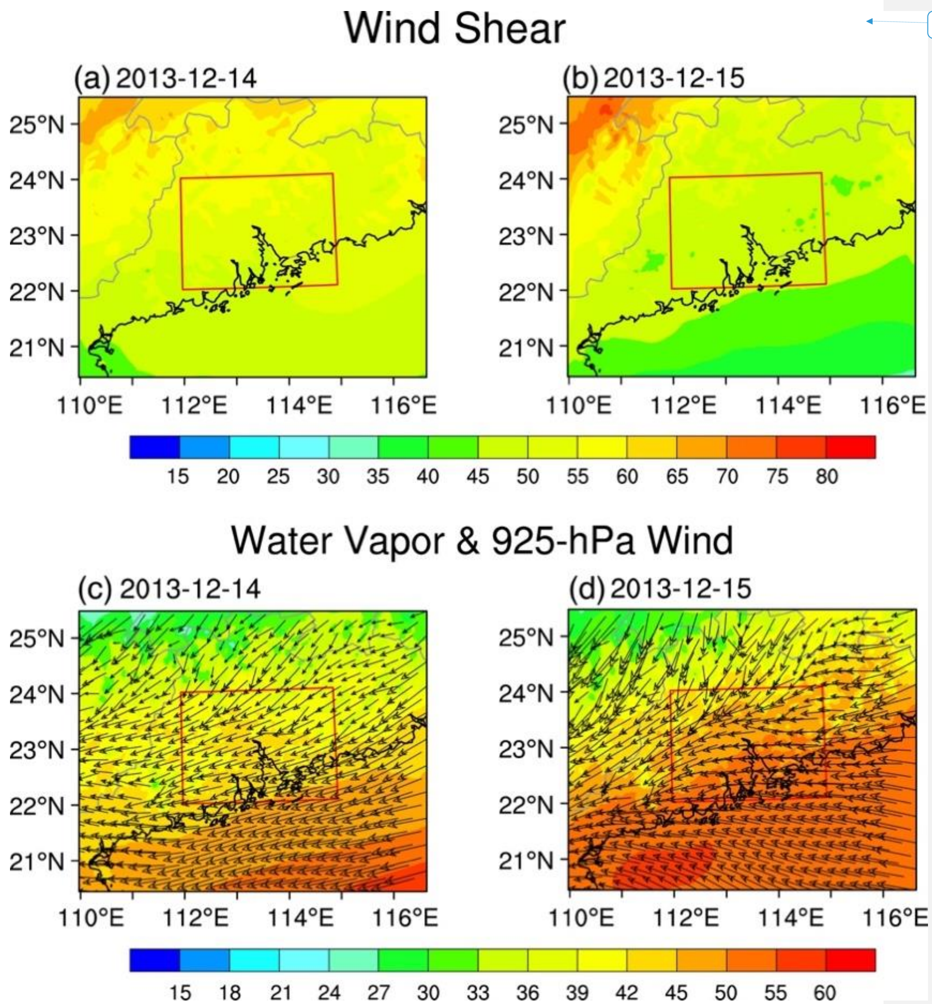

Formatted: Caption

Figure 20. S~~Figure 13. Spatial distribution of wind shear (unit: m s^{-1}) on (a) December 14 and (b) December 15 in 2013 in the CTL run (first row). Wind shear is calculated as differences between maximum wind speed and minimum wind speed at 0–10 km. Spatial distribution of column-integrated water vapor (shading; unit: mm day^{-1}) and 925-hPa wind (vector; unit: m s^{-1}) on (c) December 14 and (d) December 15 in 2013 in CTL (second row). Red boxes (22°–24° N, 112°–115° E) denote the analysis region.~~

Table 1. Model simulations. Abbreviations: CTL, control run; ARIoff, turn off aerosol-radiation interactions; D1, keep emissions in domain 1 as control run while make those except for chemical boundary conditions in domain 2 as CLEAN run; D2, keep emissions and chemical initial conditions in domain 2 as control run, make those and chemical boundary conditions in domain 1 as CLEAN run; 10×, tenfold of anthropogenic emissions and chemical initial and boundary conditions. * indicates that emissions, initial conditions (ICs), or boundary conditions (BCs), are scaled from the control run. Note the offline chemical BCs here a~~we~~re extracted from global chemical transport models and only used for domain 1.

Simulation	Anthropogenic and fire emissions, chemical ICs and BCs*		Aerosol-radiation interactions	Aerosol-cloud interactions
	Domain 1	Domain 2		
CTL	1	1	Yes	Yes
ARIoff	1	1	No	Yes
CLEAN	0.1	0.1	Yes	Yes
D1	1	0.1	Yes	Yes
D2	0.1	1	Yes	Yes
10×	10	10	Yes	Yes

~~Table 1~~

Formatted: Caption

Formatted: Font: 12 pt

Contribution of local and remote anthropogenic aerosols to ~~intensification of~~ a record-breaking torrential rainfall event in Guangdong Province, China

Z. Liu[1,2,3], Y. Ming[5], C. Zhao[6], N.C. Lau[1,2,4], J.P. Guo[7], M. Bollasina[3], Steve H.L. Yim[~~1~~4,1~~4~~,2]

[1]Institute of Space and Earth Information Science, The Chinese University of Hong Kong, Hong Kong, China
[2]Institute of Environment, Energy and Sustainability, The Chinese University of Hong Kong, Sha Tin, N.T., Hong Kong
[3]School of Geosciences, University of Edinburgh, UK
[4]Department of Geography and Resource Management, The Chinese University of Hong Kong, Sha Tin, N.T., Hong Kong
[5]Geophysical Fluid Dynamics Laboratory/NOAA, Princeton, New Jersey, USA
[6]School of Earth and Space Sciences, University of Science and Technology of China, Hefei, Anhui, China
[7]State Key Laboratory of Severe Weather, Chinese Academy of Meteorological Sciences, Beijing 100081, China

Correspondence to: Steve H.L. Yim (steveyim@cuhk.edu.hk)

1. WRF-Chem model configuration

WRF-Chem is a fully online model coupled with gas-phase chemistry mechanisms and aerosol physiochemical modules. In this model, chemical and meteorological components share the same grid coordinates, time steps, transport schemes, and subgrid physics. The meteorological component (WRF) of this coupled model uses an Eulerian dynamical core with a nonhydrostatic solver (Skamarock et al., 2008). Gas-phase chemical reactions are estimated using the carbon bond chemical mechanism (Zaveri and Peters, 1999). Aerosol physics and chemistry are treated using the Model for Simulating Aerosol Interactions and Chemistry (MOSAIC) scheme (Zaveri et al., 2008) with aqueous chemistry. The aerosol size distribution is represented by four discrete size bins within the MOSAIC scheme: 0.039–0.156 μm, 0.156–0.625 μm, 0.625–2.5 μm, and 2.5–10 μm (Fast et al., 2006). The approach to aerosol dry deposition is based on Binkowski and Shankar (1995). In-cloud (rainout) and below-cloud (washout) removal of aerosols by resolved clouds and precipitation are simulated following Easter et al. (2004) and Chapman et al. (2009), respectively. The transport and wet removal of aerosols by convective clouds are also considered using the Kain–Fritsch (KF) scheme (Kain and Fritsch, 1990) following Zhao et al. (2009, 2013~~b~~). The major physical schemes of meteorological components comprise the KF cumulus scheme; the Yonsei University (YSU) planetary boundary layer (PBL) scheme (Hong et al., 2006); the National Center for Environmental Prediction, Oregon State University, Air Force, and Hydrologic Research Lab's (NOAH) land surface model (Chen and Dudhia, 2001); the Morrison two-moment scheme for cloud microphysics (Morrison et al., 2009); and the rapid radiative transfer for global (RRTMG) for both longwave and shortwave radiation schemes (Iacono et al., 2008). Aerosol interactions with shortwave and longwave radiation are incorporated into the model by linking aerosol optical properties, including optical depth, single-scattering albedo, and asymmetry factor, to RRTMG shortwave and longwave schemes, respectively (Zhao et al., 2010, 2011). The effects of ACI

Formatted: Font: Bold

Formatted: Indent: Left: 0", Hanging: 0.19", Numbered + Level: 1 + Numbering Style: 1, 2, 3, … + Start at: 1 + Alignment: Left + Aligned at: 0.25" + Indent at: 0.5" are estimated by considering the activation of aerosols to form cloud droplets based on the maximum supersaturation in the Morrison microphysical scheme (Chapman et al., 2009; Yang et al., 2011).

2. Figures

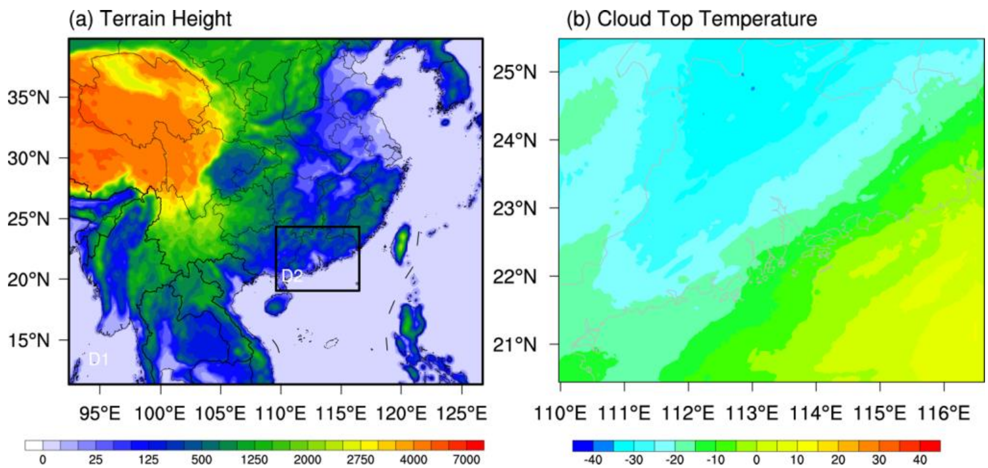

Figure S1. (a) WRF-Chem model two-nested domains with resolutions of 20 km and 4 km for domain 1 (D1) and domain 2 (D2), respectively. Shading represents terrain height (~~unit:~~ m). (b) Spatial distribution of 3-day averaged cloud top temperature (shading; ~~unit:~~ °C) during December 14–16, 2013 over domain 2 in control run.

Formatted: Font: Bold

Formatted: List Paragraph, Indent: Left: 0", Hanging: 0.19", Numbered + Level: 1 + Numbering Style: 1, 2, 3, … + Start at: 1 + Alignment: Left + Aligned at: 0.25" + Indent at: 0.5"

Formatted: English (United States)

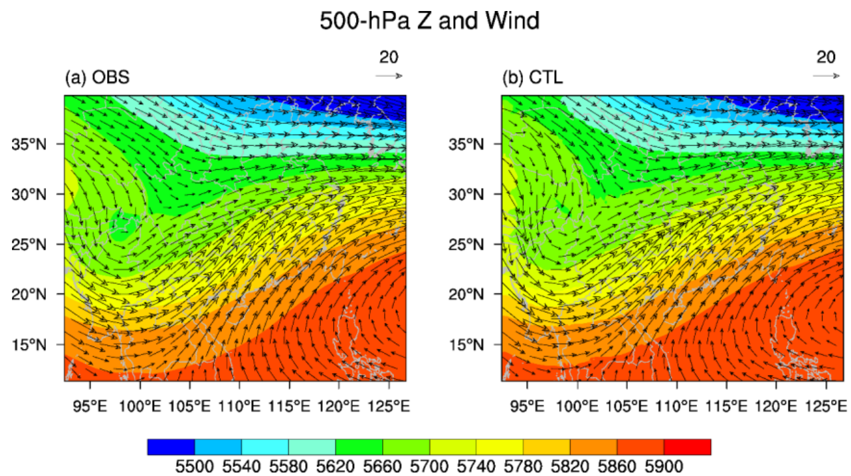

Figure S2. Spatial distribution of 3-day averaged 500-hPa wind (vector; ~~unit:~~ m s^{-1}) and height (shading; ~~unit:~~ m) during December 14–16, 2013 for (a) OBS from ERA-interim and (b) CTL from control simulation.

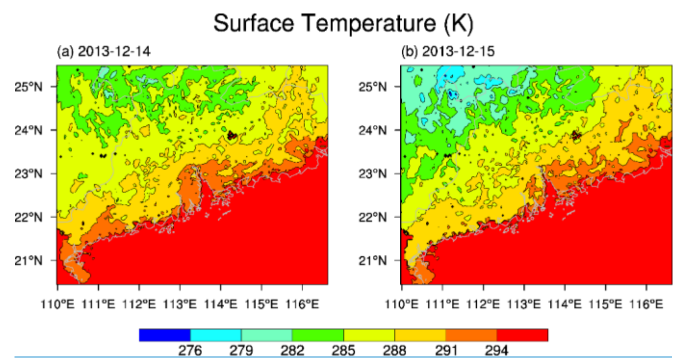

Figure S3. Spatial distribution of surface temperature (K) on (a) December 14 and (b) December 15 in 2013 in the CTL run.

Formatted: Caption

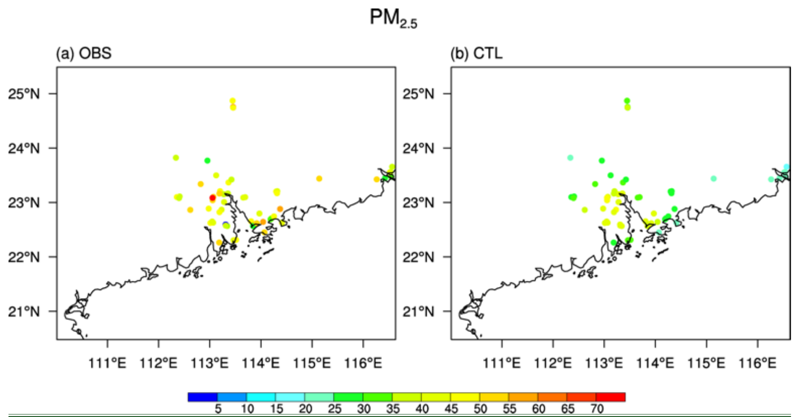

Figure S446. $PM_{2.5}$ concentration (~~unit:~~ μg m^{-3}) average during December 14–16, 2013 for (a) observation and (b) control simulation. Colored circles denote in situ station locations.

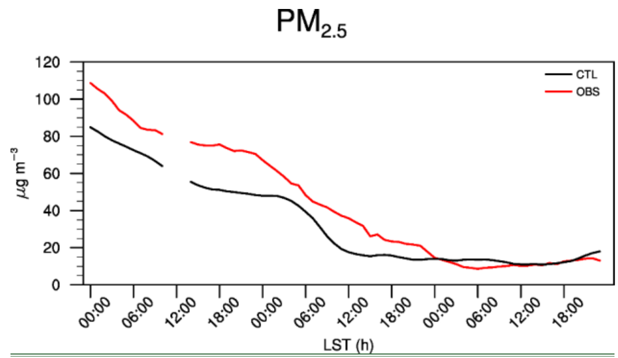

Figure S557. Time series of $PM_{2.5}$ concentration averaged over all the air quality stations during December 14–16, 2013 for CTL (black) and OBS (red).

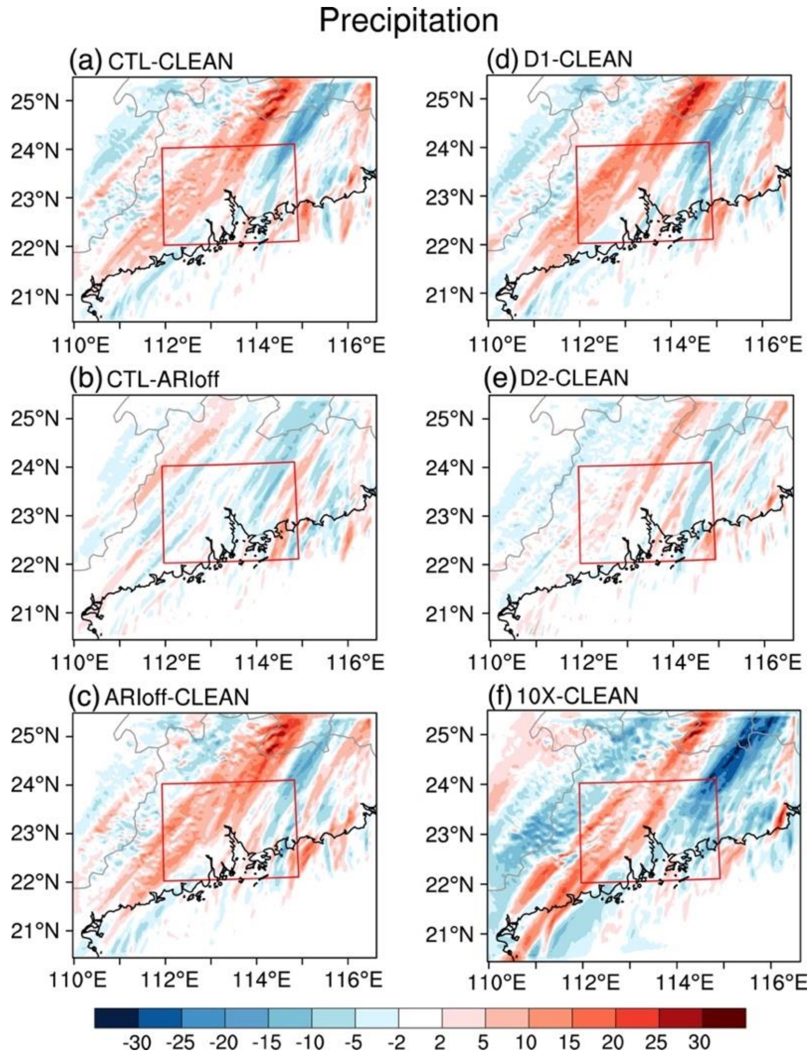

~~**Figure S3. Differences in accumulated precipitation (unit: mm) on December 16 between (a) CTL and CLEAN (i.e., CTL minus CLEAN), (b) CTL and ARIoff (i.e., CTL minus ARIoff), (c) ARIoff and CLEAN (i.e., ARIoff minus CLEAN), (d) D1 and CLEAN (i.e., D1 minus CLEAN), (e) D2 and CLEAN (D2 minus CLEAN), and (f) 10X and CLEAN (10X minus CLEAN). Red boxes (22°–24° N, 112°–115° E) denote the analysis region. ARIoff run refers to simulation with aerosol-radiation interactions off.**~~

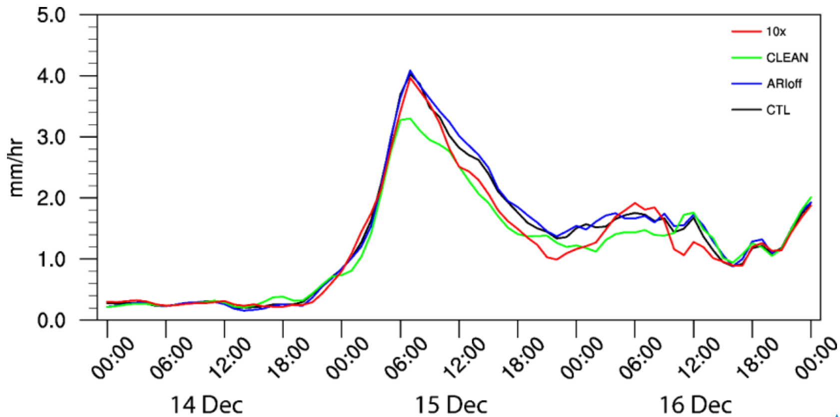

~~Figure S4. Time series of station average rain rate (unit: mm h^{-1}) over 22°–24° N, 112°–115° E (a) for OBS (red), CMORPH (black), CTL (blue), ARIoff (green), and CLEAN (purple).~~

Formatted: Caption

Formatted: English (United States)

Formatted: English (United Kingdom)

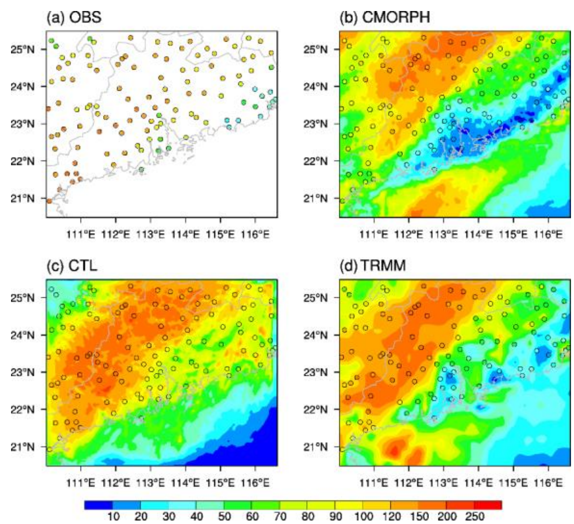

Figure S6~~65~~. Spatial distribution of accumulated precipitation (~~unit:~~ mm) from 00Z on December 14, 2013~~,~~ to 00Z on December 17, 2013 from (a) station observations (OBS), (b) CMORPH, (c) control simulation (CTL), and (d) TRMM. Circles denote locations of in situ observations.

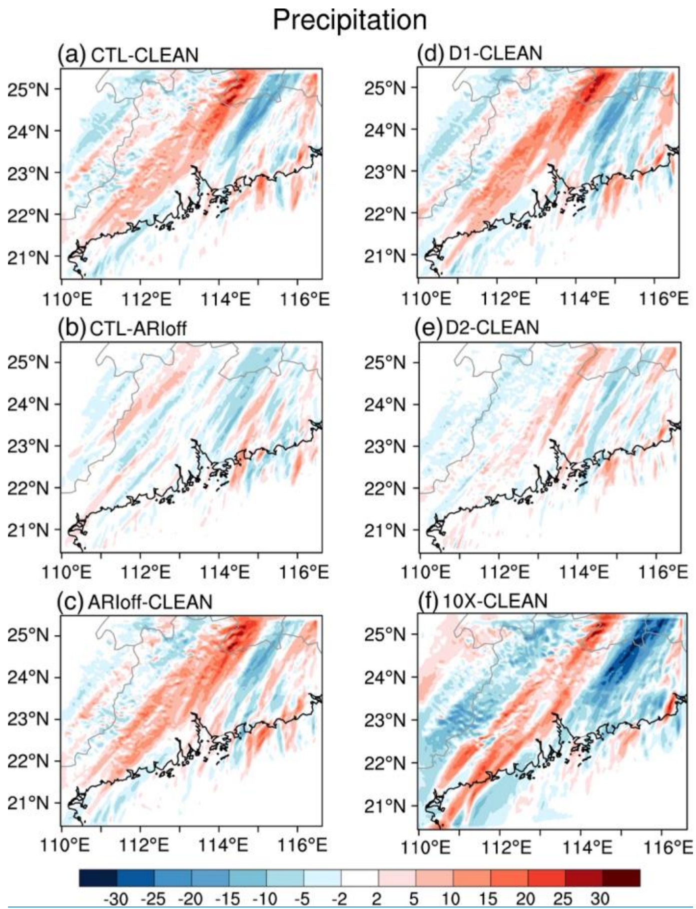

Figure S7. Differences in accumulated precipitation (mm) on December 16 between (a) CTL and CLEAN, (b) CTL and ARIoff, (c) ARIoff and CLEAN, (d) D1 and CLEAN, (e) D2 and CLEAN, and (f) 10× and CLEAN. ARIoff run refers to simulation with aerosol-radiation interactions off.

Formatted: Caption

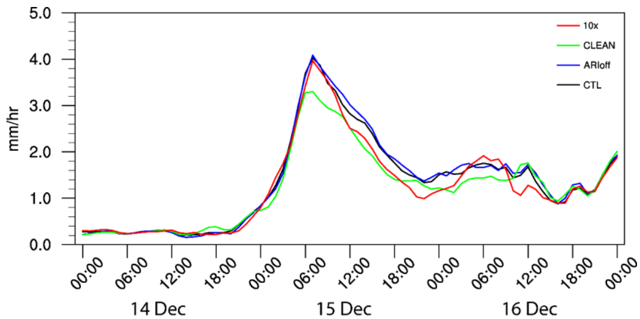

Figure S8. Time series of rain rate (mm h^{-1}) averaged over R1 (a) for 10× (red), CTL (black), ARIoff (blue), and CLEAN (green).

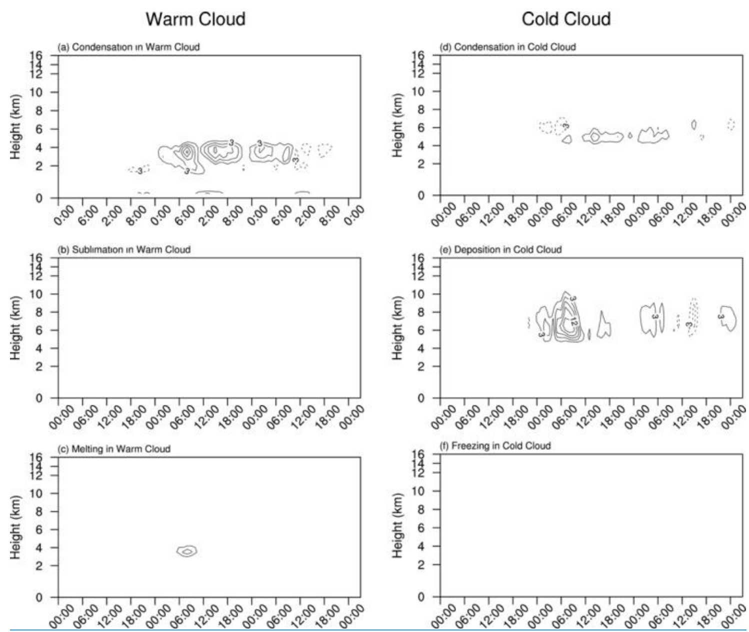

Figure S9. Differences with time (abscissa) and height (ordinate) in latent heat release (K d^{-1}) from (a) condensation, (b) deposition, and (c) freezing processes between CTL and CLEAN averaged over R1 for warm cloud. (d–f) Same as (a–c) but for cold cloud. Zero-value contour lines are omitted, and negative values are dashed. The contour interval is 3 K d^{-1}.

Formatted: Normal

Formatted: Font: 9 pt, Bold

Formatted: (Asian) Chinese (PRC), (Other) English (United States)

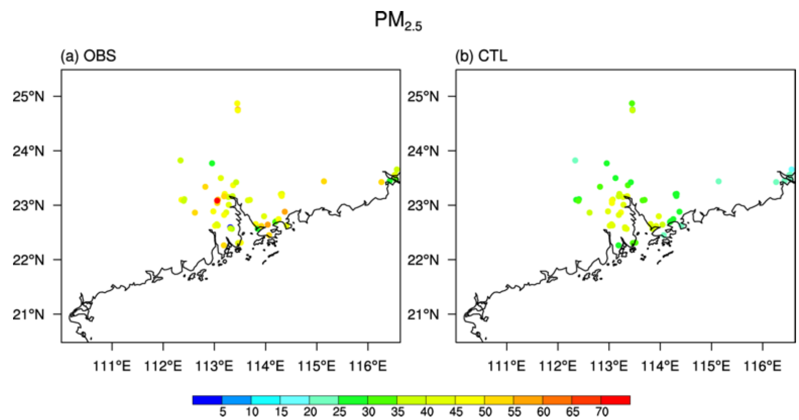

~~Figure S6. $PM_{2.5}$ concentration (unit: μg m^{-3}) average during December 14–16, 2013 for (a) observation and (b) control simulation. Colored circles denote in situ station locations.~~

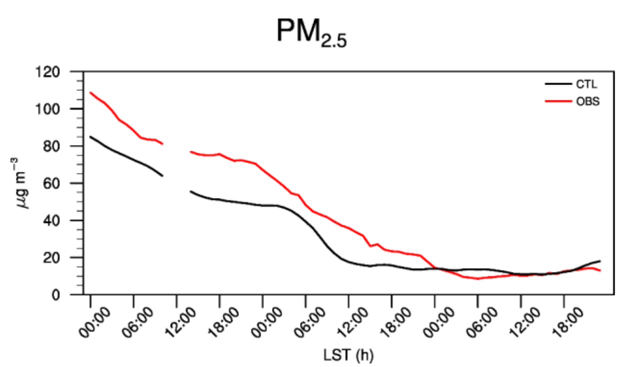

~~Figure S7. Time series of $PM_{2.5}$ averaged over all the stations during December 14–16, 2013 for CTL (black) and OBS (red).~~

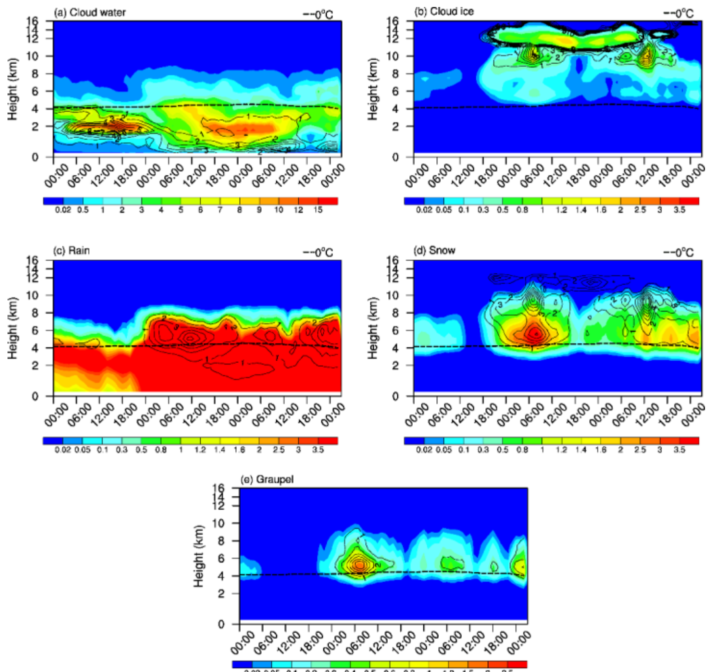

Figure S10~~108~~. Distribution with time (abscissa) and height (ordinate) in (a) cloud water (shading; ~~unit:~~ 10^{-5} kg kg^{-1}) and CDNC (contour; ~~unit:~~ 10^{7} kg^{-1}), (b) cloud ice (shading; ~~unit:~~ 10^{-5} kg kg^{-1}) and CINC (contour; ~~unit:~~ 10^{4} kg^{-1}), (c) rain (shading; ~~unit:~~ 10^{-5} kg kg^{-1}) and rain number concentration (contour; ~~unit:~~ 10^{5} kg^{-1}), (d) snow (shading; ~~unit:~~ 10^{-4} kg kg^{-1}) and snow number concentrations (contour; ~~unit:~~ 10^{3} kg^{-1}), and (e) graupel (shading; ~~unit:~~ 10^{-4} kg kg^{-1}) and graupel number concentration (contour; ~~unit:~~ 10^{3} kg^{-1}) averaged over R1 ~~the red box~~ in CTL run. ~~Only anomalies that exceed 90% significance level are depicted with shading and contour.~~

Formatted: Caption

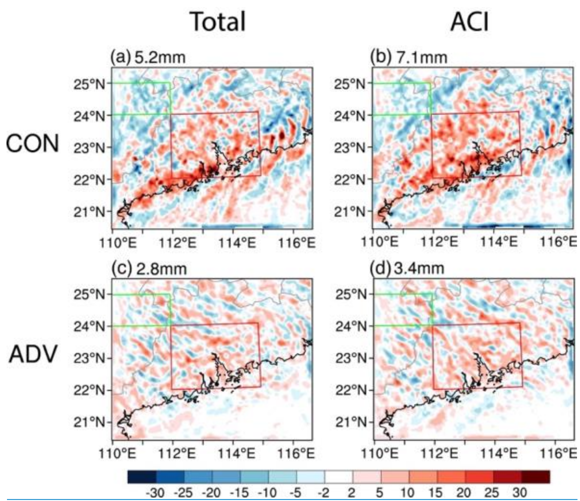

Figure S11. Differences in column-integrated moisture convergence (CON; mm) between (a) CTL and CLEAN and (b) ARIoff and CLEAN on December 15. (c, d) Same as (a, b) but for column-integrated advection of water vapor (ADV; mm). The numbers at the top-left corner of each panel represent the values averaged over R1.

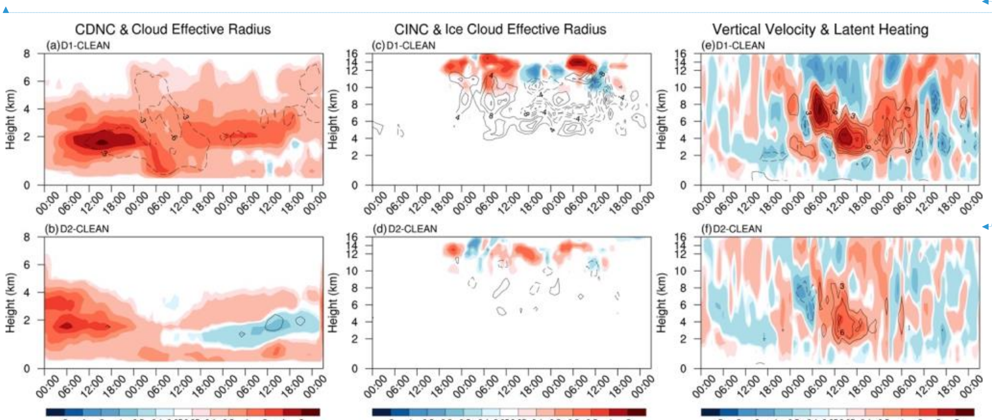

Figure S12. Differences with time (abscissa) and height (ordinate) in (a) CDNC (shading; 10^7 kg^{-1}) and cloud effective radius (contour; µm), (c) CINC (shading; 10^5 kg^{-1}) and ice cloud effective radius (contour; µm), and (e) vertical velocity (shading; cm s^{-1}) and latent heating (contour; K d^{-1}) averaged over R1 between D1 and CLEAN. (b, d, f) same as (a, c, e) but for differences between D2 and CLEAN. Zero-value contour lines are omitted, and negative values are dashed.

Formatted: English (United States)

Formatted: Normal

Formatted: Justified

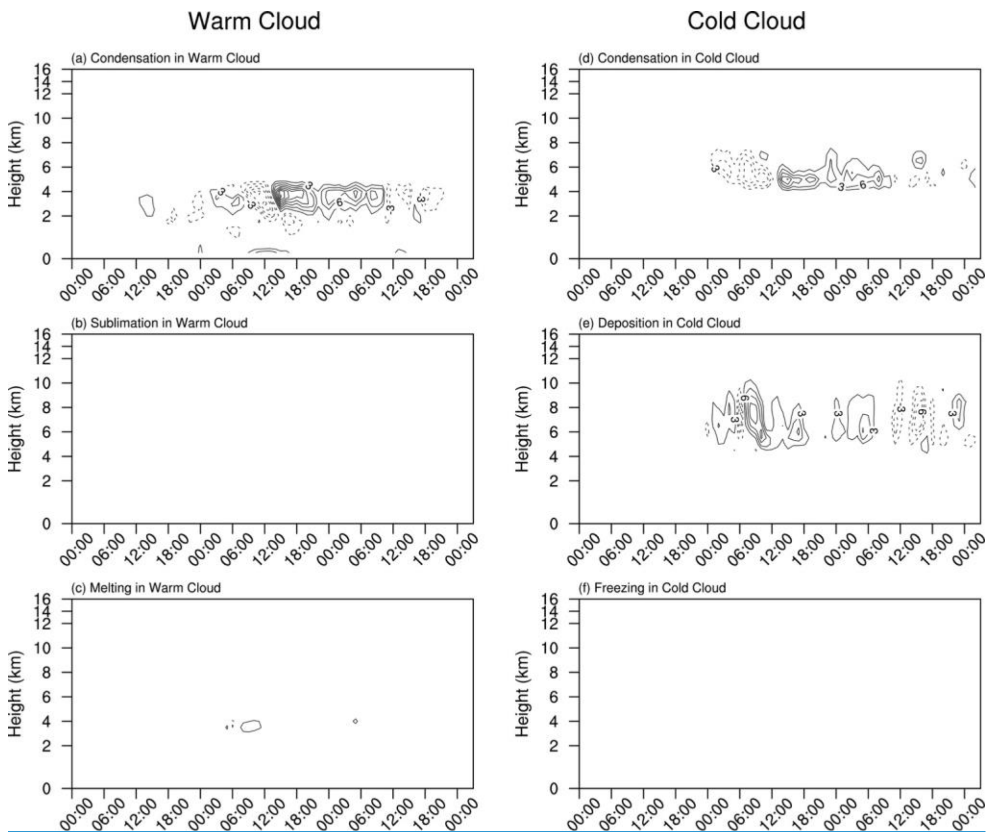

Figure S13. Differences with time (abscissa) and height (ordinate) in latent heat release (K d^{-1}) from (a) condensation, (b) deposition, and (c) freezing processes between D1 and CLEAN averaged over R1 for warm cloud. (d–f) Same as (a–c) but for cold cloud.

Formatted: Normal

Formatted: Font: 9 pt, Bold

Formatted: (Asian) Chinese (PRC), (Other) English (United States)

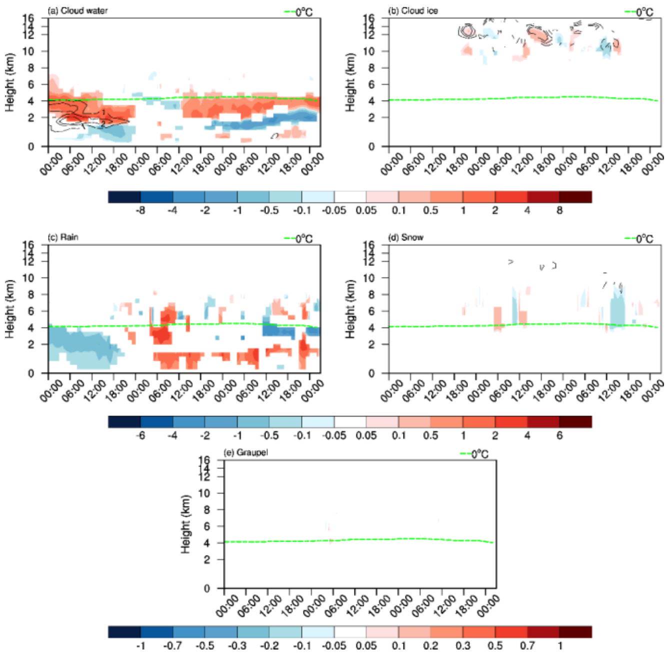
(a) Cloud water
(b) Cloud ice
(c) Rain
(d) Snow
(e) Graupel
0°C
Height (km)
00:00 06:00 12:00 18:00 00:00 06:00 12:00 18:00 00:00 06:00 12:00 18:00 00:00
-8 -4 -2 -1 -0.5 -0.1 -0.05 0.05 0.1 0.5 1 2 4 8
-6 -4 -2 -1 -0.5 -0.1 -0.05 0.05 0.1 0.5 1 2 4 6
-1 -0.7 -0.5 -0.3 -0.2 -0.1 -0.05 0.05 0.1 0.2 0.3 0.5 0.7 1

Formatted: English (United States)

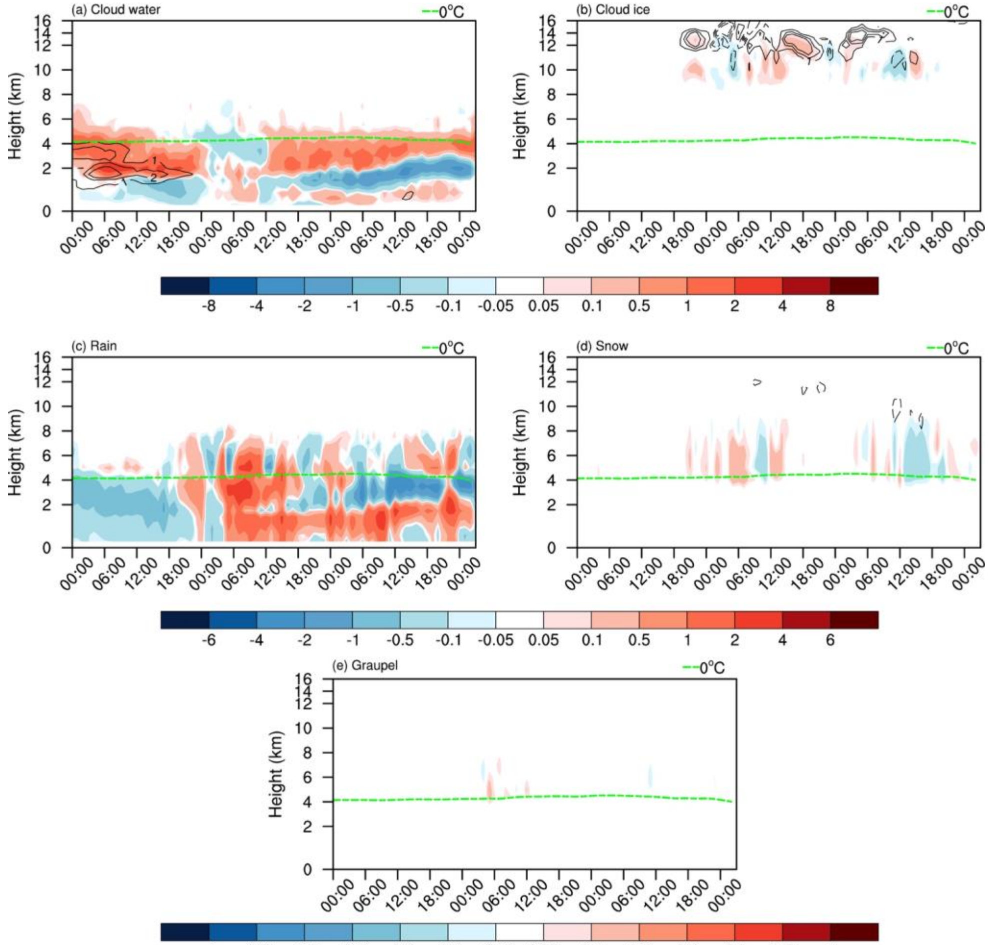

Figure S14~~149~~. Differences with time (abscissa) and height (ordinate) in (a) cloud water (shading; ~~unit:~~ 10^{-5} kg kg^{-1}) and CDNC (contour; ~~unit:~~ 10^{7} kg^{-1}), (b) cloud ice (shading; ~~unit:~~ 10^{-5} kg kg^{-1}) and CINC (contour; ~~unit:~~ 10^{4} kg^{-1}), (c) rain (shading; unit: 10^{-5} kg kg^{-1}) and rain number concentration (contour; ~~unit:~~ 10^{5} kg^{-1}), (d) snow (shading; ~~unit:~~ 10^{-4} kg kg^{-1}) and snow number concentrations (contour; ~~unit:~~ 10^{3} kg^{-1}), and (e) graupel (shading; ~~unit:~~ 10^{-4} kg kg^{-1}) and graupel number concentration (contour; ~~unit:~~ 10^{3} kg^{-1}) between D2 and CLEAN ~~(i.e. D2 minus CLEAN)~~ averaged over R1~~the red box~~. ~~Only anomalies that exceed 90% significance level are depicted with shading and contour.~~

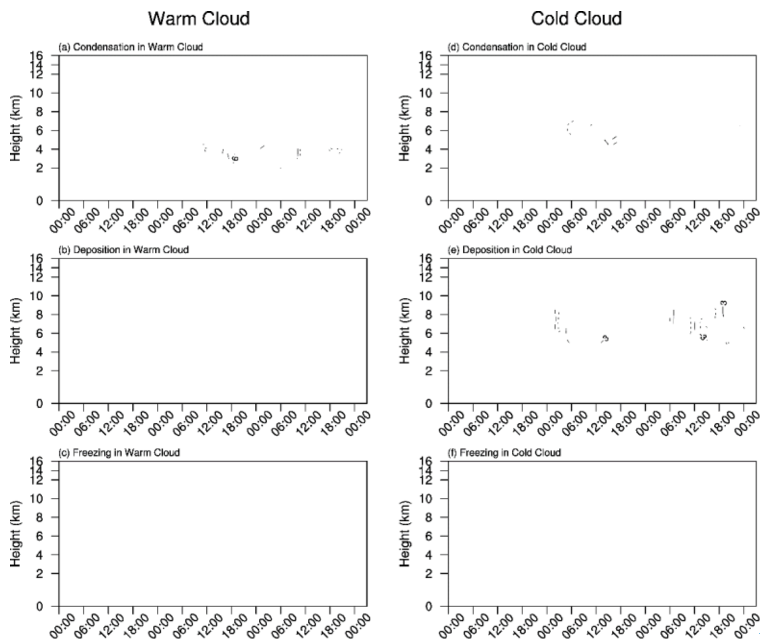

Warm Cloud
Cold Cloud
(a) Condensation in Warm Cloud
(b) Deposition in Warm Cloud
(c) Freezing in Warm Cloud
(d) Condensation in Cold Cloud
(e) Deposition in Cold Cloud
(f) Freezing in Cold Cloud
Height (km)
00:00 06:00 12:00 18:00 00:00 06:00 12:00 18:00 00:00 06:00 12:00 18:00 00:00

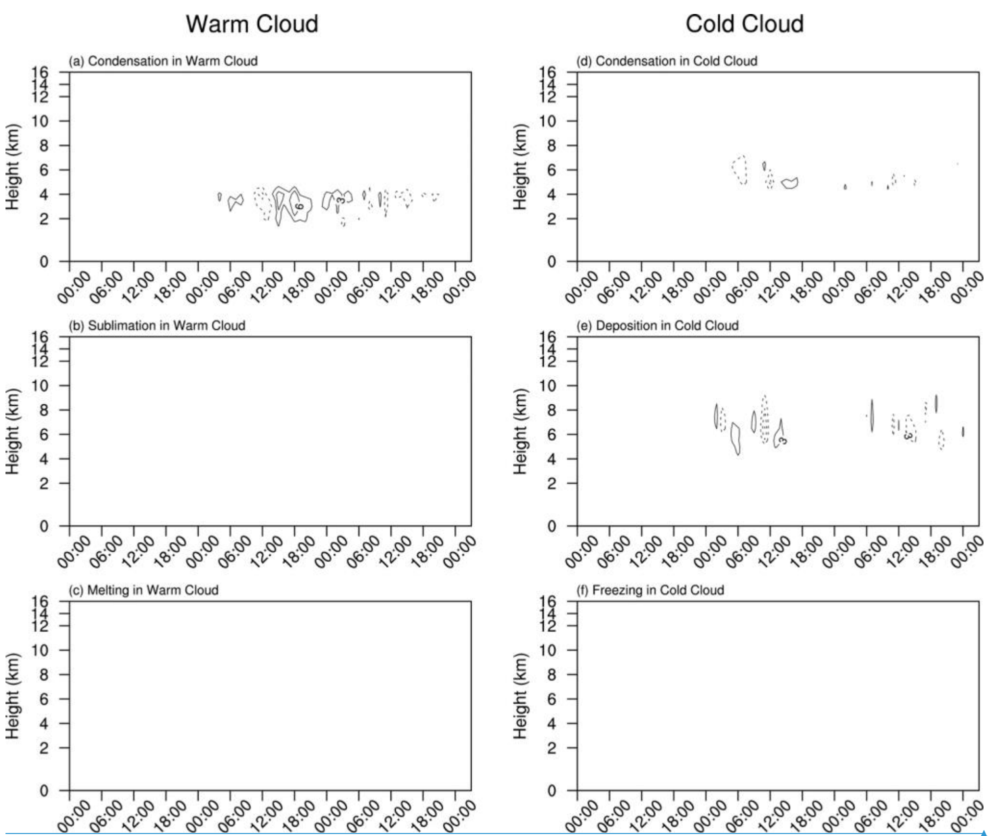

Figure S15~~15~~~~10~~. Differences with time (abscissa) and height (ordinate) in latent heat release (~~unit:~~ K d^{-1}) from (a) condensation, (b) deposition, and (c) freezing processes between D2 and CLEAN ~~(i.e. D2 minus CLEAN)~~ averaged over R1 ~~the red box~~ for ~~the~~ warm cloud. (d–f) Same as (a–c) but for~~rom~~ cold cloud. ~~Only anomalies that exceed 90% significance level are depicted with and contour.~~ Zero-value contour lines are omitted, and negative values are dashed. The contour interval is 3 K d^{-1}. ~~Note the blank represent the values are within 3 K d^{-1}.~~

Formatted: English (United States)

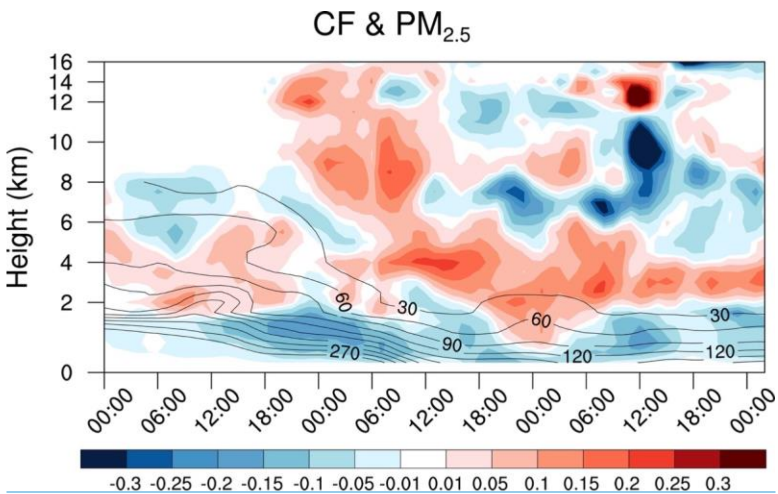

Figure S16. Differences in the time-height cross section of cloud factor CF (shading; unitless) and $PM_{2.5}$ concentration (contour; μg m^{-3}) averaged over R1 between 10× and CLEAN.

Formatted: Normal

Formatted: Font: 9 pt, Bold

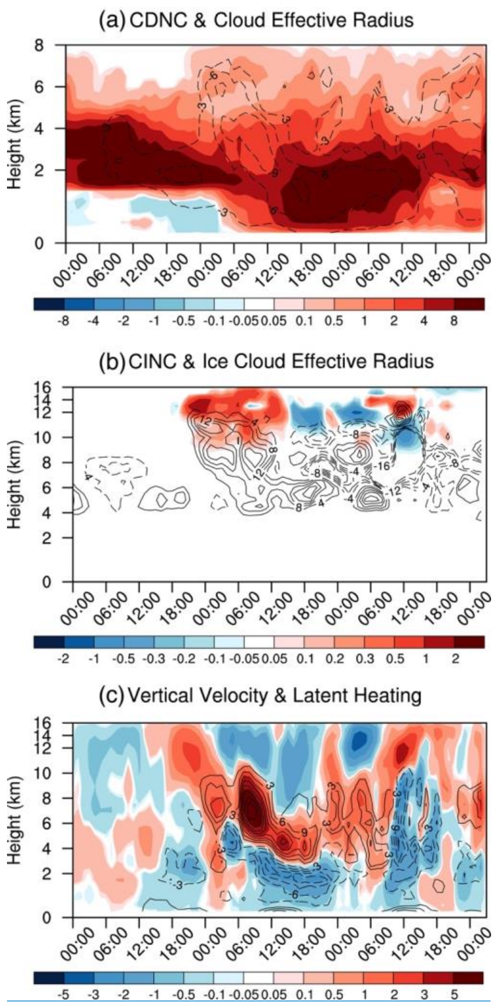

Figure S17. Differences with time (abscissa; from 00Z on December 14 to 02Z on December 17) and height (ordinate) in (a) CDNC (shading; 10^7 kg^{-1}) and cloud effective radius (μm), (b) CINC (shading; 10^5 kg^{-1}) and ice cloud effective radius (contour; μm), and (c) vertical velocity (shading; cm s^{-1}) and latent heating (contour; K d^{-1}) averaged over R1 between 10× and CLEAN.

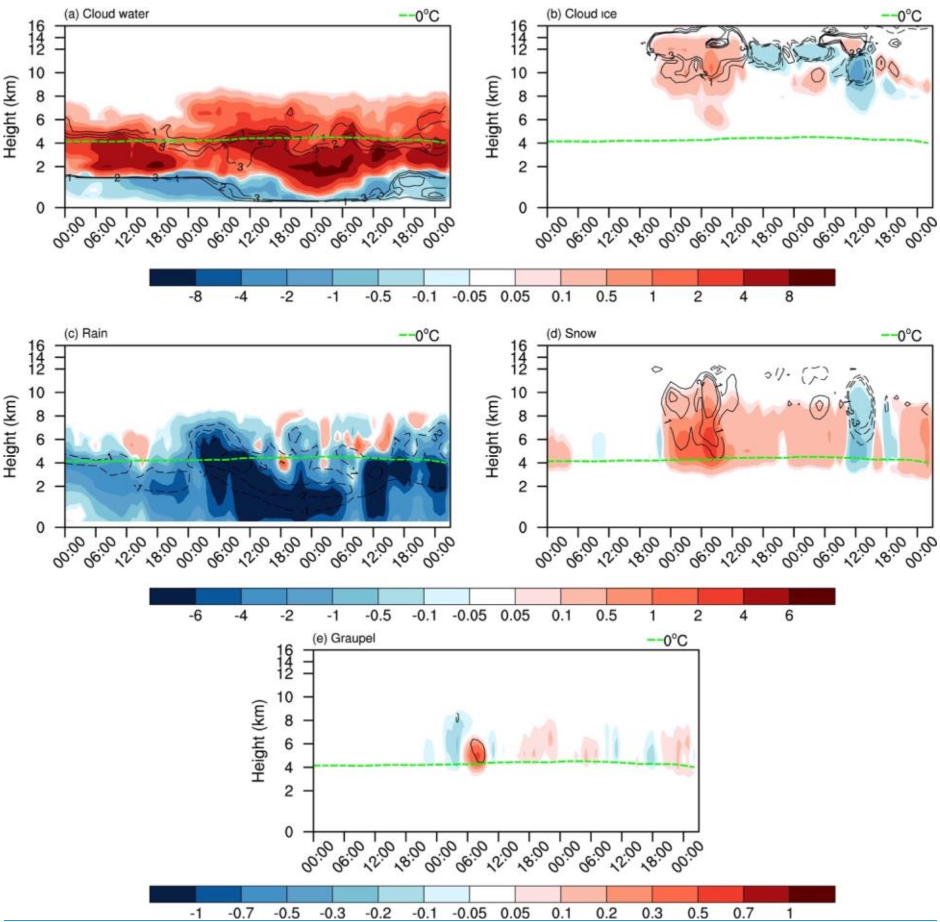

Figure S18. Differences with time (abscissa) and height (ordinate) in (a) cloud water (shading; 10^{-5} kg kg^{-1}) and CDNC (contour; 10^{7} kg^{-1}), (b) cloud ice (shading; 10^{-5} kg kg^{-1}) and CINC (contour; 10^{4} kg^{-1}), (c) rain (shading; 10^{-5} kg kg^{-1}) and rain number concentration (contour; 10^{5} kg^{-1}), (d) snow (shading; 10^{-4} kg kg^{-1}) and snow number concentration (contour; 10^{3} kg^{-1}), and (e) graupel (shading; 10^{-4} kg kg^{-1}) and graupel number concentration (contour; 10^{3} kg^{-1}) between 10× and CLEAN averaged over R1.

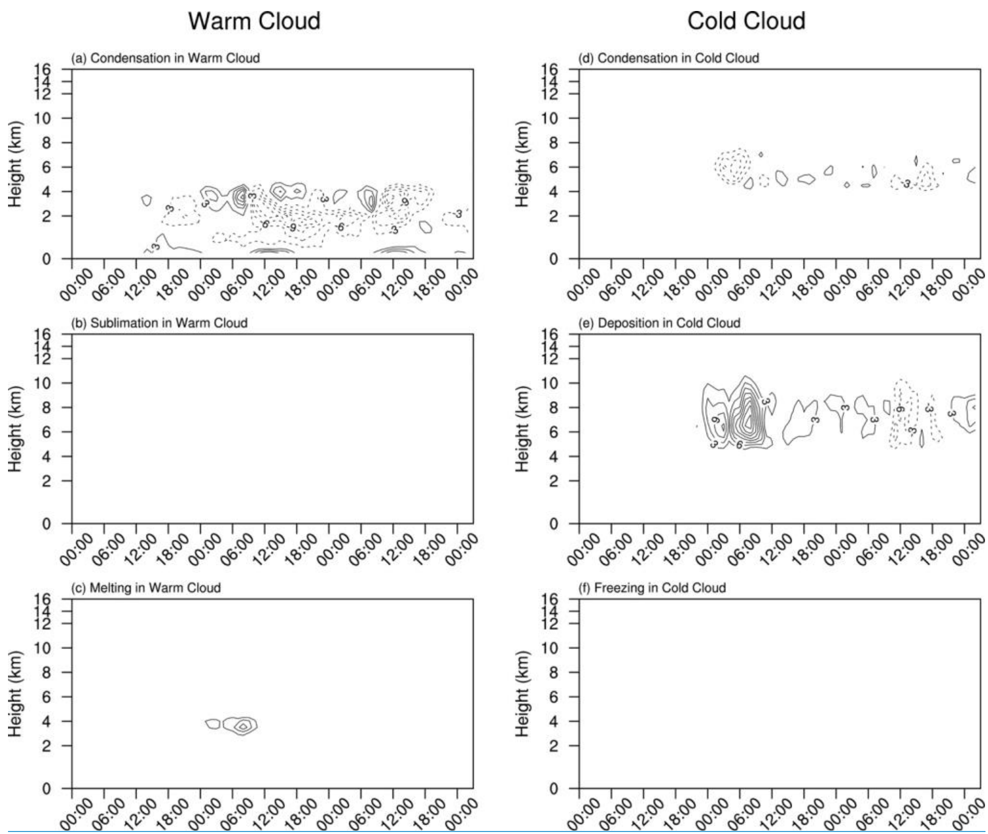

Figure S19. Differences with time (abscissa) and height (ordinate) in latent heat release (K d^{-1}) from (a) condensation, (b) deposition, and (c) freezing processes between 10× and CLEAN averaged over R1 for warm cloud. (d–f) Same as (a–c) but for cold cloud.

Formatted: Font: 9 pt, Bold

Formatted: Font: Bold

Formatted: Font: 9 pt, Bold

Formatted: Font: 9 pt, Bold, English (United Kingdom)

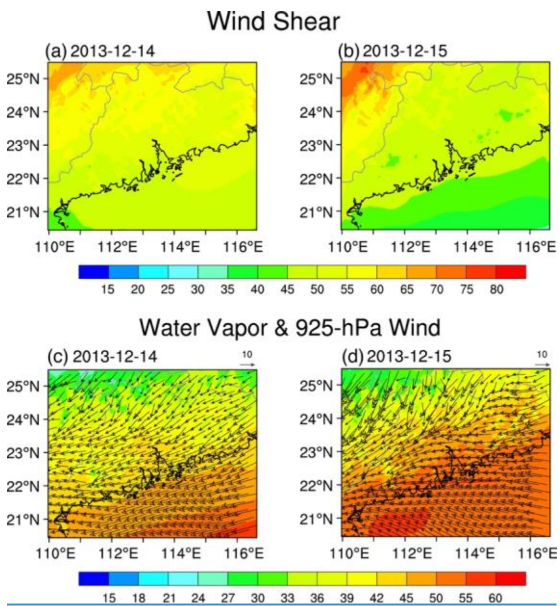

Figure S20. Spatial distribution of wind shear (m s^{-1}) on (a) December 14 and (b) December 15 in 2013 in the CTL run. Wind shear is calculated as differences between maximum wind speed and minimum wind speed at 0–10 km. Spatial distribution of column-integrated water vapor (shading; mm day^{-1}) and 925-hPa wind (vector; m s^{-1}) on (c) December 14 and (d) December 15 in 2013 in CTL.

Formatted: Centered

Formatted: English (United States)

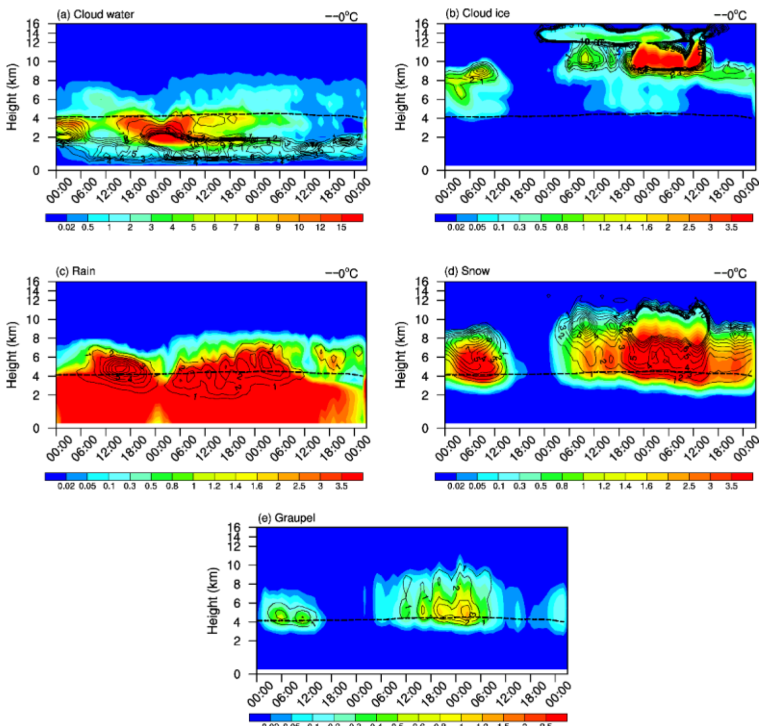

Figure S21~~2111~~. Distribution with time (abscissa) and height (ordinate) in (a) cloud water (shading; ~~unit:~~ 10^{-5} kg kg^{-1}) and CDNC (contour; unit: 10^{7} kg^{-1}), (b) cloud ice (shading; ~~unit:~~ 10^{-5} kg kg^{-1}) and CINC (contour; ~~unit:~~ 10^{4} kg^{-1}), (c) rain (shading; ~~unit:~~ 10^{-5} kg kg^{-1}) and rain number concentration (contour; ~~unit:~~ 10^{5} kg^{-1}), (d) snow (shading; ~~unit:~~ 10^{-4} kg kg^{-1}) and snow number concentrations (contour; ~~unit:~~ 10^{3} kg^{-1}), and (e) graupel (shading; ~~unit:~~ 10^{-4} kg kg^{-1}) and graupel number concentration (contour; ~~unit:~~ 10^{3} kg^{-1}) averaged over R2 ~~the region in 24°–25°N, 110°–112°E~~ from CTL run. ~~Only anomalies that exceed 90% significance level are depicted with shading and contour.~~

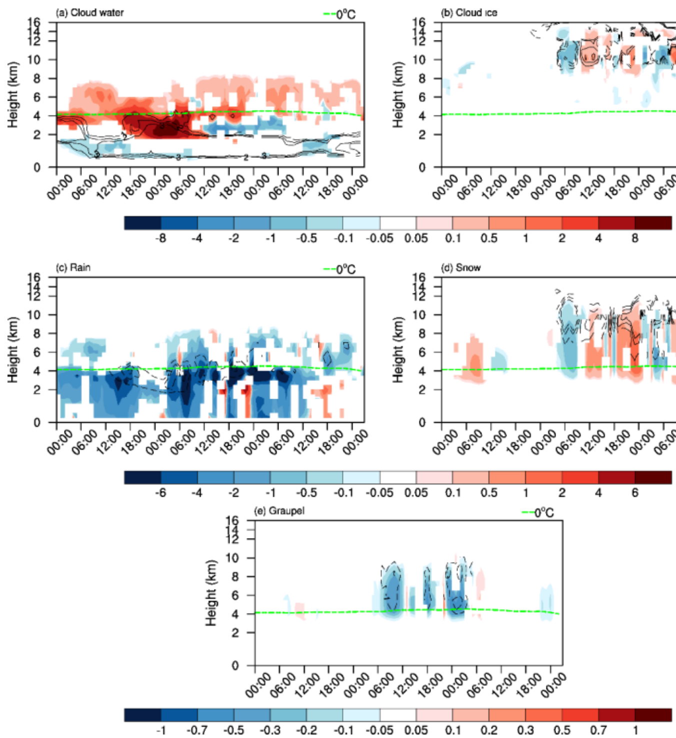
(a) Cloud water
(b) Cloud ice
(c) Rain
(d) Snow
(e) Graupel
0°C
Height (km)
-8 -4 -2 -1 -0.5 -0.1 -0.05 0.05 0.1 0.5 1 2 4 8
-6 -4 -2 -1 -0.5 -0.1 -0.05 0.05 0.1 0.5 1 2 4 6
-1 -0.7 -0.5 -0.3 -0.2 -0.1 -0.05 0.05 0.1 0.2 0.3 0.5 0.7 1

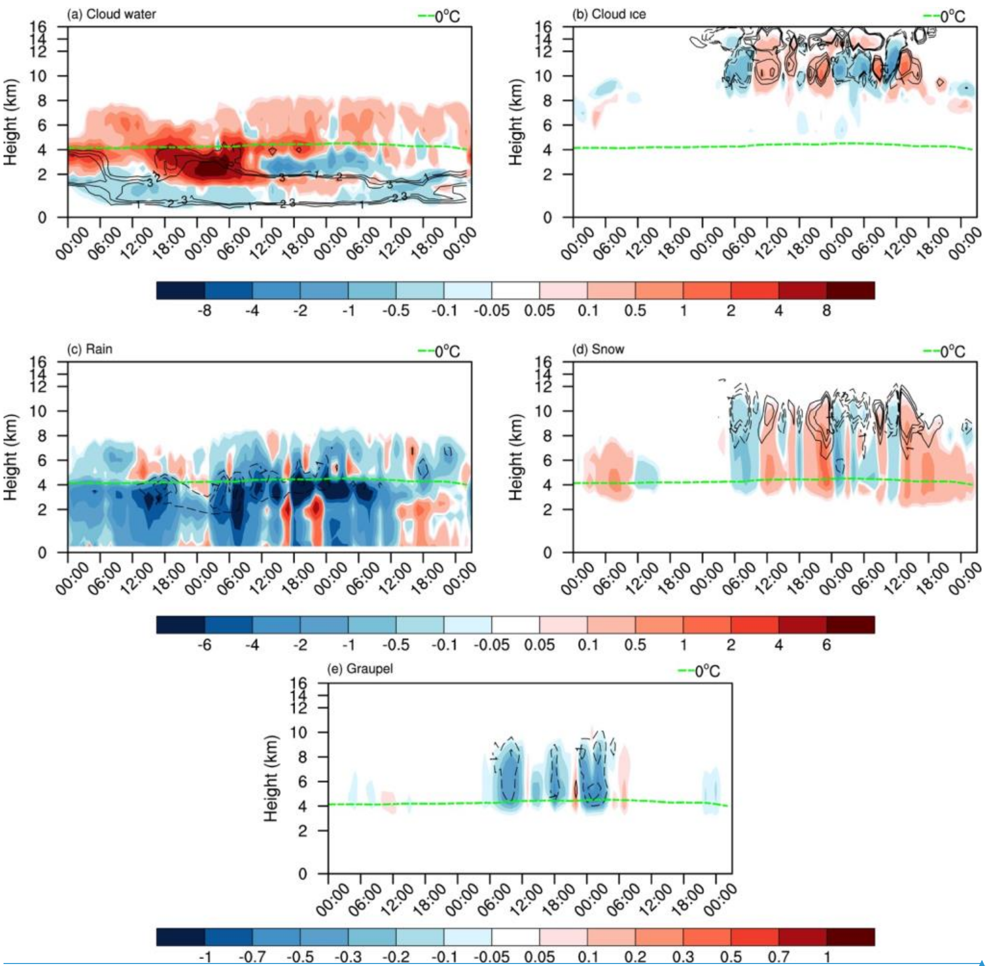

Figure S2222~~12~~. Differences with time (abscissa) and height (ordinate) in (a) cloud water (shading; ~~unit:~~ 10^{-5} kg kg^{-1}) and CDNC (contour; ~~unit:~~ 10^{7} kg^{-1}), (b) cloud ice (shading; ~~unit:~~ 10^{-5} kg kg^{-1}) and CINC (contour; ~~unit:~~ 10^{4} kg^{-1}), (c) rain (shading; ~~unit:~~ 10^{-5} kg kg^{-1}) and rain number concentration (contour; ~~unit:~~ 10^{5} kg^{-1}), (d) snow (shading; ~~unit:~~ 10^{-4} kg kg^{-1}) and snow number concentrations (contour; ~~unit:~~ 10^{3} kg^{-1}), and (e) graupel (shading; ~~unit:~~ 10^{-4} kg kg^{-1}) and graupel number concentration (contour; ~~unit:~~ 10^{3} kg^{-1}) between CTL and CLEAN ~~(i.e. CTL minus CLEAN)~~ averaged over R2~~the region in 24°–25°N, 110°–112°E~~. ~~Only anomalies that exceed 90% significance level are depicted with shading and contour.~~

Formatted: English (United States)

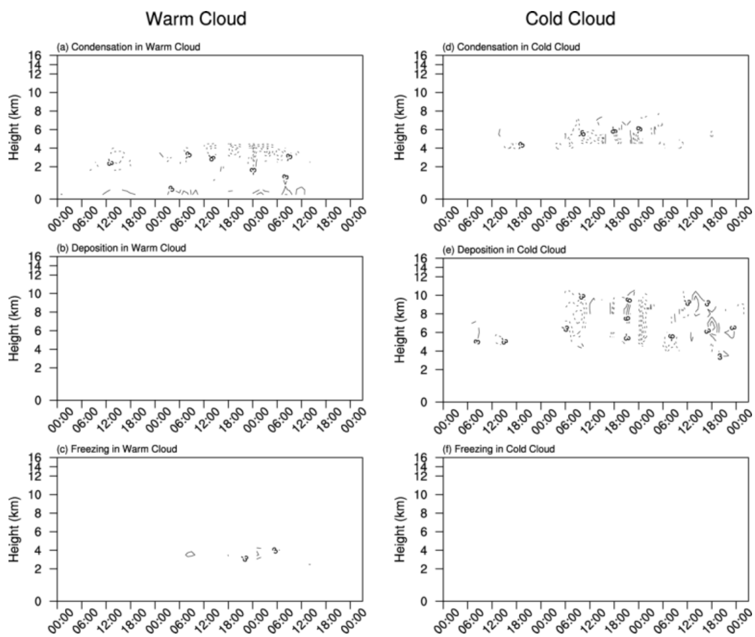

Warm Cloud
Cold Cloud
(a) Condensation in Warm Cloud
(b) Deposition in Warm Cloud
(c) Freezing in Warm Cloud
(d) Condensation in Cold Cloud
(e) Deposition in Cold Cloud
(f) Freezing in Cold Cloud
Height (km)

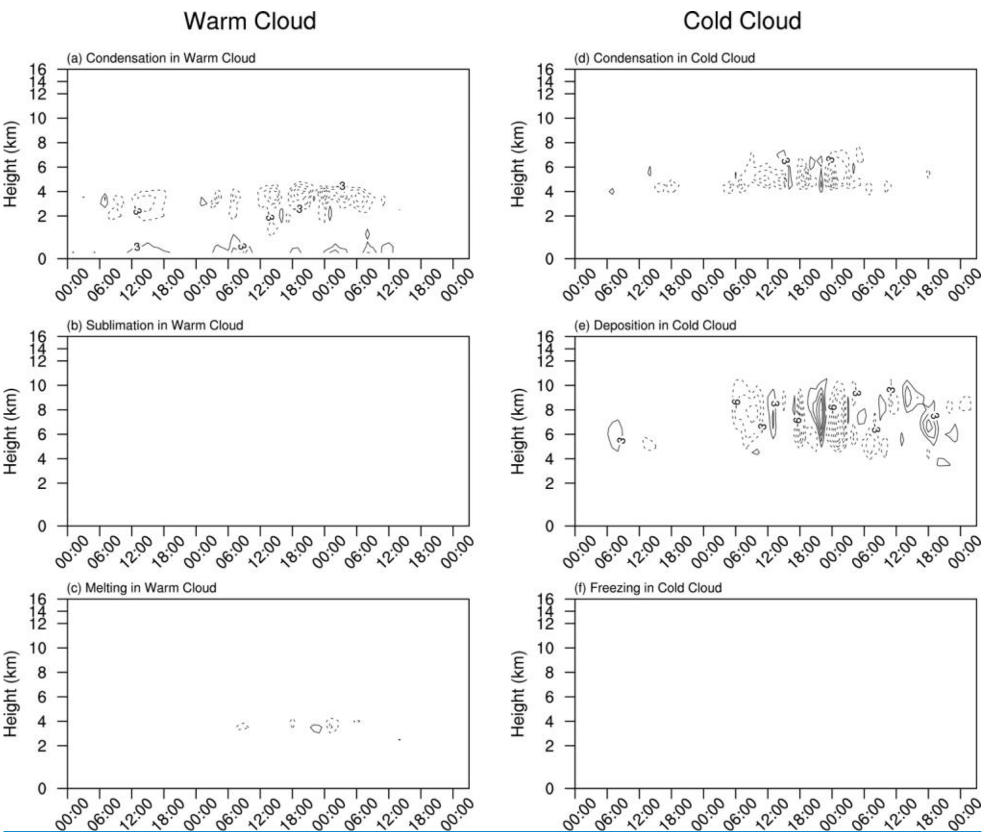

Figure S232~~313~~. Differences with time (abscissa) and height (ordinate) in latent heat release (~~unit:~~ K d^{-1}) from (a) condensation, (b) deposition, and (c) freezing processes between CTL and CLEAN ~~(i.e. CTL minus CLEAN)~~ averaged over R2 ~~the region in 24°–25°N, 110°–112°E~~ for ~~the~~ warm cloud. (d–f) Same as (a–c) but for~~rom~~ cold cloud. ~~Only anomalies that exceed 90% significance level are depicted with and contour. Zero-value contour lines are omitted, and negative values are dashed. The contour interval is 3 K d^{-1}. Note the blank represent the values are within 3 K d^{-1}.~~

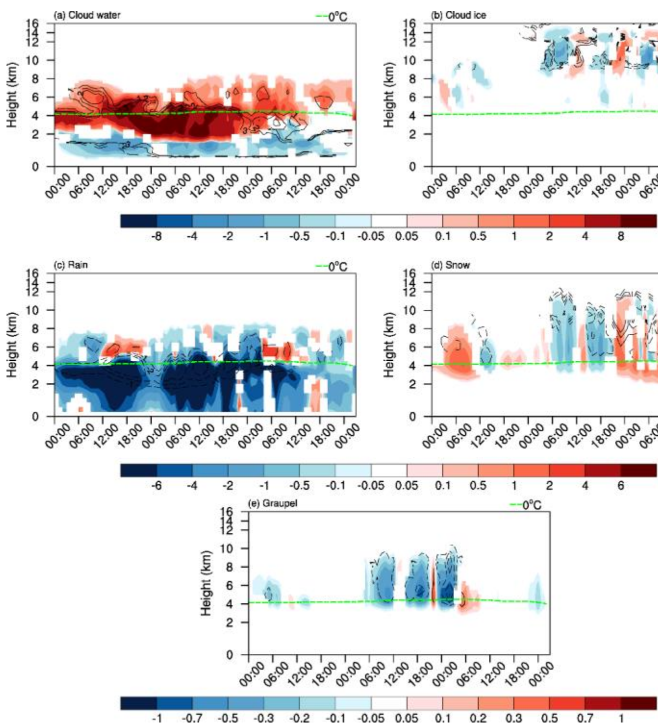
(a) Cloud water
(b) Cloud ice
(c) Rain
(d) Snow
(e) Graupel
0°C
Height (km)
00:00 06:00 12:00 18:00 00:00 06:00 12:00 18:00 00:00 06:00 12:00 18:00 00:00
-8 -4 -2 -1 -0.5 -0.1 -0.05 0.05 0.1 0.5 1 2 4 8
-6 -4 -2 -1 -0.5 -0.1 -0.05 0.05 0.1 0.5 1 2 4 6
-1 -0.7 -0.5 -0.3 -0.2 -0.1 -0.05 0.05 0.1 0.2 0.3 0.5 0.7 1

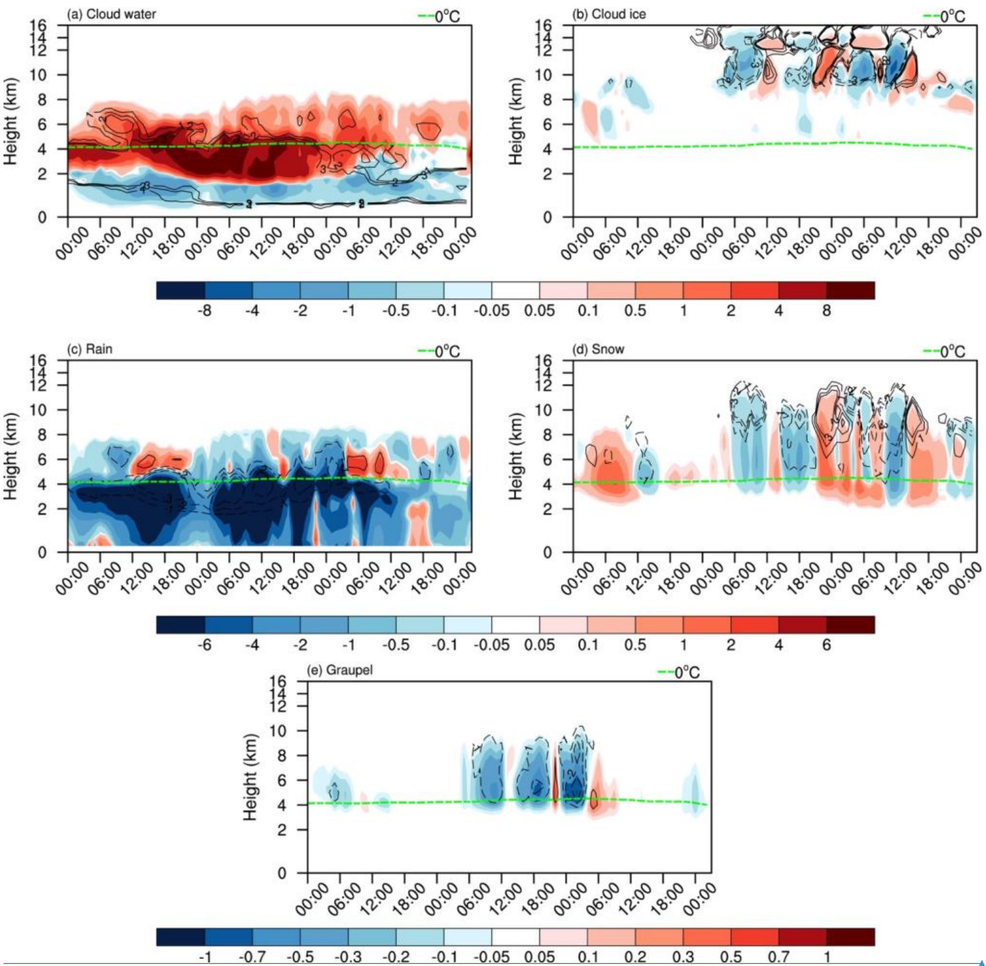

Figure S24~~24~~~~14~~. Differences with time (abscissa) and height (ordinate) in (a) cloud water (shading; ~~unit:~~ 10^{-5} kg kg^{-1}) and CDNC (contour; ~~unit:~~ 10^{7} kg^{-1}), (b) cloud ice (shading; ~~unit:~~ 10^{-5} kg kg^{-1}) and CINC (contour; ~~unit:~~ 10^{4} kg^{-1}), (c) rain (shading; ~~unit:~~ 10^{-5} kg kg^{-1}) and rain number concentration (contour; ~~unit:~~ 10^{5} kg^{-1}), (d) snow (shading; ~~unit:~~ 10^{-4} kg kg^{-1}) and snow number concentrations (contour; ~~unit:~~ 10^{3} kg^{-1}), and (e) graupel (shading; ~~unit:~~ 10^{-4} kg kg^{-1}) and graupel number concentration (contour; ~~unit:~~ 10^{3} kg^{-1}) between 10× and CLEAN ~~(i.e. 10× minus CLEAN)~~ averaged over R2~~over the region in 24°–25°N, 110°–112°E~~. ~~Only anomalies that exceed 90% significance level are depicted with shading and contour.~~

Formatted: English (United States)

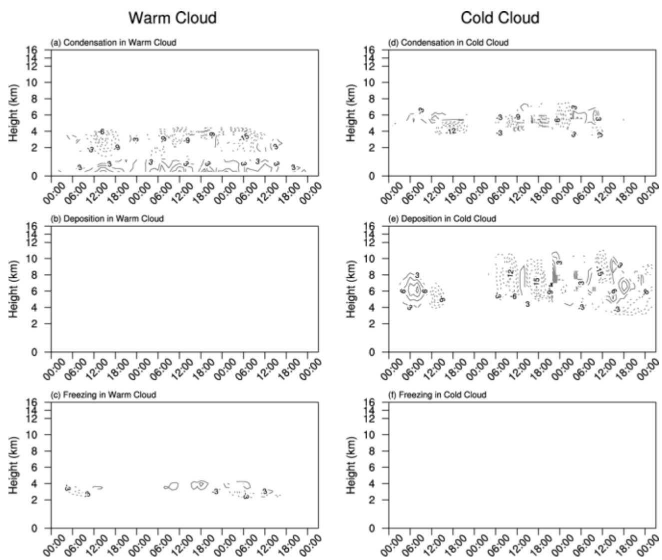

Warm Cloud
Cold Cloud
(a) Condensation in Warm Cloud
(b) Deposition in Warm Cloud
(c) Freezing in Warm Cloud
(d) Condensation in Cold Cloud
(e) Deposition in Cold Cloud
(f) Freezing in Cold Cloud
Height (km)
00:00
06:00
12:00
18:00

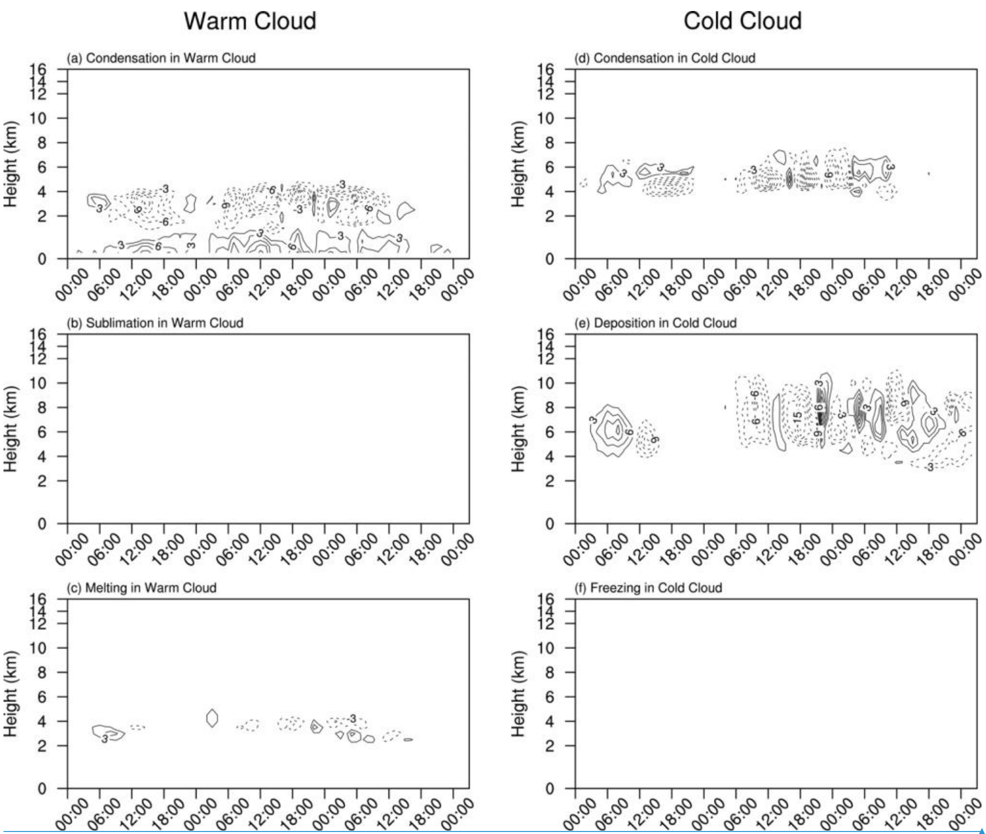

Figure S~~25~~25~~15~~15**. Differences** with time (abscissa) and height (ordinate) in latent heat release (~~unit:~~ K d^{-1}) from (a) condensation, (b) deposition, and (c) freezing processes between 10× and CLEAN ~~(i.e. 10× minus CLEAN)~~ averaged over R2 ~~the region in 24°–25°N, 110°–112°E~~ for ~~the~~ warm cloud. (d–f) Same as (a–c) but for ~~rom~~ cold cloud~~. Only anomalies that exceed 90% significance level are depicted with and contour~~. ~~Zero-value contour lines are omitted, and negative values are dashed. The contour interval is 3 K d^{-1}. Note the blank represent the values are within 3 K d^{-1}.~~

Formatted: English (United States)

Field Code Changed

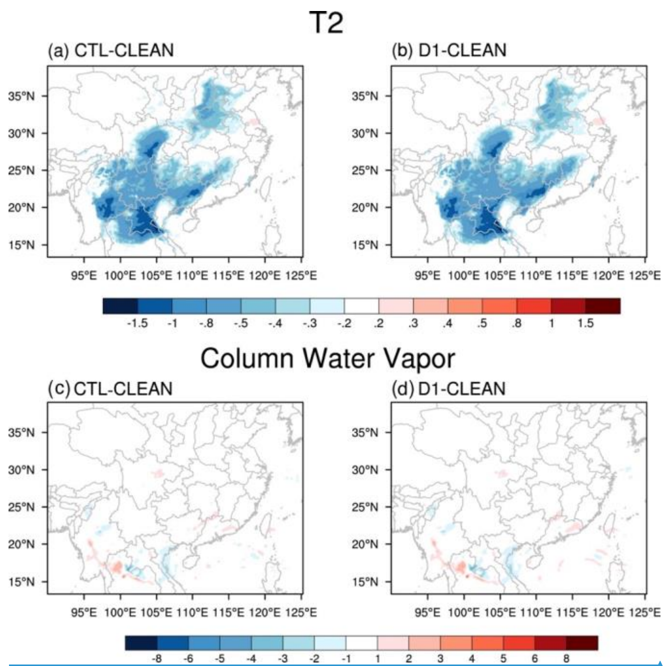

Figure S26~~26~~~~17~~. Differences in 2-m temperature (K) between (a) CTL and CLEAN and (b) D1 and CLEAN on December 15. (c, d) Same as (a, b) but for column water vapor (mm).

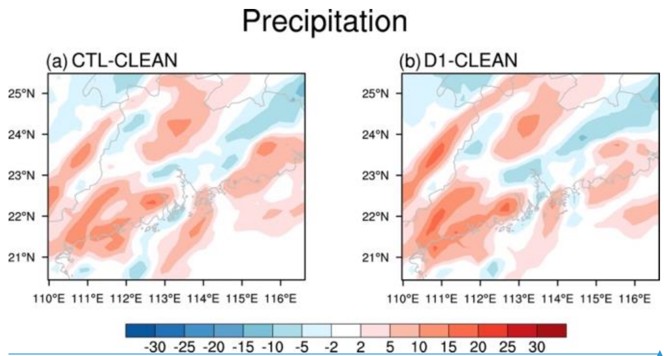

Formatted: (Asian) Chinese (PRC)

Formatted: Centered

Formatted: English (United States)

Formatted: Centered

Figure S27~~2718~~. Differences in precipitation (mm) between (a) CTL and CLEAN and (b) D1 and CLEAN on December 15 based on domain 1 output.

References

Formatted: Font: Bold, English (United States)

Formatted: Font: Bold

Binkowski, F. S. and Shankar, U.: The regional particulate matter model: 1. Model description and preliminary results, J. Geophys. Res., 100(D12), 26191, doi:10.1029/95JD02093, 1995.

Chapman, E. G., Gustafson, W. I., Easter, R. C., Barnard, J. C., Ghan, S. J., Pekour, M. S. and Fast, J. D.: Coupling aerosol-cloud-radiative processes in the WRF-Chem model: Investigating the radiative impact of elevated point sources, Atmos. Chem. Phys., 9(3), 945–964, doi:10.5194/acp-9-945-2009, 2009.

Chen, F. and Dudhia, J.: Coupling an advanced land surface–hydrology model with the Penn State–NCAR MM5 modeling system. Part I: Model implementation and sensitivity, Mon. Weather Rev., 129(4), 569–585, doi:10.1175/1520-0493(2001)129<0569:CAALSH>2.0.CO;2, 2001.

Easter, R. C., Ghan, S. J., Zhang, Y., Saylor, R. D., Chapman, E. G., Laulainen, N. S., Abdul-Razzak, H., Leung, L. R., Bian, X. and Zaveri, R. A.: MIRAGE: Model description and evaluation of aerosols and trace gases, J. Geophys. Res. D Atmos., 109(20), doi:10.1029/2004JD004571, 2004.

Fast, J. D., Gustafson, W. I., Easter, R. C., Zaveri, R. A., Barnard, J. C., Chapman, E. G., Grell, G. A. and Peckham, S. E.: Evolution of ozone, particulates, and aerosol direct radiative forcing in the vicinity of Houston using a fully coupled meteorology-chemistry-aerosol model, J. Geophys. Res. Atmos., 111(21), 1–29, doi:10.1029/2005JD006721, 2006.

Hong, S.-Y., Noh, Y. and Dudhia, J.: A new vertical diffusion package with an explicit treatment of entrainment processes., Mon. Weather Rev., 134(9), 2318–2341, doi:10.1175/MWR3199.1, 2006.

Iacono, M. J., Delamere, J. S., Mlawer, E. J., Shephard, M. W., Clough, S. A. and Collins, W. D.: Radiative forcing by long-lived greenhouse gases: Calculations with the AER radiative transfer models, , 113, 2–9, doi:10.1029/2008JD009944, 2008.

Kain, J. S. and J. M. Fritsch: A one-dimensional entraining/detraining plume model and its application in convective parameterization, J. Atmos. Sci., 47, 2784–2802, doi.org/10.1175/1520-0469(1990)047<2784:AODEPM>2.0.CO;2, 1990.

Morrison, H., Thompson, G. and Tatarskii, V.: Impact of cloud microphysics on the development of trailing stratiform precipitation in a simulated squall line: Comparison of one- and two-moment schemes, Mon. Weather Rev., 137(3), 991–1007, doi:10.1175/2008MWR2556.1, 2009.

Skamarock, W. C., Klemp, J. B., Dudhia, J., Gill, D. O., Barker, D. M., Duda, M. G., Huang, X.-Y., Wang, W. and Powers, J. G.: A description of the advanced research WRF version 3. [online] Available from: https://pdfs.semanticscholar.org/ace5/4d4d1d6c9914997ad8f4e410044fdeb95b9d.pdf (Accessed 15 May 2018), 2008.

Yang, Q., Gustafson, W. I., Fast, J. D., Wang, H., Easter, R. C., Morrison, H., Lee, Y. N., Chapman, E. G., Spak, S. N. and Mena-Carrasco, M. A.: Assessing regional scale predictions of aerosols, marine stratocumulus, and their interactions during

VOCALS-REx using WRF-Chem, Atmos. Chem. Phys., 11(23), 11951–11975, doi:10.5194/acp-11-11951-2011, 2011.

Zaveri, R. A. and Peters, L. K.: A new lumped structure photochemical mechanism for large-scale applications, J. Geophys. Res. Atmos., 104(D23), 30387–30415, doi:10.1029/1999JD900876, 1999.

Zaveri, R. A., Easter, R. C., Fast, J. D. and Peters, L. K.: Model for simulating aerosol interactions and chemistry (MOSAIC), J. Geophys. Res. Atmos., 113(13), doi:10.1029/2007JD008782, 2008.

Zhao, C., Wang, Y., Choi, Y. and Zeng, T.: Summertime impact of convective transport and lightning NOx production over North America: Modeling dependence on meteorological simulations, Atmos. Chem. Phys., 9(13), 4315–4327, doi:10.5194/acp-9-4315-2009, 2009.

Zhao, C., Liu, X., Leung, L. R., Johnson, B., Mcfarlane, S. A., Jr, W. I. G., Fast, J. D. and Easter, R.: The spatial distribution of mineral dust and its shortwave radiative forcing over North Africa: modeling sensitivities to dust emissions and aerosol size treatments, Atmos. Chem. Phys., 10, 8821–8838, doi:10.5194/acp-10-8821-2010, 2010.

Zhao, C., Liu, X., Leung, L. R. and Hagos, S.: and Physics Radiative impact of mineral dust on monsoon precipitation variability over West Africa, (2007), 1879–1893, doi:10.5194/acp-11-1879-2011, 2011.

Zhao, C., Chen, S., Leung, L. R., Qian, Y., Kok, J. F., Zaveri, R. A. and Huang, J.: Uncertainty in modeling dust mass balance and radiative forcing from size parameterization, Atmos. Chem. Phys., 13(21), 10733–10753, doi:10.5194/acp-13-10733-2013, 2013.

Formatted: Normal

Formatted: Normal, Indent: Left: 0", Hanging: 0.2", Don't adjust right indent when grid is defined, No widow/orphan control, Don't adjust space between Latin and Asian text, Don't adjust space between Asian text and numbers